UNIVERSITETET I AGDER

Design optimisation of a funnel-shaped floating dock for installation of offshore wind turbines.

Gran, Viktor A.

Pedersen, Simen N.

Widestam, Oscar

Supervisor
Zhiyu Jiang
Associate Professor

Universitetet i Agder, 2020
Faculty of Science and Technology
Department of Engineering

Obligatorisk Gruppeerklæring

Den enkelte student er selv ansvarlig for å sette seg inn i hva som er lovlige hjelpemidler, retningslinjer for bruk av disse og regler om kildebruk. Erklæringen skal bevisstgjøre studentene på deres ansvar og hvilke konsekvenser fusk kan medføre. Manglende erklæring fritar ikke studentene fra sitt ansvar.

1.	Jeg/vi erklærer herved at min/vår besvarelse er mitt/vårt eget arbeid, og at jeg/vi ikke har brukt andre kilder eller har mottatt annen hjelp enn det som er nevnt i besvarelsen.	☒
2.	Jeg/vi erklærer videre at denne besvarelsen: - ikke har vært brukt til annen eksamen ved annen avdeling/universitet/høgskole innenlands eller utenlands. - ikke refererer til andres arbeid uten at det er oppgitt. - ikke refererer til eget tidligere arbeid uten at det er oppgitt. - har alle referansene oppgitt i litteraturlisten. - ikke er en kopi, duplikat eller avskrift av andres arbeid eller besvarelse.	☒
3.	Jeg/vi er kjent med at brudd på ovennevnte er å betrakte som fusk og kan medføre annullering av eksamen og utestengelse fra universiteter og høgskoler i Norge, jf. Universitets- og høgskoleloven §§4-7 og 4-8 og Forskrift om eksamen §§ 31.	☒
4.	Jeg/vi er kjent med at alle innleverte oppgaver kan bli plagiatkontrollert.	☒
5.	Jeg/vi er kjent med at Universitetet i Agder vil behandle alle saker hvor det forligger mistanke om fusk etter høgskolens retningslinjer for behandling av saker om fusk.	☒
6.	Jeg/vi har satt oss inn i regler og retningslinjer i bruk av kilder og referanser på biblioteket sine nettsider.	☒

Publiseringsavtale

Fullmakt til elektronisk publisering av oppgaven

Forfatter(ne) har opphavsrett til oppgaven. Det betyr blant annet enerett til å gjøre verket tilgjengelig for allmennheten (Åndsverkloven. §2).

Alle oppgaver som fyller kriteriene vil bli registrert og publisert i Brage Aura og på UiA sine nettsider med forfatter(ne)s godkjennelse.

Oppgaver som er unntatt offentlighet eller tausehetsbelagt/konfidensiell vil ikke bli publisert.

Jeg/vi gir herved Universitetet i Agder en vederlagsfri rett til å gjøre oppgaven tilgjengelig for elektronisk publisering:	☒ JA	☐ NEI
Er oppgaven båndlagt (konfidensiell)?	☐ JA	☒ NEI
(Båndleggingsavtale må fylles ut) - Hvis ja:		
Kan oppgaven publiseres når båndleggingsperioden er over?	☐ JA	☐ NEI
Er oppgaven unntatt offentlighet? (inneholder taushetsbelagt informasjon. Jfr. Offl. §13/Fvl. §13)	☐ JA	☒ NEI

Preface

This thesis is written as a fulfilment of the graduation requirements of the Master of Civil and Constructional Engineering program at the Department of Engineering Sciences of the University of Agder. The research has been conducted during the fourth and concluding semester of the master's studies in structural engineering - from January to June 2020. The work is equivalent to 30 ECTs.

It is assumed that whoever is interested in this work and chooses to read it holds a fundamental knowledge in the fields of engineering and mathematics. The majority of this work is based on theoretical and mathematical research of marine structures, and it may be of help researching the potential development of offshore floating wind power.

We, the authors, would like to extend our sincerest gratitude to our main supervisor during this work: associate professor Zhiyu Jiang at the UiA Department of Engineering. For your vast knowledge, many hours of consultancy, round-the-clock availability and constant attention to detail: Thank you. In addition, we would like to thank Peter Zhi Yuan Pan at DNV GL for his inputs and thoughts while learning HydroD and the CMD-environment.

Last, but definitely not least, we would like to thank the student organisation ØVD for making the years at UiA extraordinarily eventful.

"*Wikipedia is the best thing ever. Anyone in the world can write anything they want about any subject. So you know you are getting the best possible information.*"

- Michael Scott

Abstract

Offshore wind power is a rapidly growing renewable energy industry and has a tremendous potential of further expansion. Installation of offshore wind turbines is a challenging task. Floating wind turbines are believed to be cost-effective solutions for deep water installation. This technology is extremely sensitive to wave excitation during the installation process. As deep-water wind farms often are located in areas exposed to rough weather, innovative methods of installation are investigated. The floating dock concept has been proposed in recent studies in order to expand the weather window for installing spar floating wind turbines. The idea is for the dock to shield the spar from wave excitation. Previous studies show that a funnel-shaped dock potentially has a better hydrodynamic performance compared to cylindrical and bottle-shaped docks. This master's thesis takes the previous studies into consideration and investigates how a parametric design optimisation can be carried out for a funnel-shaped dock intended for installation of floating wind turbines. The optimisation objective is defined as reduction of steel weight. While investigating how to best predict the operational constraint of piston-mode periods, the Gaussian process regression model appeared to be the best predictor. The study revealed that the heights; $T1$, $T2$ and $T3$, in addition to the diameters, $Di1$ and $Di2$, are design parameters which significantly affect the piston-mode period. The optima found in this study deviate from the predictions from the GPR based model as the geometry is outside the trained model-area. This can be solved with a new model which also includes bottle-shaped and cylindrical docks.

Table of Contents

List of Figures

List of Tables

1 | Introduction

Offshore wind power is a rapidly growing renewable energy industry. From 2009 to 2017, the electricity produced from offshore wind power worldwide increased from approximately 4416 GWh to 57331 GWh [16] and it has a tremendous potential of further expansion [17].

Installation of offshore wind turbines is a challenging task. The type of offshore wind turbine to install is dependent on the geological and environmental conditions of the wind farm site. More than 105 wind farms have been constructed in Europe to date, where the average water depth is about 30 m at the farm locations [18]. Amongst these, most wind turbines are bottom fixed, and only a few projects are floating wind turbines [18]. For water depths greater than 100 m, floating wind turbines are believed to be cost-effective solutions.

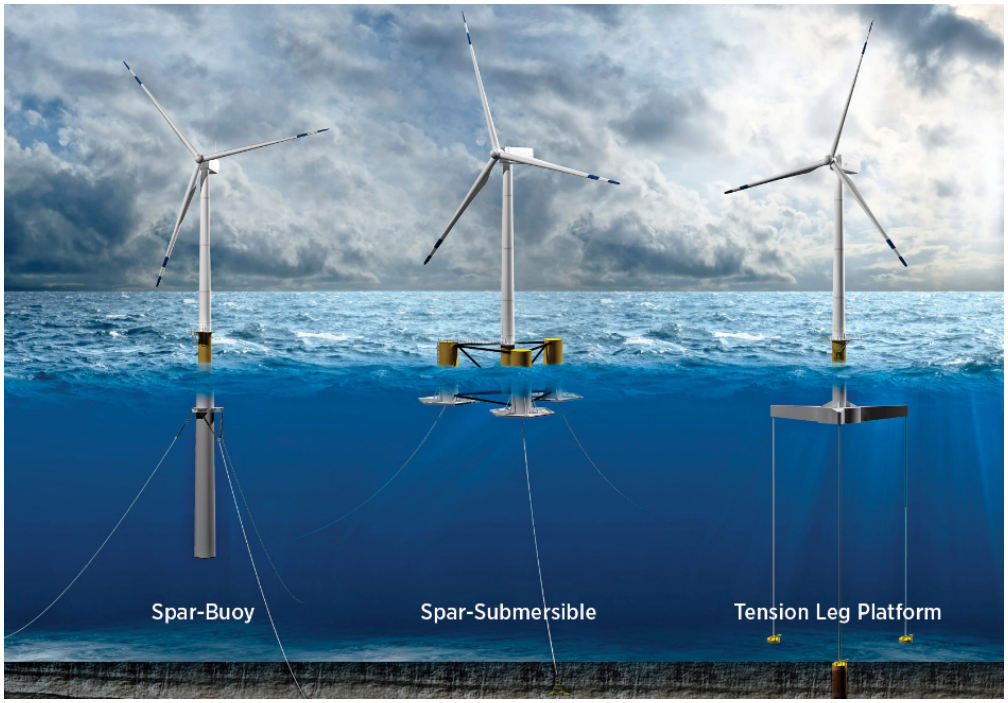

Figure 1.1: Illustration of offshore wind floating foundation concepts [1].

There are three main concepts of foundations for floating wind turbines. They are *spar*, *semi-submersible* and *tension leg* platforms. These are illustrated in Figure 1.1. For spar floating wind turbines, the platform is usually upended first, and towed to a deep-water area sheltered from harsh sea conditions, before the mating of the tower assembly with the spar platform is performed by a crane vessel. An illustration of this is shown in Figure 1.2 and 1.3. This method was used in the Hywind project before the floating wind turbines were towed to site and attached to the mooring system [19].

Figure 1.2: Transport of platform to deep-water area [2].

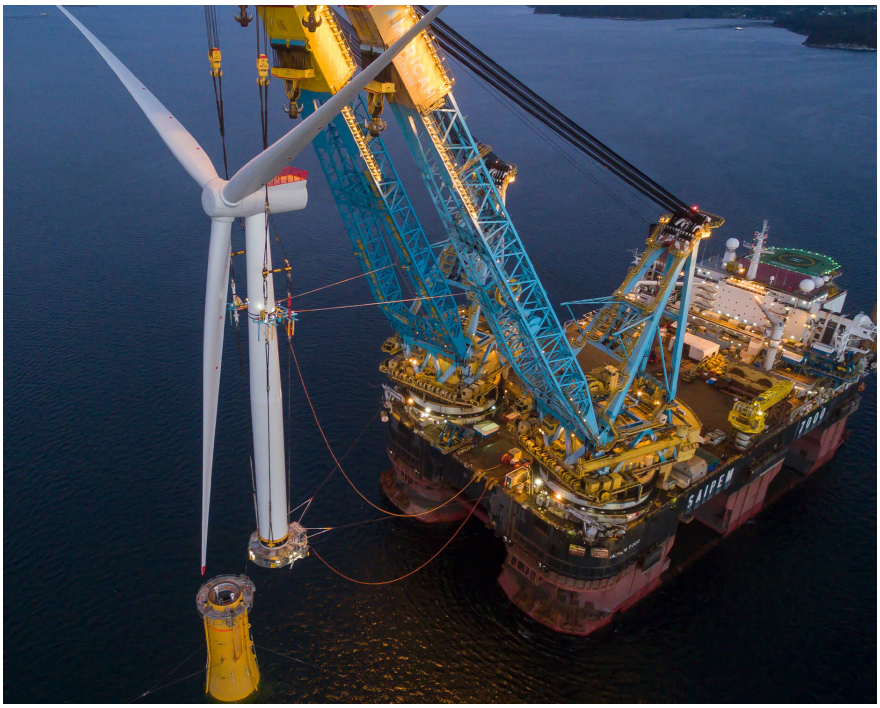

Figure 1.3: Mating of the tower assembly with the spar platform performed by a crane vessel [3].

As deep-water wind farms are often located in areas exposed to rough weather, other methods for installation of floating wind turbines are sought-after to expand the weather window and avoid delays. One recent idea is to use a wind turbine installation vessel for installation of pre-assembled rotor-nacelle-tower assemblies onto spar platforms. This concept involves a catamaran, with sliding and lifting grippers, which uses a dynamic positioning system to perform offshore installation in open seas. In this concept the motions experienced by the spar platform should be compensated during the mating process [20], [21], [22]. Another concept for installation of floating wind turbines in open seas is the floating dock concept. It has recently been proposed to expand the weather window for installing spar floating wind turbines and is further explained in Chapter 5 [23]. The concept only considered cylindrical shapes and did not include piston-mode period as a constraint. The pre-project of this master's thesis worked on improving the floating dock concept by comparing hydrodynamic analyses with alternative geometries. The result showed that a funnel-shaped dock has the potential to have improved performance in operating sea state. This master's thesis will therefore investigate how a parametric design optimisation be carried out for a funnel-shaped dock intended for installation of floating wind turbines.

2 | Social Perspective

All people on Earth directly or indirectly depend on the ocean. The Norwegian economy has always been one with especially close ties to the ocean. From the Vikings crossing the North Sea on their wooden sailing ships, through the fishing industry – a thousand-year-old-industry producing a € 2.12 BN turnover in 2019 [24], to the offshore petroleum industry which is now the cornerstone of the modern Norwegian economy. This is an industry expected to generate a net revenue of € 24.5 BN to the Norwegian state in 2020 [25][26]. Parallel to this, Norway has a proud history exploring the arctic extremes of the Earth. A history which helped form a feeling of unity within the Norwegian people following the secession from Swedish union in 1905 [27].

While world leaders are trying to find a sustainable solution to a rapidly increasing energy demand, our ever-increasing greenhouse gas-emissions are contributing to the smelting of the Earths Arctic and Antarctic regions. The smelting of land-based ice heightens ocean-levels, changes water-streams and interferes with the marine life as we know it today [28]. The Norwegian economy is heavily dependent on an industry which is contributing to the demise of the parts of the world which made Norway what it is today.

Although Norway is not by any means the world's largest contributor to global greenhouse gas-emissions, the Norwegian offshore petroleum industry did boost the Norwegian emissions of CO2-equivalents to a total of 8.3 tons per capita in 2018. Compared to Sweden (4.1 tons per capita), a comparable county without the dependency on the petroleum industry, this is an alarming number. These numbers are territorial, meaning only the production of petrochemicals on Norwegian territory is included. The consumption of exported petrochemicals does not add to these emissions [29].

As a possible solution to the excessive greenhouse gas-emissions, offshore wind power is a technology which may prove itself as a viable solution. The potential for energy harvest exceeds the combined estimated energy demand of the world eightfold, and the Norwegian industry for offshore constructions are world-leading – with the industry being very well managed and large sums having been spent on research and development. According to Næringslivets Handelsorganisasjon (NHO), there is a potential for employment of 130.000 people within the offshore wind power industry in Norway come 2050 [30].

The offshore wind industry is being foretold to become a "$ 1 trillion industry" [31]. As the industry needs rapid construction to reach it's potential, investigating optimized dock geometries is contributing to speedy growth. With a successful study, the installation of offshore wind turbines may become possible in weather conditions previously unsuited for installation. Increasing wave- and wind limits of the installation process, even by small amounts, may significantly reduce the total installation times of large wind farms. In addition, the results may open for installation in locations previously unavailable due to harsh weather conditions.

3 | Theory

This chapter elaborates on the sea environment, linear wave theory, hydrodynamic loads and motions and responses for floating structures. The chapter will also introduce the theory behind the chosen computing programs used to perform both hydrodynamic analyses and optimisation of the structure presented in this study.

3.1 Sea Environment

This sub-chapter explores introductory theory of the sea environment and will cover wave heights, wave periods and wave spectra.

3.1.1 Wave Height

The wave height is the vertical distance from the wave crest to the wave through on any given wave. On a sinusoidal wave it is two times the wave amplitude. Significant wave height H_s is the average of the highest $\frac{1}{3}$ of the waves.

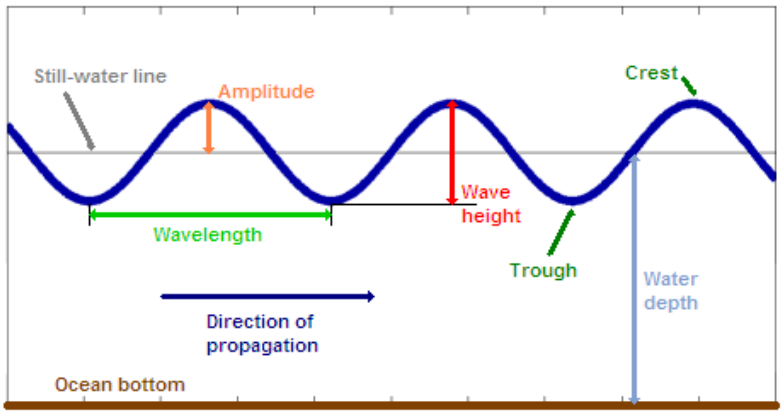

Figure 3.1: Illustration of technical terms used in sea environment [4].

3.1.2 Wave Period

The wave period T is the time, usually given in seconds, a wave uses to complete one cycle. I.e. from one wave crest to the next one. This term is important for understanding of natural periods and resonance modes covered later in this work. Wave period is inversely proportional to wave frequency f.

$$T = \frac{1}{f} \tag{3.1}$$

3.1.3 Wave Spectrum

A wave spectrum is a simplified way to describe the sea surface containing various waves with different wave periods and wave heights by their energy contributions. Two of the most recognised approaches are the Pierson-Moskowitz (PM) and The Joint North Sea Wave Project (JONSWAP). The PM spectrum defines the energy distribution of waves with the respect to the wave frequency. This approach is based on measurements of constant environmental conditions during an extended time-period in the North Atlantic in 1964 [32]. A modified PM spectrum is described by the equation

$$S_p m\ (\omega) = \frac{5}{16} {H_s}^2 {\omega_p}^4 \omega^{-5} e^{(-\frac{5}{4}\frac{\omega}{\omega_p}^{-4})} \tag{3.2}$$

Where ω_p, *the angular spectral peak*, is equal to $\frac{2\pi}{T_p}$ and T_p is the *spectral peak period* [5].

The JONSWAP approach is meant to describe the conditions of the North Sea. It is a modified version of the PM spectrum and can be described by the equation

$$S_j\ (\omega) = A_y S_p m(\omega) y^{e^{0,5(\frac{\omega-\omega_p}{\rho\omega_p})^2}} \tag{3.3}$$

Where A_y is a *normalizing factor*, y is a non-dimensional *peak shape parameter* and ρ is a *spectral width parameter*. If y equals 1 it is reduced to the PM spectrum. Different y values are shown in Figure 3.2 [5].

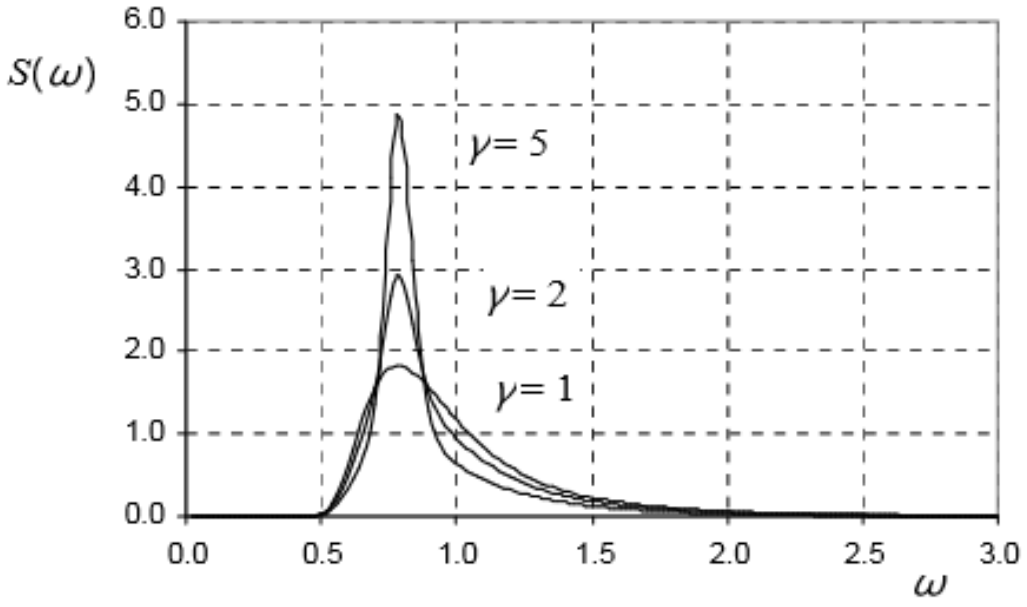

Figure 3.2: JONSWAP spectrum with variable peak shape parameter [5].

3.2 Hydrostatics of Marine Structures

This sub-chapter aims to serve as a brief introduction to some of the definitions, stability calculations and considerations needed to verify the structural integrity of a marine structure.

3.2.1 Hydrostatic Stability

The centre of gravity, G, is defined as the imaginable point within the structure where all mass may be concentrated to a force vector in the *negative* z-direction. The center of buoyancy, B may be defined as an imaginable centre of volume for the *submerged* parts a structure [33] where buoyancy may be simplified to a force vector in *positive* z-direction. The metacentre, M, is defined as the point where a vertical line through a heeled centre of buoyancy crosses the line of the original vertical centre of buoyancy. See figure 3.3 for illustration. The metacentric height, GM, is the distance between the centre of gravity and the metacentre. A larger metacentric height will initially give a larger *righting moment* in a heeled state [34]. Righting moment refers to the *righting arm* between G and B_1 in figure 3.3, and if this is poorly designed the marine structure may capsize.

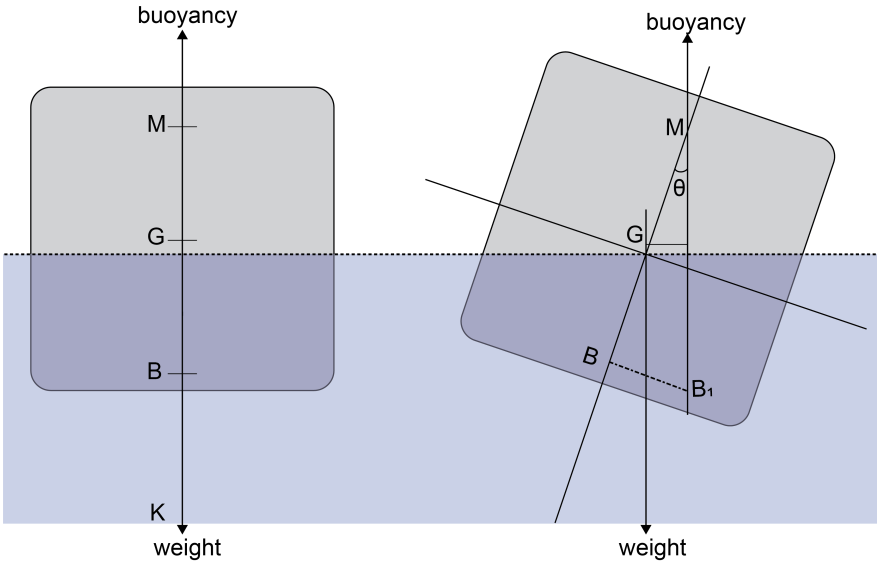

Figure 3.3: Some of the parameters influencing the hydrostatic stability of a floating body.

3.2.2 States of Operation

There are three main *states* of a marine structure:

- *Operational state*, where the structure is being used as intended.
- *Transit state*, where the structure is being transported to an installation site. For ships, transit and operations may coincide.
- *Survivability state*, where the structure is imagined caught in severe weather conditions, with 50- or 100-year return periods, and is no longer in operation or in transport. The constraints in the survivability state are not as strict as in the other states.

3.3 Linear Wave Theory

Linear wave theory, also known as Airy wave theory, is often used for modelling of random sea states in ocean engineering. One of the main reasons to use linear wave theory in modelling is that irregular waves can be described by adding together regular waves with different properties.

Given that the seabed is horizontal and infinite in the horizontal direction, airy wave theory can be deduced using the derivatives of the flow potential $\phi(x, z, t)$, the continuity equation for incompressible flows, boundary conditions at seabed and free surface boundary conditions.

The flow velocity:

$$v_x = \frac{\partial \phi_w}{\partial x} \quad and \quad v_z = \frac{\partial \phi_w}{\partial z} \tag{3.4}$$

The continuity equation:

$$\frac{\partial^2 \phi_w}{\partial x^2} + \frac{\partial^2 \phi_w}{\partial z^2} = 0 \tag{3.5}$$

Boundary condition for the seabed:

$$\frac{\partial \phi_w}{\partial x} = 0 \quad for \quad z = -h \tag{3.6}$$

This means that the seabed is impermeable and the vertical flow velocities of water particles at the seabed is zero.

Boundary condition for the free surface dynamic:

$$\frac{\partial \phi_w}{\partial t} + g\zeta = 0 \quad for \quad z = \zeta \tag{3.7}$$

where constants are included in $\frac{\partial \phi_w}{\partial t}$.

The free surface pressure is equal to the atmospheric pressure at the surface of the fluid $z = \zeta$, and the free surface dynamic boundary condition can be deduced from the Bernoulli equation for unstationary irrotational flow. ζ is equal to the free surface elevation.

Boundary condition for the free surface kinematic:

$$\frac{\partial z}{\partial t} + \frac{1}{g}\frac{\partial^2 \phi_w}{\partial t^2} = 0 \quad for \quad z = 0 \tag{3.8}$$

The water particles on the free surface and the free surface itself has the same vertical velocity due to no leak condition. The free surface kinematic condition is known as the Cauchy-Poisson condition. $\frac{\partial z}{\partial t}$ is equal to the vertical velocity of the wave surface and $\frac{\partial^2 \phi_w}{\partial t^2}$ is equal to the flow acceleration.

These boundary conditions are used in boundary element method to calculate hydrostatic and hydrodynamic problems [6] [35].

3.4 Hydrodynamic Loads

This sub-section explains how hydrodynamic loads on a floating structure can be simplified by superposition due to linear theory and how added mass and radiation damping is found.

3.4.1 Radiation and Diffraction

Multiple loads acting on a floating body is a complex problem. This can, however, be simplified using the concept of superposition from linear theory. A floating structure is affected by both passing waves, and waves generated by the structure itself due to oscillation. Radiation is connected to the added mass, damping and restoring loads. This can be understood by picturing the floating structure being forced to oscillate in still water. The radiating waves represent the energy taken out of the system. The diffraction loads are from the passing waves acting on the structure given that it is fixed.

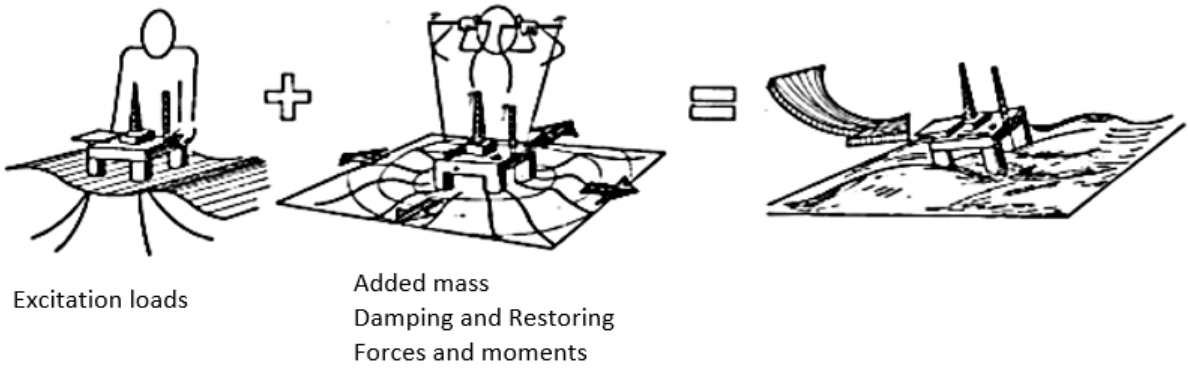

Figure 3.4: Superposition of wave excitation, added mass, damping and restoring loads [6].

3.4.2 Added Mass and Radiation Damping

Added mass and damping can be explained from forced harmonic rigid body motions in steady-state conditions. This motion generates outgoing waves from the structure and results in oscillating fluid pressure on the body surface. Resulting forces and moments can be found by integration of the fluid pressure over the body surface. This means that added mass is not affected by excitation loads, so a fixed dock will have the same added mass as a floating dock.

3.5 Motions and Responses of Floating Structures

This section shows the degrees of freedom of a floating structure and explains how the equation of motion can be used to calculate motions, natural periods and response amplitude operators. It also explains what piston mode excitation and linear sloshing look like.

3.5.1 Degrees of Freedom

Floating structures in ocean environment have six degrees of freedom (DOF). The six DOFs consist of three directions like the Cartesian coordinate system (Surge, Sway and Heave), and three rotations around these, respectively Roll, Pitch and Yaw. Hydrostatic and hydrodynamic pressures acts on the rigid structure and will exert forces and moments which try to move or rotate the body in its given DOF.

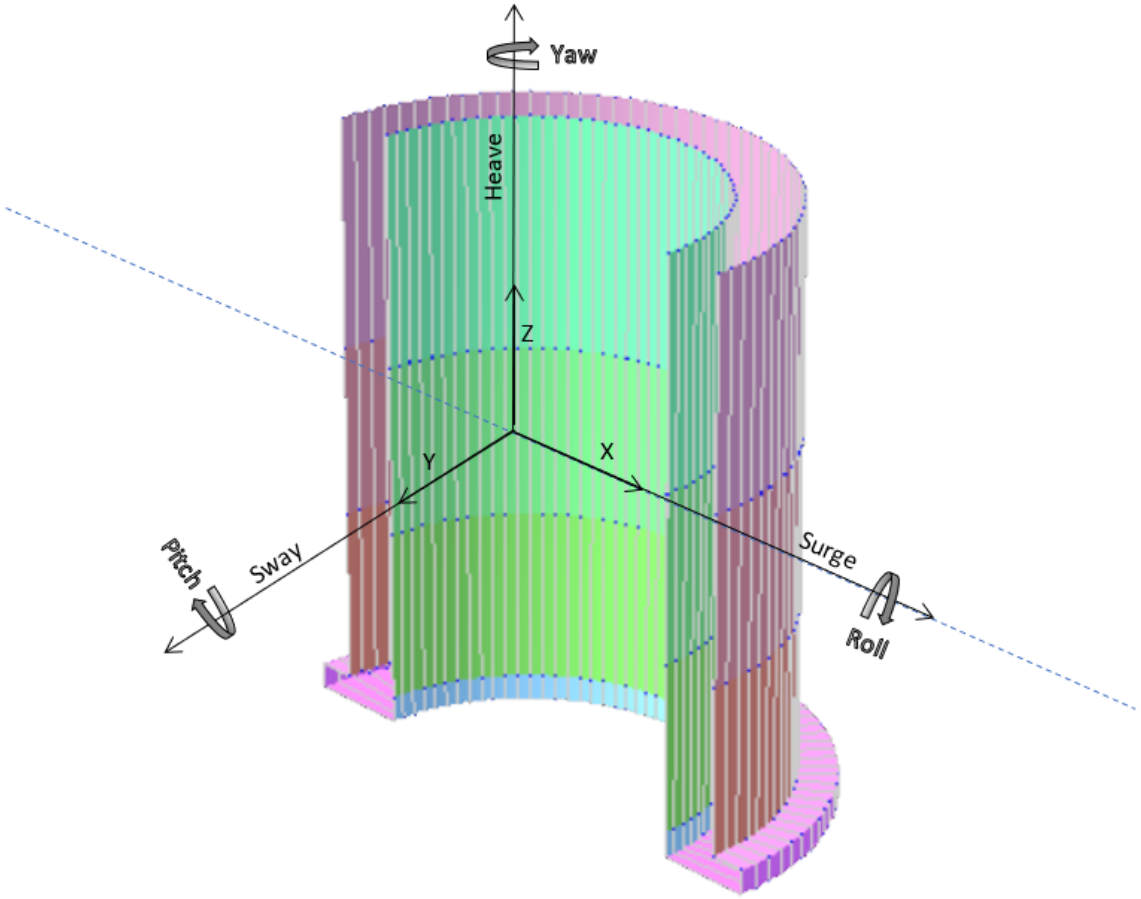

Figure 3.5: The six DOF shown on a cylindrical floating dock.

3.5.2 Equation of Motion

The equation of motion is used to describe the motions of the system. It is derived from Newtons second law. The basic equation of motion is given by

$$(M + A)\ddot{x} + B\dot{x} + Cx = F_{exc} \tag{3.9}$$

where F_{exc} is the exciting force, A is the added mass, B is the damping and C is the hydrostatic restoring force.

For six DOF the formula can be written as:

$$\sum_{j=1}^{6} \left[(M_j + A_j)\, \ddot{x} + B_j \dot{x} + C_j x \right] = F e^{i\omega_e t} \tag{3.10}$$

This formula can be used to calculate body motions in all six DOFs.

3.5.3 Natural Periods

Natural periods of a system with multiple DOFs can be found by first guessing an answer for the second-order differential equation, which is a variant of Newton's second law for a spring system.

$$\boldsymbol{M}\ddot{x} + \boldsymbol{K}x = 0 \tag{3.11}$$

Here guessing

$$x = \Phi \cos(\omega t + \varphi) \tag{3.12}$$

Where Φ is the eigenvectors, ω is the angular eigenfrequency, t is the time and φ is the phase of the oscillation.

Through double differentiation of eq. 3.11 and insertion of the guessed solution x from eq. 3.12, an equation for natural periods emerge:

$$(\boldsymbol{K} - \omega^2 \boldsymbol{M})\phi = 0 \tag{3.13}$$

Where $\boldsymbol{K}$ is the stiffness matrix.

To solve this equation for the system when it is in motion the solution is when $\boldsymbol{K} - \omega^2 \boldsymbol{M} = 0$. This means that the matrix is singular and the solution can be written as

$$det \left| \boldsymbol{K} - \omega^2 \boldsymbol{M} \right| = 0 \tag{3.14}$$

3.5.4 Response Amplitude Operator

The response surface amplitude (RAO) are the transfer functions which determine the effects different sea states will have on the motion of a floating structure.

For regular wave conditions RAO can be calculated by dividing the response amplitude by the excitation amplitude. In this case this can be done by dividing the dock motion by the wave amplitude.

$$(M + A)\ddot{x} + B\dot{x} + Cx = F_{exc} \tag{3.15}$$

With $x = ae^{i\omega t}$ and $F_{exc} = F_0\zeta_a e^{i\omega t}$

Where a is the distance the dock has moved and ζ_a is the wave amplitude. Figure 3.6 shows an example for surge.

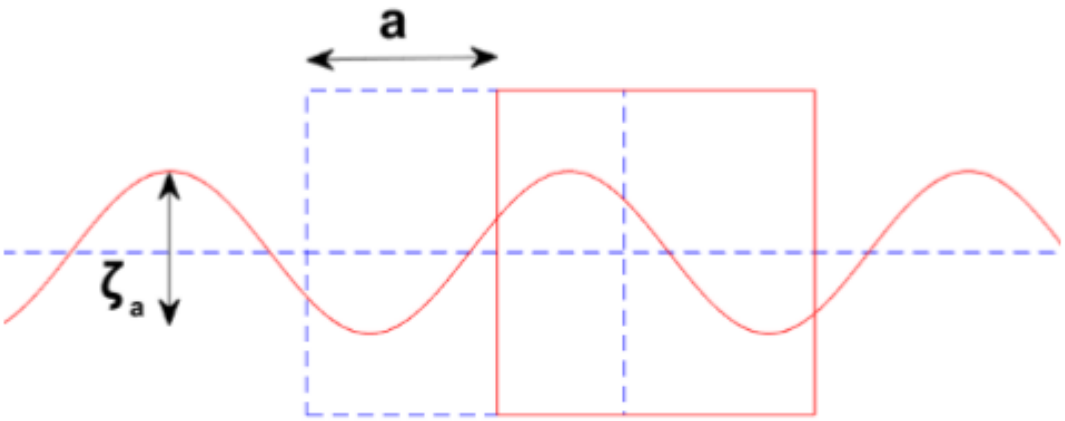

Figure 3.6: RAO variables surge [7].

Inserting for F_{exc}, x and its derivatives give:

$$(M + A)(-\omega^2 ae^{i\omega t}) + B(i\omega ae^{i\omega t}) + C(ae^{i\omega t}) = F_0\zeta_a e^{i\omega t} \tag{3.16}$$

And as RAO is the dock motion divided by the wave amplitude this gives:

$$RAO = \frac{a}{\zeta_a} = \frac{F_0}{-\omega^2(M + A) + i\omega B + C} \tag{3.17}$$

3.5.5 Piston Mode Exication

The piston-mode excitation is a resonance oscillation where the water surface moves as a rigid body in the heave direction. When studying the floating dock, piston-mode is one of the important resonance modes. Piston-mode can cause trouble if it is on wave periods that occur during installation. When wave periods are in the vicinity of the period that piston mode occurs, the water surface inside the dock oscillates significantly.

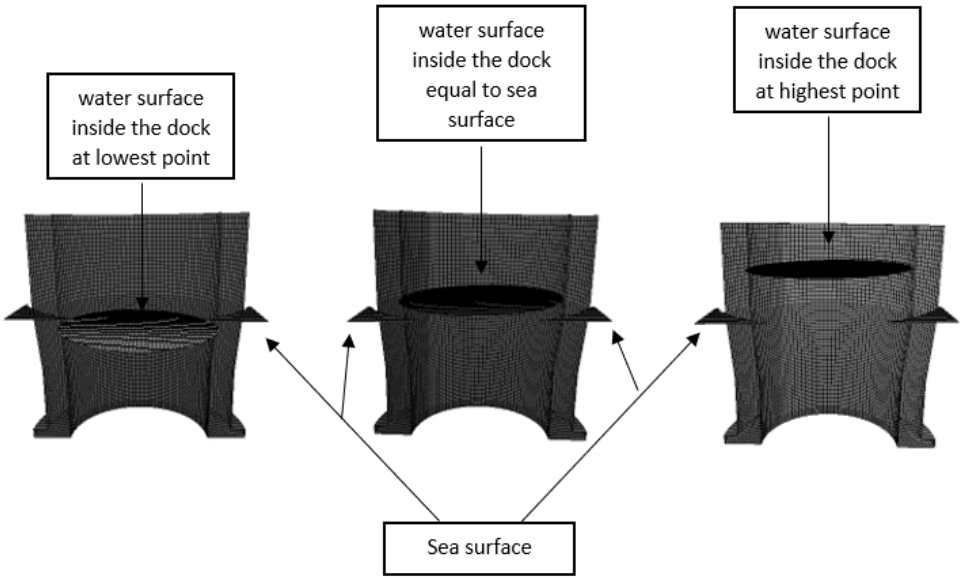

Figure 3.7: Example of piston-mode oscillation inside a floating dock.

The period of the piston mode excitation can be predicted by looking at the added mass in heave direction for the structure.

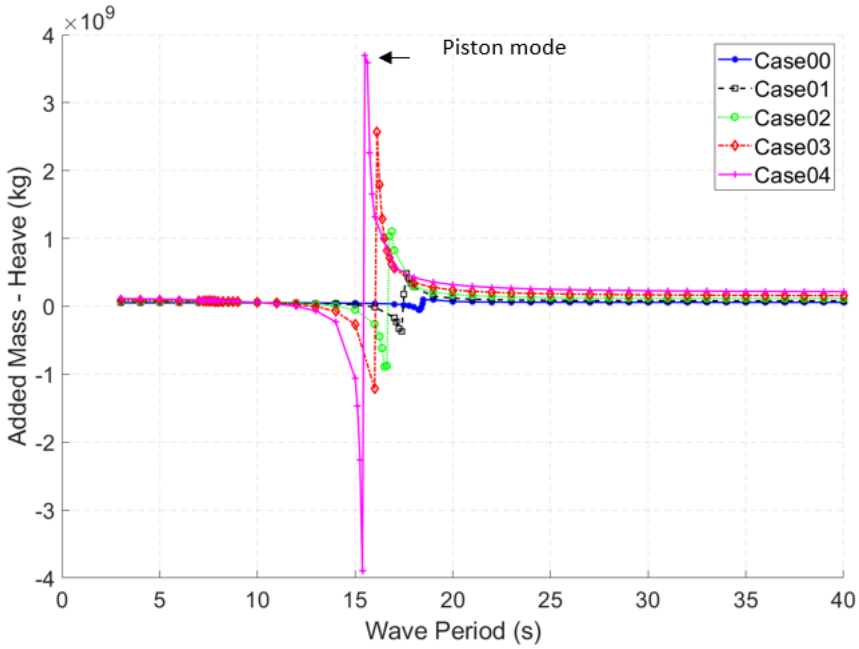

Figure 3.8: Example of how piston-mode is predicted by looking at added mass in heave.

It can be predicted by Molin's formula that has proven to provide good accuracy for simple cylindrical docks [23].

$$\omega_{piston} = \sqrt{\frac{g}{T_0(1 + \frac{D_i(\frac{3}{2} + ln\frac{D_0}{2D_i})}{\pi T_0})}} \tag{3.18}$$

Where g is the gravity, D_i is the inner diameter, D_0 is the outer diameter and T_0 is the height of the part of the dock that is submerged.

This gives

$$T_{piston} = \frac{2\pi}{\omega_{piston}} \tag{3.19}$$

3.5.6 Linear Sloshing

Sloshing effects occur when a liquid with a free surface is inside a vehicle or a structure and it is moved and can be a result of resonant excitation of the tank liquid. Sloshing can also be a result of transient motions like when coffee gets spilled form a coffee cup [36]. This study focuses on linear sloshing and not nonlinear sloshing like swirling. Linear sloshing is an important resonance mode coupled to surge and pitch motions. When waves hit the period that the linear sloshing mode occurs the water surface inside the dock gets higher on one side while it gets lower on the other symmetrical around the middle of the dock and shifts.

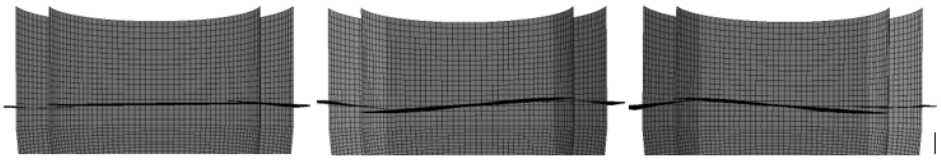

Figure 3.9: Example of linear sloshing oscillation inside a floating dock.

For a 2d case a good estimation of the linear sloshing period for a rectangular planar tank is equal to the cylindric one, and can be found with the following equation with $i = 1$

$$T_i = \frac{2\pi}{\sqrt{g\pi i \frac{\tanh\frac{\pi i h}{l}}{l}}} \tag{3.20}$$

Where g is the gravity, h is the height of the water and l is the breadth of the tank [36].

For a 3d case the linear sloshing period for an upright cylindric tank can be estimated with

$$T_{1.1} = \frac{2\pi}{\sqrt{g l_{1.1} \frac{\tanh\frac{l_{1.1} h}{R_0}}{R_0}}} \tag{3.21}$$

Where $l_{1.1} = 1.841$, g is the gravity, h is the height of the water and R_0 is the inner diameter [36].

3.5.7 Wave Particle Transfer Function

The sloshing and piston period can also be found by inspecting the movement of the docks and the water surface elevation inside the docks for every frequency for every case in the Xtract program [37]. This program can generate animations of motions of the buoy with radiated and diffracted waves around it for every wave frequency and makes it easy to visually investigate the piston and sloshing phenomena. Figure 3.10 and 3.11 shows examples where piston and sloshing period is found from the animation. This method is referred to further in this paper as from wave particle transfer function. The wave particle transfer function can be regarded as the most direct representation of the physical phenomena of linear sloshing and piston mode resonance, whereas the added mass in heave or pitch is an assisting indicator since it is only relating to a hydrodynamic force from the radiation problem.

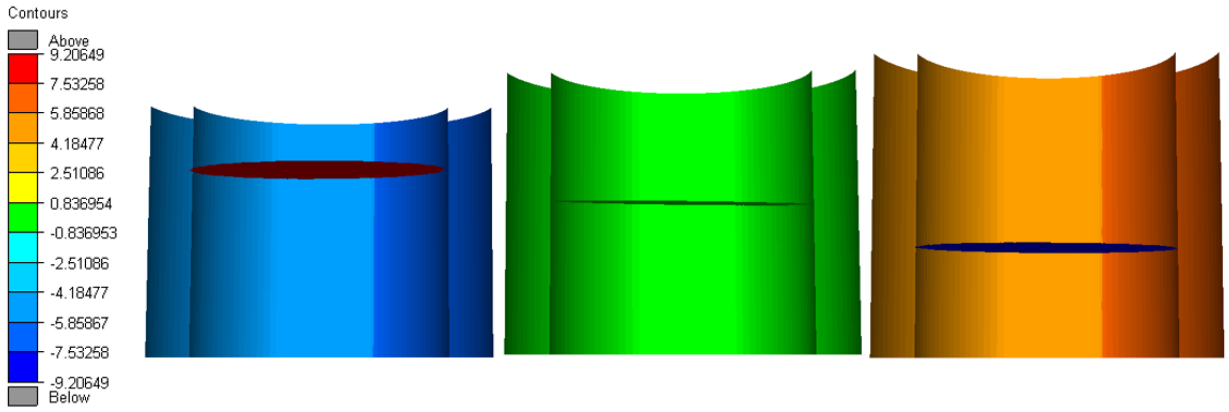

Figure 3.10: illustration of piston mode resonance found from wave particle transfer function.

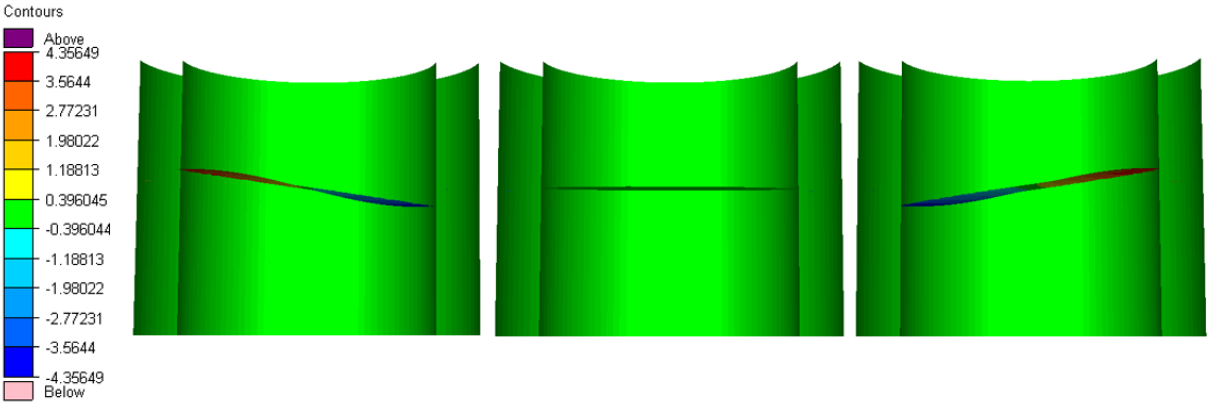

Figure 3.11: illustration of linear sloshing mode found from wave particle transfer function.

3.6 Design of Experiments

Design of experiments (DOE) refers to the process of planning an experiment so that the appropriate data is collected and analyzed by statistical methods, resulting in a valid and objective conclusion [38]. When analyzing a process, experiments are often used to evaluate which inputs have a significant impact on the output, and what the target level of those inputs should be to achieve the desired output. In addition to understanding how a particular variable affects product performance, interactions between different process and product variables are identified. The observations made are never exactly representative of the process we think we are observing. Mathematically, this is conceptualized as:

$$measured\ value = true\ value \pm error [39] \tag{3.22}$$

The process involved in conducting a successful DOE can be broken down into five steps:

1. Define the problem.
2. Plan the experiment.
3. Run the experiment.
4. Analyze the data with the help of statistical methods.
5. Report the results.

Figure 3.12: Flowchart for the DOE process.

3.6.1 Problem Definition

It is important to verify that the problem is properly defined and clearly understood before starting any work. Usually, it is collected input from concerned parties with insight regarding the problem. Questions that are recommended to get asked are:

- Do dimensional changes occur in the x, y, or z direction over time?
- Is one dimension outside the specification limit, and is this temperature related?
- Do the parts warp inconsistently from piece to piece?
- Do the dimensions change in a controlled manner over time?
- Have the dimensions changed because of a change in raw materials?
- Are the dimensional issues due to shrinkage caused by the raw materials?
- Are the dimensions different from run to run because of process changes?

Before deciding on the course of action it is critical to fully understand the problem. To understand the problem is critical in order to solve it.

3.6.2 Experiment Planning

After the problem is defined, it is important to define and select the independent variables with limits for the evaluation and dependent variables. Independent variables or factors are parameters of either processing or product that are set at specific values (levels) and controlled in the experimental design. Independent variables are usually quantitative. However, in some experimental designs, the independent variables are qualitative in the form of a control variable is yes or no, or high or low setting is used. It is better to use quantitative factors if possible. With quantitative variables, the high and low levels for each factor are defined [39].

Dependent variables or factors are the responses being measured for each experiment to determine whether the independent variables have an effect on properties or processing conditions being evaluated. Dependent variables or responses are easy to measure and evaluate when using quantitative tests, which provide very specific values for each experiment. In some situations, responses are more qualitative than quantitative. Normal qualitative responses such as pass/fail, good/bad, or yes/no do not provide a good response to model. The number of data points evaluated for each experimental response depends on the number of tests required for statistical significance, based on the precision and accuracy of the test [38].

3.6.3 Data Run and Collection

The third step in the process is data collection. Once the experiments are defined, it is time to execute the experiments and collect the data. It is easier to run the experiments in a nonrandom order, however, this may result in errors that can lead to the wrong conclusion. Randomize the experimental order as much as possible and do not run all the replicates or duplicate experiments one after the other. Collect all available processing data during the experimental phase on both the fixed and manipulated independent variables. Measure the response variables for each experimental test condition.

3.6.4 Analysis

There are good computer programs available to analyze the data. Computer programs like MATLAB predict which independent factors and interactions are significant for a particular response , generate models to predict the dependent response at any experimental point or composition within the experimental matrix, plot the model equations to provide a visual comparison of the data, predict the experimental process condition or composition where the response is maximum, and predict or define an experimental operating range or composition where the properties meet the specifications or desired values[38].

3.6.5 Result Report

The final step is to report the obtained results. Without a summary report, the work will probably be repeated in the future because people will not remember that the work was done or the results were generated. Graphical methods are often useful in this stage, particularly in presenting the results to others. Follow-up runs and confirmation testing should also be performed to validate the conclusions from the experiment [38].

3.7 Response Surface Methods

Response surface methods are well-established statistical and mathematical ways of visualizing and mapping correlations between a set of variables and an interesting output. In engineering and optimisation RSM is often used for reducing material use, production times and cost during the design process. This chapter elaborates on the three types of respnse surfaces used in this thesis.

3.7.1 Polynomial Response Surfaces

This sub-chapter will elaborate on different kinds of regressions and interpolations suitable for fitting and visualizing piston-mode period as a function of two different design variables.

Linear Regression

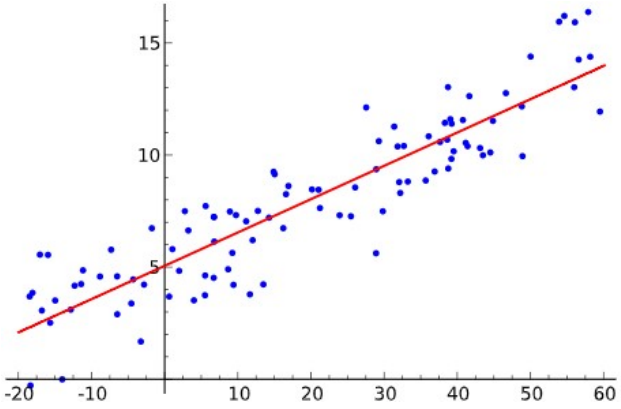

Figure 3.13: Visual representation of linear regression [8].

As a line is given on the form $y = a_0 + a_1\ x_j$, where an are unknown constants placing the line in the plane, one needs to calculate $|y_j - (a_0 + a_1\ x_j)|$ for j number of values of data. Where $a_0 ... a_n$ are random constants. One needs to decide a_0 through a_n such that the squares of these values are of the lowest possible value [40]. This sum is put on the following form and is referred to as lowest mean squares;

$$q_{min} = \sum_{j=1}^{n} (y_j - a_0 + a_{1x_j})^2 \tag{3.23}$$

For a lowest possible value, we have:

$$\frac{\partial q}{\partial a_0} = 0\ and\ \frac{\partial q}{\partial a_1} = 0 \tag{3.24}$$

Nonlinear Regression

Similar to linear regression, the technique of calculation is the same. Although the mathematical shape of the curve is not the same. A polynomial to the n^{th} degree is a curve in 2D is described by:

$$y = \ \beta_0 + \beta_1\ x + \beta_2\ x^2 \dots \beta_n\ x^n + \varepsilon \tag{3.25}$$

Where ε is the unobserved random error and $\beta_0 ... \beta_n$ are constants.

The rest of the regression methodology is similar to the linear regression-method - β-values need to be chosen so that y fits the data sets [41].

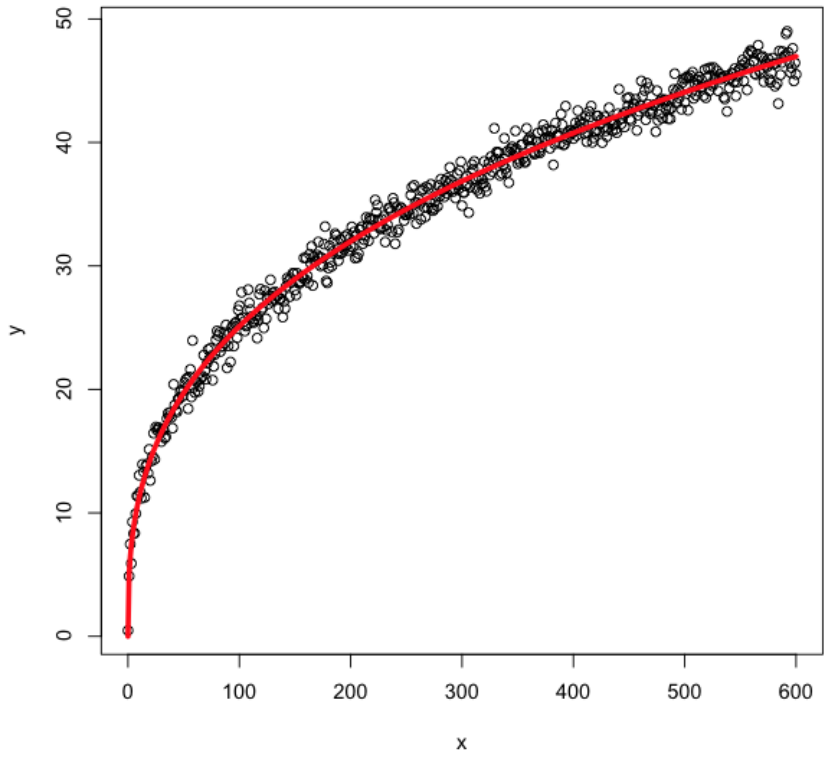

Figure 3.14: Visual representation of nonlinear regression [9].

Interpolation

As with regression, interpolation may be done in both linear and polynomial terms. Linear interpolation assumes a linear relation between data sets. Using data points 1 and 2, one may create the straight line between any data points on figure 3.15a utilizing:

$$f(x) = f_1 + \frac{(f_2 - f_1)(x - x_1)}{x_2 - x_1} \tag{3.26}$$

Polynomial interpolation as illustrated in 3.15b is done by choosing a polynomial such that:

$$f(x) = ax + bx^2 ... + nx^n \tag{3.27}$$

when working with a $(n + 1)$-sized data set, polynomial interpolation is possible for a n^{th} degree polynomial. Spline interpolation is a generalization of linear interpolation, where one may utilize the simplicity of linear interpolation between points and the sophistication of polynomial interpolation. This method of interpolation creates a polynomial interpolation between all data sets, removing the need of a high-order polynomial to create curvature. A quadratic function may very well provide a reasonable result for a data set with a high number of data, using the spline-approach.

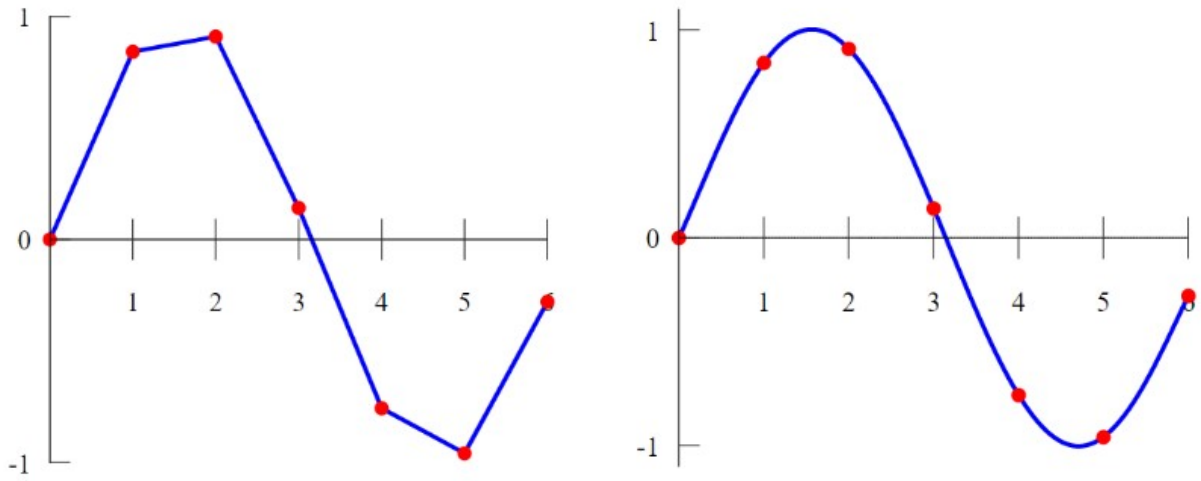

(a) Linear interpolation.

(b) Nonlinear interpolation.

Figure 3.15: Linear and nonlinear interpolations illustrated [10][11].

3.7.2 Gaussian Process Regression

Machine learning teaches computers to learn from experience, like humans . Machine learning algorithms use computational methods to "learn" information directly from data without relying on a predetermined equation as a model. The algorithms adaptively improve their performance as the number of samples available for learning increases [15]. Supervised learning can be divided into regression and classification problems. Whereas the outputs for classification are discrete class labels, regression is concerned with the prediction of continuous quantities [42]. Gaussian process regression, GPR, are nonparametric kernel-based probabilistic models [12]. GPR has several benefits, working well on small datasets and having the ability to provide uncertainty measurements on the predictions.

Background

Unlike many popular supervised machine learning algorithms that learn exact values for every parameter in a function, the Bayesian approach infers a probability distribution over all possible values.

Consider the training set

$$[(xi, yi); i = 1, 2, ..., n], \ where\ xi \in \mathbb{R}d\ and\ yi \in \mathbb{R}\ [12] \tag{3.28}$$

is drawn from an unknown distribution. A GPR model addresses the question of predicting the value of a response variable y_{new}, given the new input vector x_{new}, and the training data. Rather than calculating the probability distribution of parameters of a specific function,GPR calculates the probability distribution over all admissible functions that fit the data [42]. A linear regression model is of the form:

$$y = xT\beta + \varepsilon, \ where\ \varepsilon \sim N(0, \sigma 2)\ [12] \tag{3.29}$$

The error variance σ^2 and the coefficients β are estimated from the data. A GPR model explains the response by introducing latent variables, $f(xi), i = 1, 2, ..., n$, from a Gaussian process (GP), and explicit basis functions, h. The covariance function of the latent variables captures the smoothness of the response and basis functions project the inputs x into a p-dimensional feature space [42].

Covariance Functions

In supervised learning, it is expected that the points with similar predictor values have close response -or target values. In Gaussian processes, the covariance function expresses this similarity. It specifies the covariance between the two latent variables, where both values are d-by-1 vectors. In other words, it determines how the response at one point is affected by responses at other points. The covariance function k can be defined by various kernel functions. It can be parameterized in terms of the kernel parameters in vector v. For many standard kernel functions, the kernel parameters are based on the signal standard deviation and the characteristic length scale. The characteristic length scales briefly define how far apart the input values can be for the response values to become uncorrelated. Both the characteristic length value and the signal standard deviation need to be greater than 0, and this can be enforced by the unconstrained parametrization vector v. The covariance -or kernel funtions used in this study are the following:

Exponential Kernel

The exponential kernel function can be specified using the "KernelFunction","exponential" name-value pair argument. This covariance function is defined by:

$$k\left(x_i, x_j|\theta\right) = \sigma_f^2 exp\left(-\frac{r}{\sigma_l}\right), \tag{3.30}$$

where σ_l is the characteristic length scale and $r = \sqrt{(xi - \ xj)^T (xi - \ xj)}$ [12]

Matern 5/2

Matern 5/2 kernel function can be specified using the 'KernelFunction','matern52' name-value pair argument. The Matern 5/2 covariance function is defined as

$$k(x_i, x_j) = \sigma_f^2 \left(1 + \frac{\sqrt{5r}}{\sigma_l} + \frac{5r^2}{\sigma_l^2}\right) exp\left(-\frac{\sqrt{5r}}{\sigma_l}\right) \tag{3.31}$$

where $r = \sqrt{(xi - \ xj)^T (xi - \ xj)}$ is the Euclidean distance between x_i and x_j [12]

Rational Quadratic Kernel

The rational quadratic kernel function is specified using the 'KernelFunction','rationalquadratic' name-value pair argument. This covariance function is defined by

$$k\left(xi, xj|\theta\right) = \sigma_f^2 exp\left(1 + \frac{r^2}{2\alpha\sigma_l^2}\right)^{-a} \tag{3.32}$$

where σ_l is the characteristic length scale, α is a positive-valued scale-mixture parameter, and $r = \sqrt{(xi - \ xj)^T (xi - \ xj)}$ is the Euclidean distance between x_i and x_j [12].

When providing the initial kernel parameter values for a built-in kernel function, input the initial values for signal standard deviation and the characteristic length scale(s) as a numeric vector. When providing the initial kernel parameter values for a custom kernel function, input the initial values the unconstrained parametrization vector$v$. "fitrgp" uses analytical derivatives to estimate parameters when using a built-in kernel function, whereas when using a custom kernel function it uses numerical derivatives [12].

The covariance function $k(x, x\prime)$ is usually parameterized by a set of kernel parameters or hyperparameters, θ. Often $k(x, x\prime)$ is written as $k(x, x\prime|\theta)$ to explicitly indicate the dependence on θ.

The GPR model is probabilistic, which makes it possible to compute the prediction intervals using the trained model. The figure below is considering some data observed from the function $g(x) = x * sin(x)$, and assuming that they are noise free. The subplot on the left in the following figure illustrates the observations, the GPR fit, and the actual function. It is more realistic that the observed values are not the exact function values, but a noisy realization of them. The subplot on the right illustrates this case. When observations are noise free (as shown on the left), the GPR fit crosses the observations, and the standard deviation of the predicted response is zero. Hence, you do not see prediction intervals around these values [12].

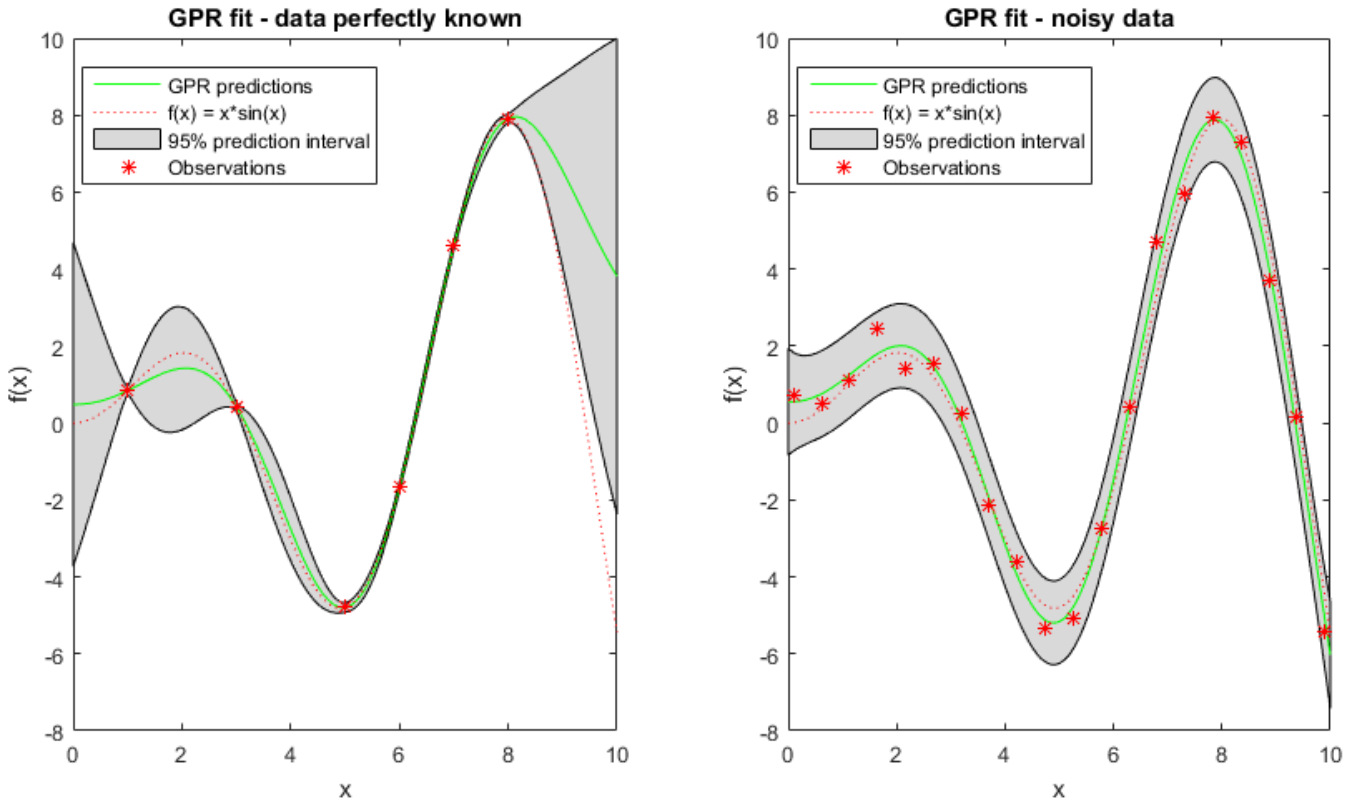

Figure 3.16: Visual representation fitting of data using GPR [12]

3.7.3 Artificial Neural Networks

Artificial neural networks, ANN, are a great tool for recognizing patterns. ANN are computing systems inspired by the biological neural networks such as the brain of a human or animal. Systems like ANN "learn" to perform task from given examples by recognizing patterns by identifying characteristics from the examples given, often referred to as "training data". Although every neural network are unique, the typical process of developing a network tend to follow and evaluate these steps:

1. Access and prepare your data
2. Create the neural network
3. Configure the network's inputs and outputs
4. Tune the network parameters (the weights and biases) to optimize performance
5. Train the network
6. Validate the network's results
7. Integrate the network into a production system

This study used shallow neural networks as a tool to identify patterns from the pre-tests done.

Shallow Neural Networks

Neural networks that operate on two or three layers of connected neuron layers are known as shallow neural networks. Deep learning networks can have many layers, even hundreds. Both are machine learning techniques that learn directly from input data. As shown in the figure below, the neural network consists of an input layer, one or more hidden layers, two in this case, and an output layer. The layers are interconnected with nodes that are called "neurons", with each layer using the output of the previous

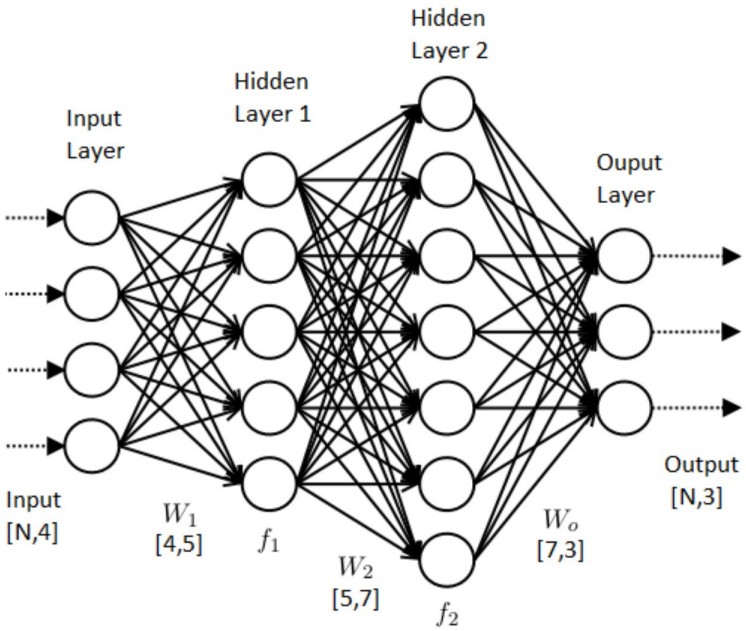

Figure 3.17: Visual representation of an Artificial Neural Network [13]

Neurons

ANNs are composed of artificial neurons inspired by the biological concept of neurons which receive input, combine the input with their internal state and an optional threshold using an activation function, and produce output using an output function. The initial inputs are external data, such as documents or images/figures. The ultimate outputs accomplish the task, such as recognizing an object in an image. The important characteristic of the activation function is that it provides a smooth, differentiable transition as input values change, i.e. a small change in input produces a small change in output.

Activation function

The Activation function is important for an ANN to learn and also make sense of a system that is usually really complicated. The main purpose of the activation function is to convert an input signal of a node in an ANN to an output signal. This output signal is used as input to the next layer in the stack.

Learning

Learning involves adjusting the weights of the network to improve the accuracy of the result. This is done by minimizing the observed errors. Learning is complete when examining additional observations does not usefully reduce the error rate. Even after learning, the error rate typically does not reach 0. If after learning, the error rate is too high, the network typically must be redesigned. Practically this is done by defining a cost function that is evaluated periodically during learning. As long as its output continues to decline, learning continues. The cost is frequently defined as a statistic whose value can only be approximated. The outputs are actually numbers, so when the error is low, the difference between the output and the correct answer is small. Learning attempts to reduce the total of the differences across the observations. The tool used to define a neural network often has the option to choose a training algorithm. This study compared three different algorithms of backpropagation : Levenberg-Marquardt, Bayesian regularization and Scaled conjugate gradient.

Levenberg Marquardt

Levenberg-Marquardt in ANN supports training with validation and test vectors if the network's property is set to a data division function. Validation vectors are used to stop training early if the network performance on the validation vectors fails to improve or remains the same for max_fail epochs in a row. Test vectors are used as a further check that the network is generalizing well, but do not have any effect on training. This method is often the fastest backpropagation algorithm when using matlab as a tool for ANN, and is highly recommended as a first-choice supervised algorithm, although it does require more memory than other algorithms[43].

Bayesian Regularization

Bayesian regularization algorithm is a network training function that updates the weight and bias values according to Levenberg-Marquardt optimisation. It minimizes a combination of squared errors and weights, and then determines the correct combination so as to produce a network that generalizes well. Validation stops are disabled by default (max_fail = inf) so that training can continue until an optimal combination of errors and weights is found. However, some weight/bias minimization can still be achieved with shorter training times if validation is enabled by setting max_fail to 6 or some other strictly positive value[44].

Scaled Conjugate Gradient

Scaled conjugate gradient is a network training function that updates weight and bias values according to the scaled conjugate gradient method. Any network can be trained by this algorithm as long as its weight, net input, and transfer functions have derivative functions. Backpropagation is used to calculate derivatives of performance with respect to the weight and bias variables X. The algorithm is based on conjugate directions, but does not perform a line search at each iteration[45].

Testing

To ensure the network has learned the system well enough before actually using it, it can be tested. When testing the network the size of the training data needs to be split in two. The first one is used to train the network, and the second one is served to assess the performance of the network after the training is complete. In the testing phase, the input patterns are fed to the network and the desired output patterns are compared with those given by the ANN. The agreement or the disagreement of these two sets gives an indication of the performance of the neural network model. The trained network should be validated with the third independent data matrix completely independently. If enough examples are available, the data may be divided randomly in two parts into the training and test sets. However, the training set still has to be large enough to be representative of the problem and the test set has to be large enough to allow correct validation of the network. This procedure of partitioning the data is called "k-fold crossvalidation", sometimes named the holdout procedure.

3.8 Optimisation

From a mathematical point of view, an optimisation process is minimising or maximising a function, f, relying on variables $x_0, x_1 ... x_n$ [46]. There are several ways of minimising the cost-function of this floating dock. In addition to the *gradient descent*-method of optimisation, which is the chosen method for this thesis, this chapter elaborates on some different available families of optimisation.

3.8.1 Summary of Optimisation Methods

Evolutionary algorithms (EA) are a set of algorithms based on the theory of evolution by Charles Darwin. One good example is the genetic algorithm, which is an EA presented in the 1960's by John Henry Holland. The algorithm creates a population of n samples of randomized parameter-combinations. The samples are then evaluated against the optimisation benchmark. Each sample is then given a score based on how it's function value compares to the other samples [47]. Each variable is defined as a 'gene'. The algorithm then uses the 'best' samples as 'parents' for a new generation. The new generation then replaces the previously lowest ranked samples. This continues until there is a solution, or a pre-defined number of generations are completed [48].

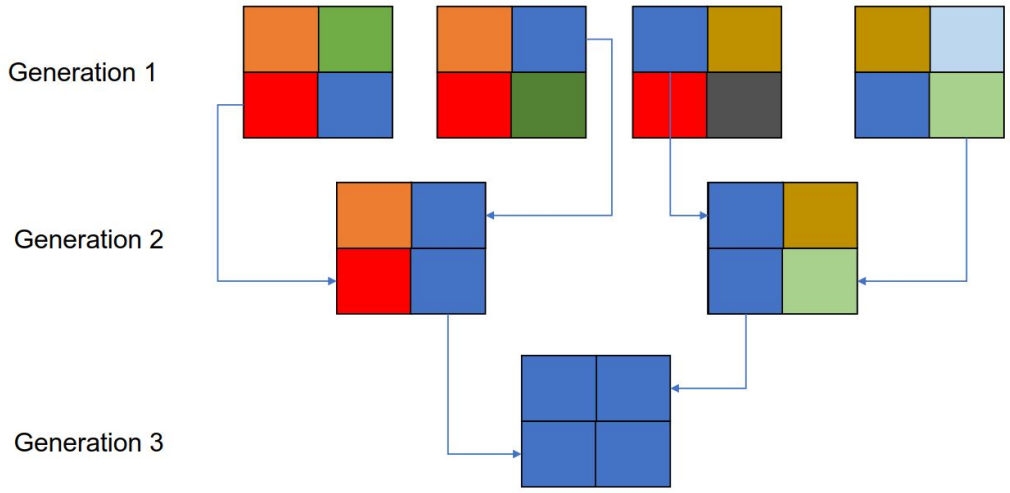

Figure 3.18: Visualized simplification of a genetic algorithm.

Imagine having a simple optimisation problem. As illustrated in figure 3.18 every sample contains four colors (genes), where blue is optimum. All individuals are evaluated, and combined with a matching mate to create a new generation. In this simple example optimum (all genes are blue) is reached within the third generation. Usually the program has a lot of variables, and evaluating a large number of individuals with many variables will take a lot of computing power. This means that the evolutionary algorithms are not suitable for optimisation problems where the number of variables is large, if their boundaries are not strict. For binary optimisation problems (such as the problem illustrated in figure 3.18 where 'optimum' is either blue or not blue) the algorithm is very efficient [47].

Combinatorial optimisation algorithms are a set of algorithms which good at finding optima given a *finite* number of combinations. Meaning that they are good at choosing the optima from a set of available variable-combinations.

One type of combinatorial optimisation algorithm is the *Greedy randomized adaptive search pro-*

cedure, also known as GRASP. In this type of optimisation the algorithm adds more and more information as it iterates along the function. Meaning it would at first optimize for instance height, then diameters, before attempting to optimize thicknesses [49]. These types of algorithms would not be suitable to the non-linear constraints of this thesis.

3.8.2 Gradient-Based Optimisation

Gradient-based optimisation is a common denominator for optimisation algorithms which depend on differentiation of variables. Gradient descent is such an optimisation algorithm, commonly used to minimize a multivariable function. Gradient descent is used for the optimisation in this thesis. The minimization is done by iterating gradients of the function. The gradients are found by differentiating with respect to every variable. Imagine optimizing a function $f(x_1, x_2, x_3)$. This function gives a multi-dimensional surface, and the gradients of this function will be:

$$f'(x_1, x_2, x_3) = \begin{bmatrix} \frac{\partial f}{\partial x_1} \\ \frac{\partial f}{\partial x_2} \\ \frac{\partial f}{\partial x_3} \end{bmatrix} \tag{3.33}$$

with each gradient representing how steeply the function will change given a change within every variable [50]. The algorithm evaluates the gradients of the point in which it stands at all times. Given a *learning rate*, practically a step size, the algorithm may move in the direction of the steepest descent. A large step size may move the algorithm in the direction of a *local* minimum quicker, but the risk of overstepping the *global* minimum is present [51]. Smaller steps may lead to large computing times. Given this info, a different starting point, and a different step size may lead to different optimisation-results. This creates a need of large amounts of randomized starting points for this type of optimisation. Some results may be local saddle points, while others may be global minimums. The user needs to be able to separate the two [52]. The gradient descent method also has a weakness in that it will create a zig-zaging path, which will use a lot of processing power to find a minimum. Especially of the step sizes are small.

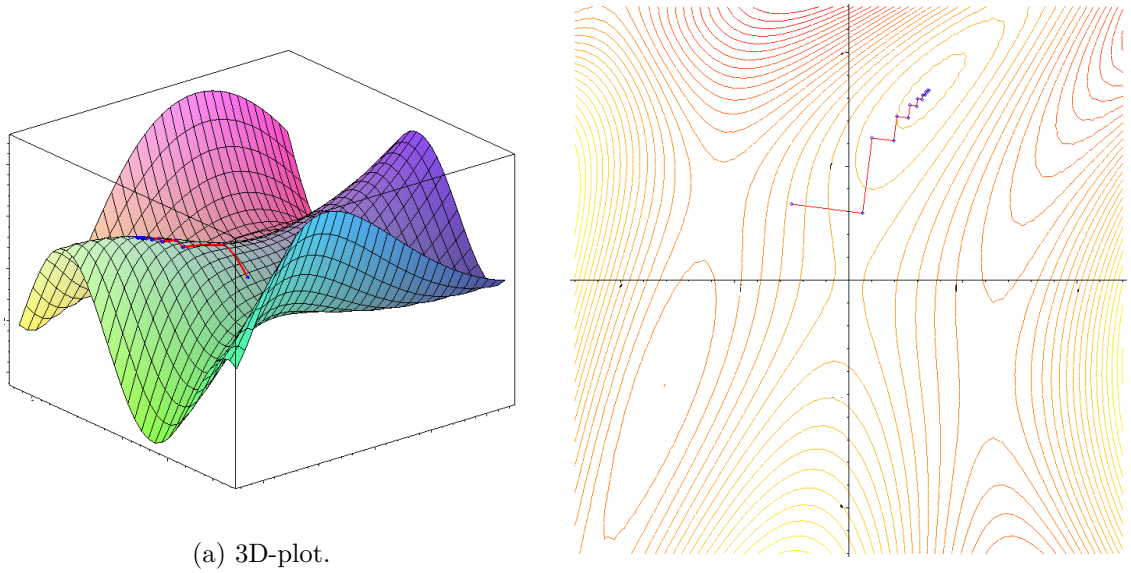

(a) 3D-plot.

(b) 2D-plot.

Figure 3.19: The zig-zaging nature of the gradinent descent method illustrated in 3D and 2D [14]. It is also imaginable how different starting points may lead to different paths and different minimums in this figure.

3.9 Key Statistics

This chapter describes the key statistical values which are used as guidelines in the process of choosing the best model for creating response surface models.

3.9.1 Residual Sum of Squares

The Residual sum of squares (RSS) is the sum of the squares of residuals. Residuals are the deviations of predicted values from a fit, compared to the actual value of empirical data. Hence RSS is a measure of the discrepancy between estimated and actual values from a model. A small RSS indicates a model fitting closely to the measured values. RSS is often used as a criterion for choosing an optimum fitting model for data sets. This value may be referred to as SS_{res} [50].

$$RSS = \sum_{i=1}^{n} (y_i - f(x_i))^2 \tag{3.34}$$

3.9.2 Sum of Squares and Coefficient of Determination

Given a mean of all data points, $\bar{y} = 1/n \sum_{i=1}^{n} (y_i)$, the total sum of squares (variance) is equal to:

$$SS_{tot} = \sum_{i=1} (y_i - \bar{y})^2 \tag{3.35}$$

Given RSS and SS_{tot}, R^2 may be calculated using the following relation below. This shows that a better regression model yields an R^2 closer to 1.

$$R^2 = 1 - \frac{SS_{res}}{SS_{tot}} \tag{3.36}$$

4 | Scope

With sustainable power in exponential demand, the potential for growth and profit of offshore wind power is ever increasing. One of the largest issues with offshore wind power development is installation times and weather limitations. To reach the full energy potential of offshore wind power there is a need of installation in areas with harsh weather. One of the limitations of installations is spar movement due to waves during lifting of tower, nacelle, and rotor. Being able to reduce the movements of, and loads on, the spar during installation may increase efficiency and reduce cost of offshore installation. Henceforth, the research question of this thesis is:

How can a parametric design optimisation be carried out for a funnel-shaped dock intended for installation of floating wind turbines?

This thesis builds on the previous work of Jiang et. al *Design, modelling, and analysis of a large floating dock for spar floating wind turbine installation* [23]. The possibility of a floating dock is investigated in this work. The work of Gran et. al, *Hydrodynamic Analysis of Floating Docks With Alternative Geometries for Floating Wind Turbine Installation* [53], which further investigates what dock geometries may increase piston-mode periods is built on - which is where the funnel-shape was first investigated. With this previous work in mind the following sub-questions have emerged:

- What are the most important design parameters?
- How can a response surface be created for certain operational constraints?
- Which constraints will have the greatest impact on the optimum design?
- How will the design objective vary along design iterations?

As the idea of a floating dock and its shape was already laid out, this thesis looks at how to minimise the cost of such a structure. The cost is defined as steel weight, where the cost of steel is $1 per tonne. There is no welding, customization or other forms of labour included in this cost estimate. There are certain simplifications and assumptions made, which are further elaborated on in chapters *Case and Materials* and *Methods*.

5 | Case and Materials

This chapter introduces the floating dock concept, panel model and test parameters for the preliminary study, the design variables, sequential and randomized analyses and the gradient based optimisation.

5.1 The Floating Dock Concept

The floating dock concept has recently been proposed to expand the weather window for installing spar floating wind turbines. This is because it is not always possible to find deep-water areas that are sheltered for harsh sea conditions close to the wind farms [23]. The concept uses a floating dock to shield the spar platform from motions caused by waves under the installation process of the floating wind turbine. The installation process for the concept consists of six main steps shown on Figure 5.2. Even though the floating dock shields the spar platform from motions caused by waves, piston-mode still occurs inside the dock in a given period based on the dock geometry, as seen in Figure 3.7 and 3.10. The effect of different geometries has been studied in a pre-project for this master thesis. This master thesis focuses on finding optimum funnel-shaped dock where the objective is to minimize the weight given different constraints. Constraints are explained in section 5.5. The dock is analysed both in operational and transit conditions, and uses ballast inside the bilgebox and the side walls in form of scrap steel and water to adjust the draft, as transit needs a lower draft to increase towing efficiency. The ballast can be used to adjust the center of gravity to secure stability, and the bilgebox can contribute to dampen motions on the dock.

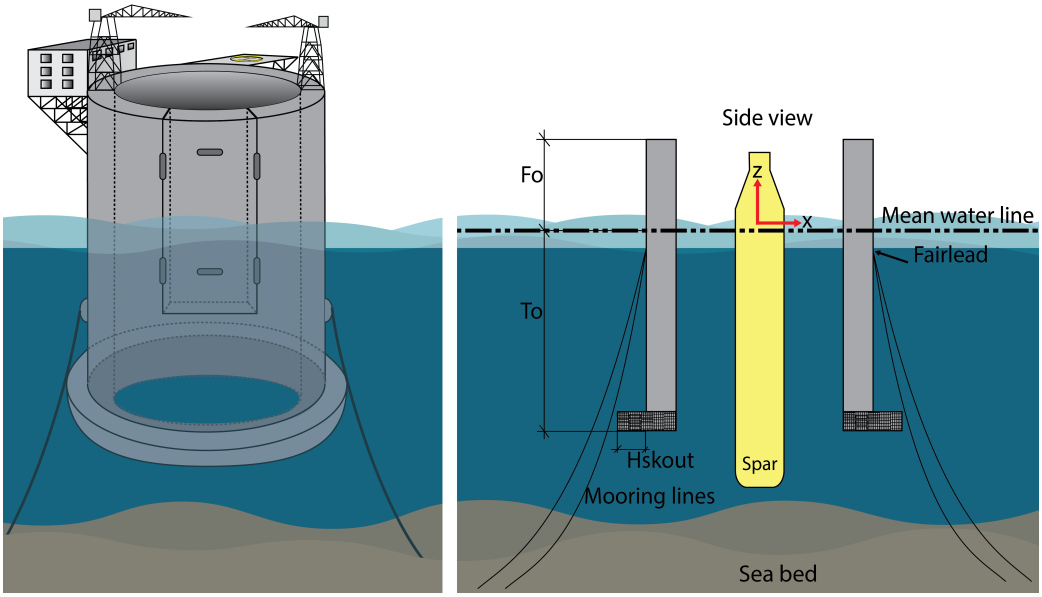

Figure 5.1: Schematic of the floating dock concept and a spar platform inside the dock concept.

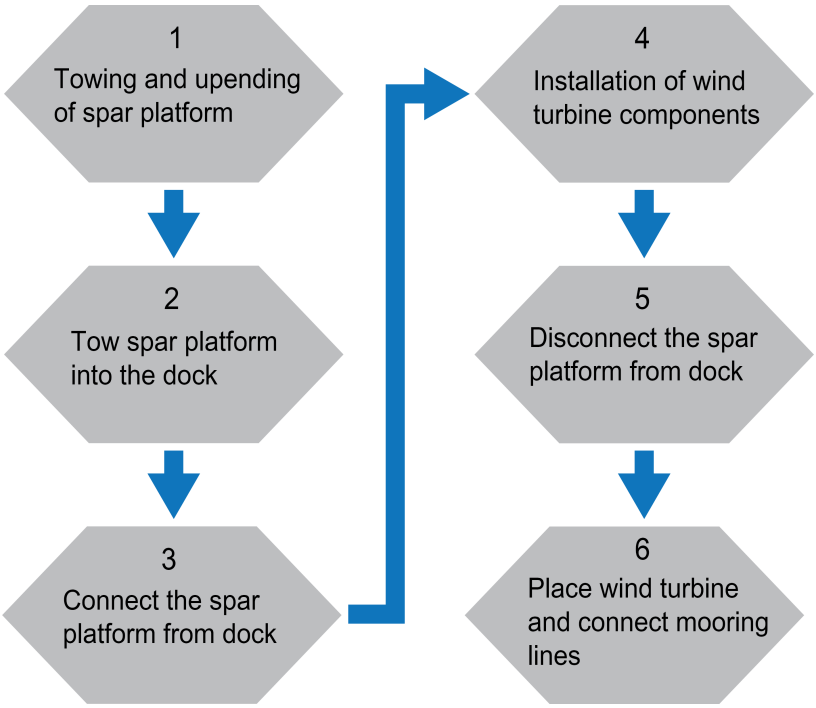

Figure 5.2: Main installation steps for a spar floating wind turbine.

- First, the spar platform is towed horizontally to the site and is upended.
- Second, the gate at the dock is opened and the spar foundation is moved to the middle of the floating dock with help of tugboats.
- Third, tugger lines are connected between the platform and the dock to avoid drift-off of the spar.
- Fourth, the mating process which is the most important step where relative motions between the parts can cause structural failure if impacts to the guide pins occur. This is done by a heavy-lift vessel with cranes.
- Fifth, the spar foundation will be disconnected from the dock.
- Sixth, the floating wind turbine is towed to a designated location and will be installed with mooring lines.

5.2 Preliminary Study

Figure 5.3 shows a panel model of a funnel shaped dock used for the preliminary study as a reference case. The figure also includes a table containing the test points of the preliminary study. The preliminary study investigates how changes in T1, T2, T3, Di1, Di2 and Dt individually affect piston mode for a dock with a homogeneous density panel model. Explanation of the design variables is found in Section 5.3. A total of 13 hydrodynamic analysis was performed, where one was for the base case for comparison and one for each individual change on the geometry.

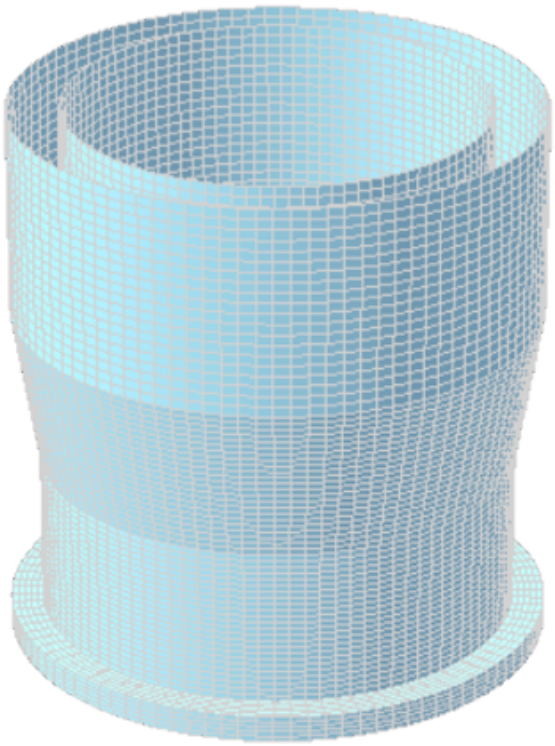

Symbols	***Test points (m)***
Di1	35, 40, 45
Di2	30, 35, 40
T1	20, 30, 40
T2	20, 30, 40
T3	20, 30, 40
Hsk	5
Dt	5, 10, 15

Figure 5.3: Panel model of reference dock and the test points (T1 = 30, T2 = 30, T3 = 30, Hsk = 5, Di1 = 40, Di2 = 35, Dt = 10).

5.3 Design Variables

The variables used to define the geometry of the dock in operation and transit are illustrated in Figure 5.4a and 5.4b. An explanation of the design variables and their lower and upper bounds is shown in Table 5.1. These lower and upper bounds were chosen based on the earlier work regarding the floating dock concept and after discussion with our supervisor.

Design variables	***Symbols***	***Lower and upper bounds (m)***
Dock upper inner radius	Di1	35 to 75
Dock lower inner radius	Di2	30 to 69
Dock thickness	Dt	5 to 15
Dock height upper	T1	1 to 80
Dock height middle	T2	20 to 50
Dock height lower	T3	1 to 80
Bilge tank height	Hsk	4 to 20
Bilge tank outward extension	Hskout	6 to 15
Bilge tank inward extension	Hskin	0 to 10
Height of water ballast in operation	Hbwo	Dependent
Height of water ballast in transit	Hbwt	Dependent
Dock freeboard in operation	Fo	20
Dock draft in operation	To	60 to 100
Dock freeboard in transit	Ft	Dependent
Dock draft in transit	Tt	20 to 60

Table 5.1: Lower and upper bounds of the design variables.

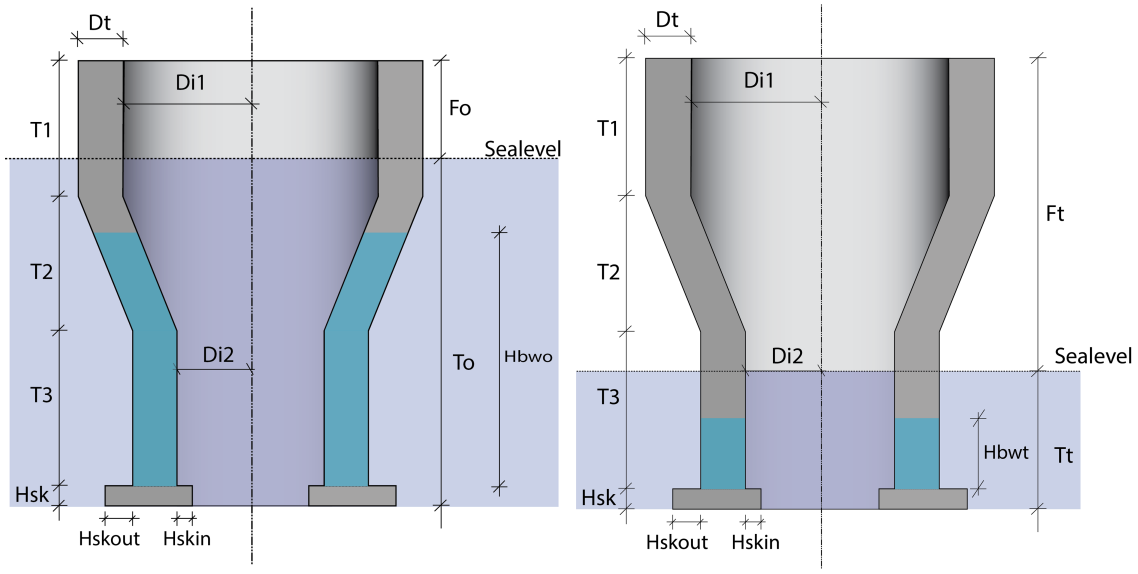

(a) Operation.

(b) Transit.

Figure 5.4: Design variables illustrated on a funnel shaped dock.

5.4 Sequential and Randomized Analyses

A test matrix was generated for thorough testing of the design variables between the determined lower and upper bounds to establish a way to predict piston mode resonance for a funnel shaped dock. The test matrix was generated in MATLAB by using initial upper and lower bounds to produce vectors consisting of 9 points between the lower and upper bounds for $Di1$, $Di2$, $T1$, $T2$, and $T3$. These vectors were used to make a matrix with each possible combination (59049 combinations). Combinations where $Di1 \leq Di2$, and where the the total height was outside the interval $[80, 125]$ were removed. The remaining 10296 combinations were each given an unique ID. A hydrodynamic analysis was run for each of these combinations. The results were used to generate different models for predicting of piston-mode resonance. 1000 tests with randomly generated points within these boundaries were run for verification of the models generated. Constant values, because these do not affect the piston-mode period, for DT, Hskin, Hskout and Hsk were also included in the test matrix. The initial lower and upper bounds are shown in Table 5.2, and the test points for the sequential analyses used as training data are shown in Table 5.3.

Table 5.2: Initial lower and upper bounds.

Symbols	***Initial lower and upper bounds (m)***
Di1	30 to 75
Di2	30 to 75
T1	1 to 80
T2	20 to 50
T3	1 to 80

Table 5.3: Test points used in the sequential analyses after unwanted combinations is removed

Symbols	***Test points (m)***
Di1	35.625, 41.250, 46.875, 52,500, 58,125, 63,750, 69,375, 75,000
Di2	30.000, 35.625, 41.250, 46.875, 52,500, 58,125, 63,750, 69,375
T1	01.000, 10.875, 20.750, 36.625, 40.500, 50.375, 60.250, 70.125, 80.000
T2	20.000, 23.750, 27.500, 31.250, 35.000, 38.750, 42.500, 46.250, 50.000
T3	01.000, 10.875, 20.750, 36.625, 40.500, 50.375, 60.250, 70.125, 80.000
Dt	10
Hsk	5
Hskin	0
Hskout	6

5.5 Gradient-Based Optimisation

The optimisation focused on getting the cost, in this case defined as steel weight, as low as possible given a set of pre-defined constraints and lower and upper bounds for the design variables. During the search for optimum docks the dock draft in transit is set to a maximum of 20m, 25m, 30m and one without a boundary for draft in transit while the piston-mode period in operation is set to a minimum of 17,19, 21 and 23 seconds and is calculated by the generated gaussian process regression based model.

5.5.1 Objective Function

In mathematical terms, this may be represented in a way where the goal is to minimize F_x, where F_x is the objective function that is subjected to a constraint function $\vec{C}_{ix} < 0$ where each i is a constraint $i = 1, ...n$; and the design variables is set between x^L the lower and x^U the upper bound. $x^L < x < x^U$. The lower and upper bounds for the variables used in the optimisation is shown in Table 5.1.

The objective function would ideally cover the dock lifetime costs, but is simplified to only include the cost (weight) of structural steel in this study. This means that the simplified objective function can be expressed as:

$$F = \sum_{i=1}^{N} f(Di1, Di2, T1, T2, T3 \ldots, Hsk, t_i, a_i) \tag{5.1}$$

where F is the cost, N is the number of components, t_i is the thickness of the component and a_i is a factor for the steel price. Thus, the function calculates the volume of steel and multiplies it by a price factor.

5.5.2 Assumptions

Some mass assumptions are used in the optimisation after discussion with our supervisor and is based on earlier work floating dock concept in addition to the steel from the geometry:

- The price of steel is set to 1 [USD/ton]
- The steel used as fixed ballast is scrap steel and is set to 0 [USD/ton]
- The mass of the living quarter is set to 1000 tons.
- The mass of the wind turbine tower is set to 1200 tons which corresponds to a 10MW wind turbine.
- The number of nacelles in storage is 5 during operation and 0 during transit and has the weight of 700 tons each.
- The mass of the cranes is set to 5000 tons.

Some assumptions used for the sequential and randomized analyses that the piston-mode period calculation model used as a constraint in the gradient based optimisation:

- The total mass of the dock is calculated to be equal to the buoyancy caused by the volume under water.
- For the center of gravity calculation the density of the bilgebox is assumed to be 3600 kg/m^3, while the rest of the mass is even divided over the volume of the steel.
- Approximate formulas for calculating the radius of gyration given the upper and lower diameter of the funnel shaped dock has been made based on early hydrodynamic analyses.

  $$RX = (Di1 + Di2) \cdot ((0.00002345 \cdot ((Di1 + Di2)^2)) - (0.00792295 \cdot (Di1 + Di2)) + 1.11629446)$$
  $$RY = (Di1 + Di2) \cdot ((0.00002345 \cdot ((Di1 + Di2)^2)) - (0.00792295 \cdot (Di1 + Di2)) + 1.11629446)$$
  $$RZ = (Di1 + Di2) \cdot ((0.00000514 \cdot ((Di1 + Di2)^2)) - (0.00177414 \cdot (Di1 + Di2)) + 0.69104909)$$

- The specific product of inertia uses the approximated radius of gyration and the mass calculated. For example $I_x = MASS \cdot (RX)^2$

The assumptions was used to write the JS files that HydroD reads to start a hydrodynamic analysis. It used the the parameters that explained the geometry from the test matrix in the sequential and randomized analyses to calculated the values needed in the JS file. All the cases was in statically equilibrium since the hydrodynamic analysis automatically stops if it is unbalanced.

5.5.3 Constraints

Linear and nonlinear constraints are required for the results to be accepted, these constraints demand:

- That the metacentric height is equal to or larger than minimum required value in operation.

  $(GM_o \geq 1m)$

- That the metacentric height is equal to or larger than minimum required value in transit.

  $(GM_t \geq 1m)$

- That height of side ballast is not larger than what there is room for in operation.

  $(0 \leq Hbwo + Hbfo \leq To + Fo)$

- That height of side ballast is not larger than what there is room for in transit.

  $(0 \leq Hbwt + Hbft \leq Tt + Ft)$

- That the piston-mode period is equal to or greater than minimum required value in operation.

  $(T_{piston} \geq Tmin_{piston})$

- That the maximum heeling angle less than limits in operation.

  $\eta_5 o \leq 2deg$

- That the maximum heeling angle less than limits in survival.

  $\eta_5 s \leq 7deg$

- That the maximum heeling angle less than limits in transit.

  $\eta_5 t \leq 2deg$

- That it is equilibrium between weight and buoyancy in operation and transit.

  $(W_o = B_o)$ *and* $(W_t = B_t)$

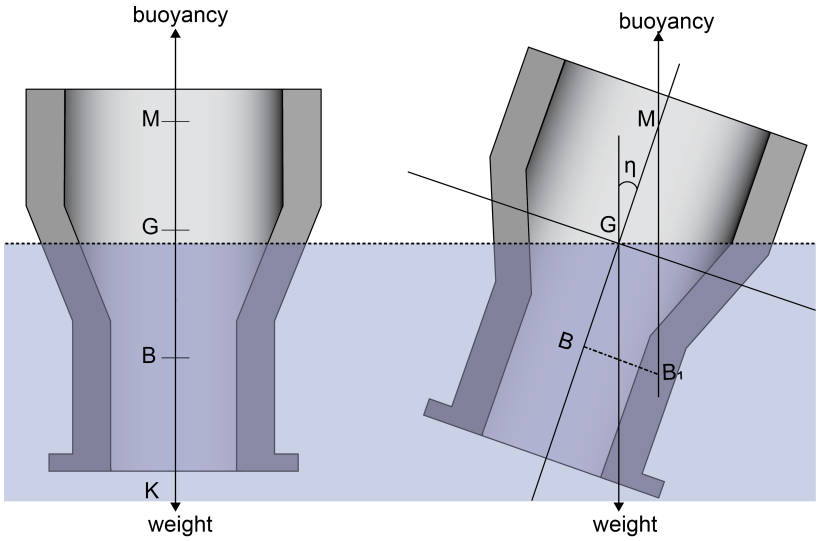

Figure 5.5: Illustration of metacentric height, center of gravity, center of buoyancy and heeling angle on a funnel shaped dock.

Figure 5.5 illustrates the metacentric height, center of gravity, center of buoyancy and heeling angle on a funnel shaped dock which is used in contraint 1, 2, 6, 7, 8 and 9. Refer to chapter 3.2.1 for theory on the hydrostatics of marine structures. The first two constraints ($GM_o \geq 1m$) and ($GM_t \geq 1m$) is required for initial stability for offshore units. Constraint 3 and 4 ($0 \leq Hbwo + Hbfo \leq To + Fo$) and ($0 \leq Hbwt + Hbft \leq Tt + Ft$) are physical limitations so the dock doesnt calculate more water than what it is room for. Constraint 5 sets a minimum required piston-mode period which is calculated by the gaussian process regression based predictor model. Constraint 6,7 and 8 is required to achive stringent stability requirement where the wind speed for operation and transit condition is set to 36 m/s and 52 m/s for survival condition which is based on offshore standards [54]. The last constraints ($W_o = B_o$) *and* ($W_t = B_t$) is required for the dock to float in a given position.

6 | Method

This chapter describes the fundamental methods of data gathering, software training, the building of models, analyses and processing of the simulation results. As this thesis is research-based, the methodology is qualitative, gaining test results through computer programs and their calculations and simulations.

6.1 Research

As an introductory phase to this project, quite a large amount of time was spent acquiring basic knowledge of floating offshore wind turbines and hydrodynamic wave theory. One of the authors wrote a pre-project on this subject, which greatly steepened the learning curves of the remaining authors. As the authors are all completing their masters within the discipline of civil engineering, the knowledge of hydrodynamics and marine structures were, as expected, quite limited.

6.2 Software

This chapter describes the different software used to complete this thesis.

6.2.1 HydroD

The DNV-GL-developed HydroD-package is used as a cornerstone of this project. The WADAM-analyses run by HydroD are used for every single test case. As this software package uses JavaScript (JS) as its application programming interface (API), the authors benefited greatly from the pre-project which created JS-models in HydroD. These JS-scripts were further developed to create model templates used to run the necessary WADAM-analyses.

HydroD was used in the introductory phase of the work, testing all the geometries listed in the test matrix for a piston mode resonance frequency (PMR). These results were listed and further used by MATLAB to create a function estimating PMR given any geometries within the constraints. As the numerous sets of WADAM-analyses were run, the different cases were saved in numbered case-folders made by CMD [55].

6.2.2 MATLAB

As MATLAB is a *'multi-paradigm numerical computing environment and proprietary programming language developed by Mathworks'* [56], this programming language is something which needed to be studied separately. Internet tutorials, trial-and-error through logical assumptions, and previously coded similar problems by the project supervisor dr. Jiang were the main sources of learning. MATLAB is a very high functioning application, with a lot of different toolboxes available for simplification of the coding [57].

MATLAB was used throughout the work. In the beginning it was used to create JS-files and batch-files for HydroD to run all test-matrix combinations of the geometries. Later it was used to read the wave particle transfer function (WPTF) to automatically read the PMR-results for all geometries. MATLAB was later used to generate a function estimating PMR-values for all possible geometries, before it was used for the optimisation process.

6.2.3 Windows Command Promt

One of the earliest barriers to be overcome during the data-collection for this project was MATLAB failing to automatically run the HydroD-package with its WADAM- and analyses. To outmaneuver this issue, the automated running of HydroD was elected to be done through CMD. Learning CMD was done in a similar way to MATLAB, with the supervisor being dr. Pan. A batch-file containing a kill-command for both the WADAM-applications soon appeared to be a necessity throughout the trial-and-error-phase of CMD-coding.

The windows command prompt was used to overrun HydroD, so that one batch-file, created by Matlab, would start and run a series of HydroD-simulations automatically. As the computation times were massive, HydroD-simulations were run simultaneously on multiple computers in the computer laboratory on the UiA Campus. CMD was used to keep these simulations running and organizing the files in correct and traceable folders.

6.2.4 Microsoft Excel

Microsoft Office Excel (MOE) is a computer program developed by Microsoft and is a part of the Microsoft Office-package. The program is based on spreadsheets, where one may conduct calculations and list data. The program also has a large amount of inbuilt formulae [58]. MOE may also be used to visualize numbers and statistics through diagrams.

MOE was used for caching data in this project. MATLAB was used to read WADAM-results and write the results to MOE. The results were then read back into MATLAB for further evaluation with NNF, GPR and RS.

6.3 Script Architecture and Procedure

The chapter aims to illustrate the script architecture built in JavaScript, Matlab and CMD. Including the build-up and sequence of the program-codes and points of manual input and procedures.

6.3.1 Preliminary Analyses

The preliminary analyses consisted of thirteen singular tests in HydroD. One reference and twelve indicator tests. These tests were run to investigate coherence between design parameters and piston mode resonance frequency. The JavaScrip-files which input info to HydroD were manually changed for each test case. This practice was used for a limited number of tests to get a certain familiarity with the scripting which runs HydroD. Parallel to getting to know HydroD,

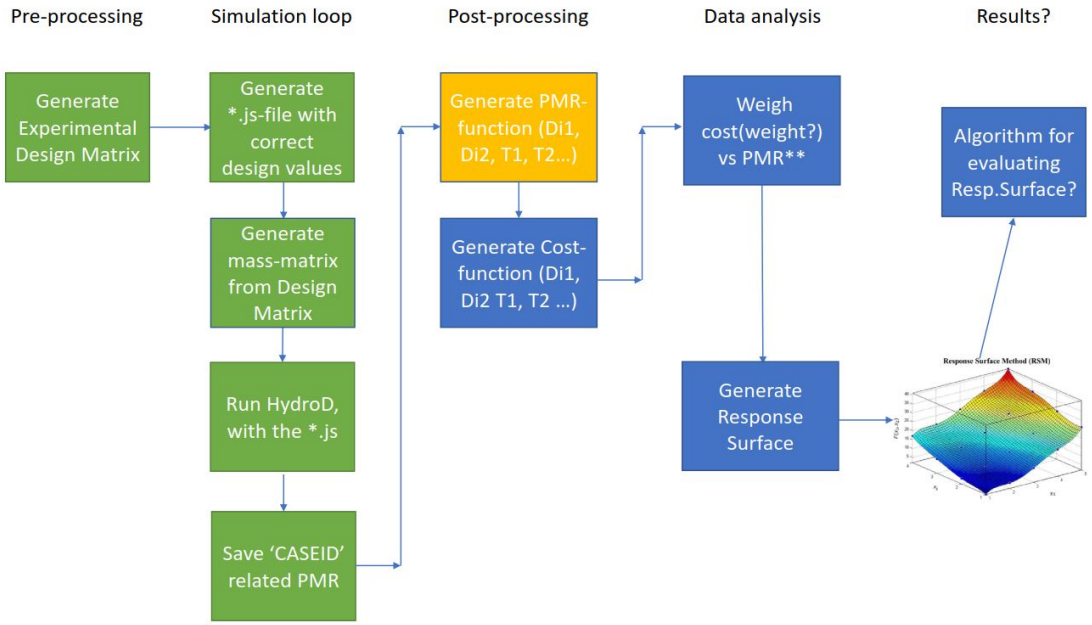

Figure 6.1: Early visualization of the planned work flow (January 2020).

6.3.2 Sequential and Randomized Analyses

Having found the set of design parameters which impacted piston mode resonance frequency, a plan for investigating a function piston mode resonance frequency, given the design parameters, was laid out. Creating a valid test matrix is the first step to creating a set of multi-variable tests. To ensure there is a combination of all values for all variables available for simulation, this test matrix was generated within MATLAB. The test-matrix-code needs inputs of maximum and minimum values of the tested variables, with a step between the test values. The code will then create an array for each variable, with its stepped values. The code will then proceed to generate a full factorial design matrix, where the level of each variable is represented by the number of steps. Further, the code will continue by analyzing the full factorial matrix and change the values to the represented values in the variable-arrays.

As it soon became obvious that HydroD kept crashing when called from Matlab, CMD was chosen for running an automated loop with several HydroD-analyses. This meant dividing the automated process into segments. Creating the test-matrix and and a set of *.bat-files in Matlab. The *.bat-files creating test directories, sorting the tests and running HydroD.

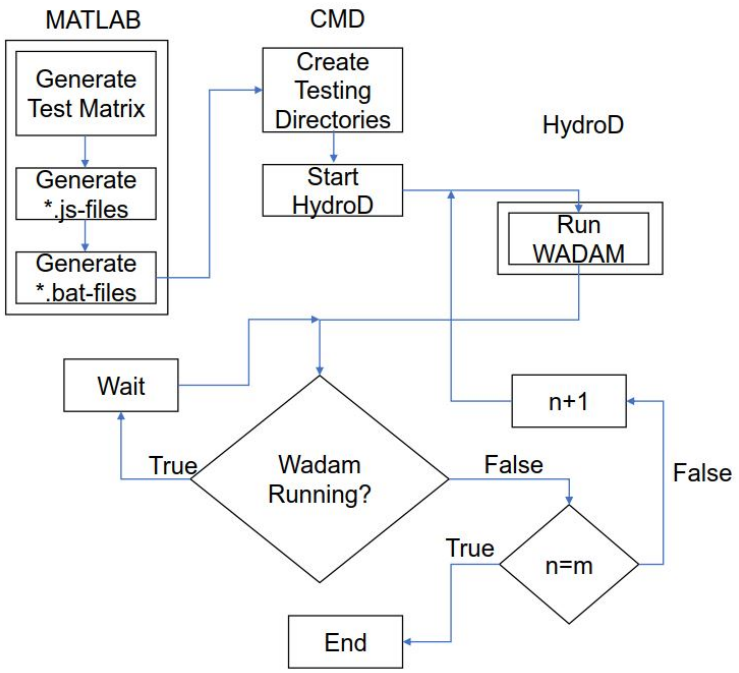

Figure 6.2: Visualization of the randomized and sequential analyses.

The *.bat-files were run on several computers, over several days, in room A0314 on UiA campus. The number of simulations run on each computer were adjusted according to the processing power of each computer. i9-processors were used for a larger number of tests than i7-processors.

What computers were used for which simulations was at all time logged on a purpose-made piece of paper to keep control of every simulation. The properties of each computers hardware was also tracked in the same document. There were two types of computer; one with i7 processor and 16 GB ram, marked with (i7) and the other with i9 processor and 32 GB ram, marked with (i9) in the document. The document worked as a map over the computer lab, with each row and column representing one computer with a total of 29 computers. One computer in the room did not work and therefor got "blacked out" on the map. The document was used to keep track of what tests was done at which computer, at what time. The figure below shows a part of the full document used in the analysis process. the full version is to be seen in the Appendix 1. One document was used for each test-series, and collected to keep track of the progress. The document was filled in with what number of tests that were run (BAT-file), if it was done and checked. When all simulations were run, the directories were saved on an external hard drive as a backup for the original file at the computer. This was also logged in the document consecutively over the test process. The total data volume reaching an excess of 800 gigabytes. An independent MATLAB-script was used to automatically read the piston-mode resonance frequencies of each simulation, before writing the PMR into a new column of the test matrix and caching all data to Microsoft Excel for quicker and easier access.

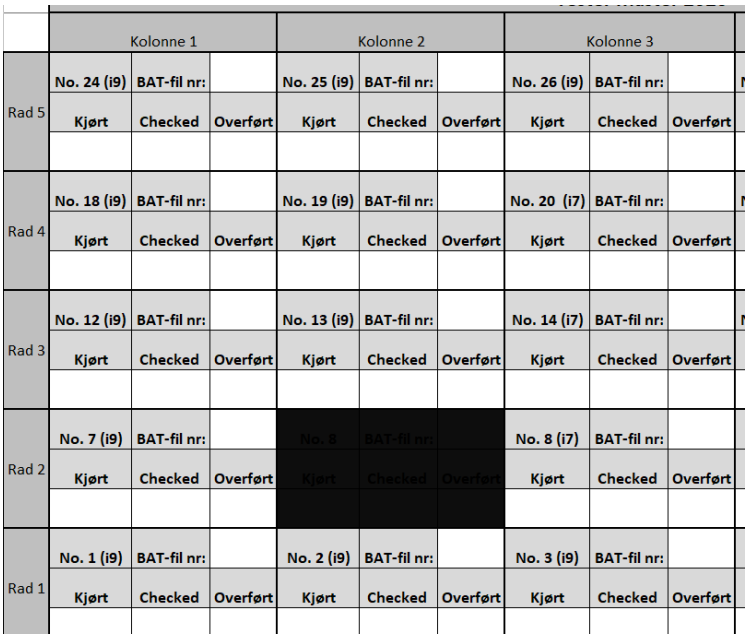

Figure 6.3: Section of the map over the computers used to log the progress of the analyses.

6.3.3 Polynomial Response Surfaces

With the sequential and randomized testing complete, a coherence between design variables leading to a PMR was explored. This was done through MATLAB, in Curve Fitting Toolbox. This toolbox allows the user to choose what form of interpolation, extrapolation or regression the user wants to utilize, and then returns a 3D-plot with statistical figures and deviations. Polynomial regressions of orders between second and fifth were used, with the polynomial order dependent on the data set size. A coherence between design variables was then read from the 3D-plots. The response surface scripts start off by reading the test matrix, with corresponding PMR-values, from an Excel-spreadsheet. Given this data, the code using regression theory for visualizing the comparison of different design variables separates the matrix columns into named variable-strings. Using polynomial regression of the 3^{rd} order, the code combines all design variables in x and y directions, while reading the corresponding PMR-value and fitting it into the z-direction. This outputs a 3D-plane, visualizing the impact of changing design variables and their correlation to PMR. All design variables are plotted against each other, like a round of '*round robin*'.

6.3.4 Artificial Neural Network

Deep Learning Toolbox in matlab provides a framework for designing and implementing deep neural networks with algorithms, pretrained models, and apps. The toolbox nntool has been used in this study to create an artificial neural network model. Input data from the tests done earlier was imported and then used for training, testing and validation of the neural network before using it to simulate new results. Three different algorithms was applied, and then compared to check the accuracy to the original test results.

The network that was used in the MATLAB nntool consisted of a two-layer feedforward network, with a sigmoid transfer function working as an activation function in the hidden layer and a linear transfer function in the output layer. The default number of hidden neurons is set to 10.

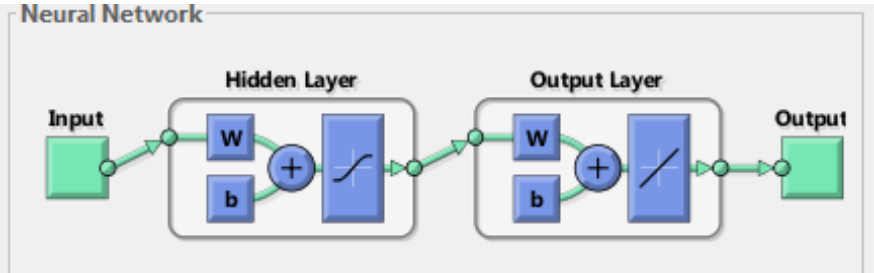

Figure 6.4: Artificial Neural network

The tool provides three different training algorithms; Levenberg-Marquardt (trainlm), Bayesian Regularization (trainbr), Scaled Conjugate Gradient (trainscg). Levenberg-Marquardt (trainlm) is recommended for most problems, but for some noisy and small problems Bayesian Regularization (trainbr) can take longer but obtain a better solution. For large problems, however, Scaled Conjugate Gradient (trainscg) is recommended as it uses gradient calculations which are more memory efficient than the Jacobian calculations the other two algorithms use. All of the algorith was testet and is compared in the result section to evaluate the accuracy of the results.

6.3.5 Gaussian Process Regression

Machine learning uses supervised and unsupervised learning. In this case supervised learning has been implemented in the form of guassian process regression, GPR. Supervised learning trains a model on known input and output data so that it can predict future outputs [15].

Similar to ANN, Matlab was used as a tool to create Gaussian Process Regression model aiming to learn and predict the future data which was suppose to be used in the optimisation-process.

Machine learning algorithms use computational methods to “learn” information directly from data without relying on a predetermined equation as a model. The algorithms adaptively improve their performance as the number of samples available for learning increases. A supervised learning algorithm takes a known set of input data and known responses to the data (output) and trains a model to generate reasonable predictions for the response to new data. Regression techniques predict continuous responses [15].

In Matlab, the regression learner toolbox was used to train regression models to predict data (output) using supervised machine learning. The data set containing input, such as variables, and output in the form of from the tests done in HydroD was used as input, learning data. The learning data is used to recognize patterns, so that the tool can generate predictions by its own. Three different type of algorithms was used for the machine learning; Exponential Kernel (3.7.2), Matern 5/2 (3.31), Rational Quadratic Kernel (3.32). Therefore, choosing the right algorithm

requires trading off one benefit against another, including model speed, accuracy, and complexity. Trial and error is at the core of machine learning—if one approach or algorithm does not work, you try another[15].Presented below is a flowchart of a typical machine learning procedure:

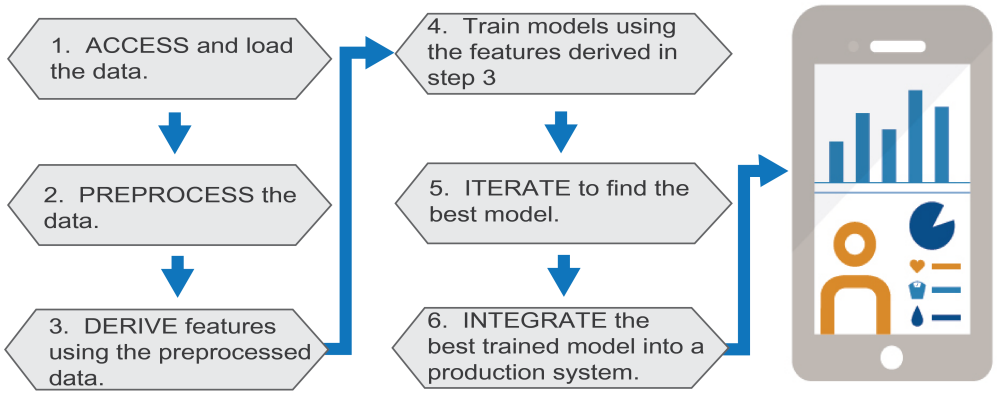

Figure 6.5: Flowchart, Machine learning procedure [15]

The exact procedure is described below with the following steps[15]:

1. On the Apps tab, in the Machine Learning group, click Regression Learner
2. Click New Session and select data from the workspace or from file. Specify a response variable and variables to use as predictors. See Select Data and Validation for Regression Problem.
3. On the Regression Learner tab, in the Model Type section, click the arrow to expand the list of regression models. Here the suited algortihm for the machine learning is choosed.
4. Click train
5. Click models in the History list to explore results in the plots.

   The trained machine learning matlab code gets exported and used as a tool to predict future results based on the training performed in each algorithm for GPR. The result will be evaluated and compared with other types of machine learning methods to see which has the most accurate future prediction.

6.3.6 Optimisation

The optimisation-script is based on the function $fmincon$, built into Matlab. $fmincon$ is a gradient descent-based optimisation program where there are manual inputs defining the constraints of the optimisation. Both in regards to geometry of the dock and in number of iterations and function evaluations. $fmincon$ finds the minimum value for $f(x)$, given a set of constraints defined as:

$$f_{min}(x) \begin{cases} A\,x & \leq & b \\ Aeq\,x & = & beq \\ c(x) & \leq & 0 \\ ceq(x) & = & 0 \\ lb & \leq & x & \leq & ub \end{cases} \tag{6.1}$$

where b and beq are problem boundaries defined as vectors, A and Aeq are problem boundaries defined as matrices. $f(x)$ is a function which returns a scalar. In this case a steel weight. c and ceq are nonlinear constraints defined in the function $nlcon.m$ in this work. x, lb and ub are either matrices or vectors, depending on the case. In this thesis they are used as vectors. $fmincon$ utilizes the gradient descent algorithm to minimize the function value within the constraints defined. When $fmincon$ finishes running, it leaves an $exitflag$ as a sort of trace to indicate it's performance:

- -2 - No feasible point found
- 0 - Number of iterations exceeded options
- 1 - First-order optimum
- 2 - Function change smaller than options

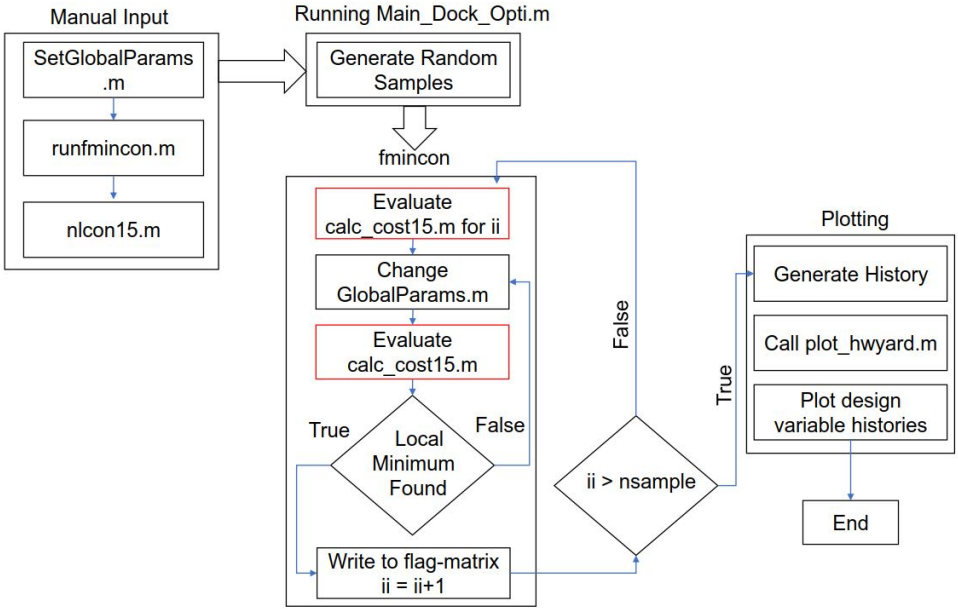

Figure 6.6: Flowchart, visualizing the process of optimisation and plotting of results.

In the script $SetGlobalParams.m$ the user defines global parameters such as upper and lower bounds for all geometric variables, material densities, global loading to the dock, etc. In the script $runfmincon.m$ the user defines step-lengths, maximum number of function evaluations and maximum number of iterations for the optimisation function. In addition, the *linear* constraints,

A, Aeq, b and beq are defined within $runfmincon.m$. Constraints set as linear in this case are for instance $Di_1 > Di_2$, $Di_1 < 120$ or $T_{Piston} > 19$. The lower and upper bounds of all optimisation parameters are also defined in this script, although read from $SetGlobalParams.m$. Within the script $nlcon15.m$, c and ceq are defined as nonlinear constraints for the optimisation. Nonlinear constraints in this case refers to stability in both operational and transit states. Stability refers to parameters such as $center\ of\ gravity$, $center\ of\ buoyancy$, $metacentres$ and $displacements$, to name a few. All of these parameters are calculated using the function values for each iteration of differentiation, called from different Matlab-codes. For every iteration the program loads an external code checking the piston-mode period of the geometry. This code takes about two seconds to load, and significantly reduces processing speeds.

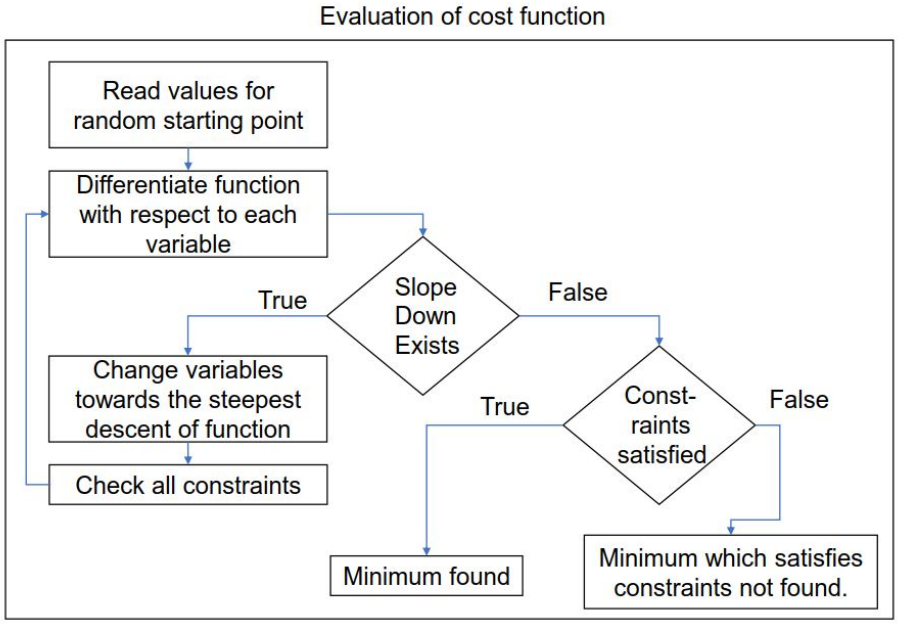

Figure 6.7: Flowchart, visualizing one function evaluation.

When the number of samples as defined in $Main\_Dock\_Opti.m$ is run, the program looks through its $flag$-matrix searching for the number 1, minimum found. As it searches, the code also creates a parallel string, where the runs which found an optimum are collected. When the string is complete, the code creates history-matrices for all optimised variables and continues to plot these, with each iteration from $fmincon$ saved as one step.

7 | Results

In this chapter the results from the four main steps from the test procedure are presented. This includes:

- Hydrodynamic analysis from the preliminary study.
- Polynomial response surfaces of the variables, comparison between models using Gaussian process regression and artificial neural network for the calculation of piston period.
- Gradient based optimisation looking at different optimums found.
- Verfication of the optimums from gradient based optimisation.

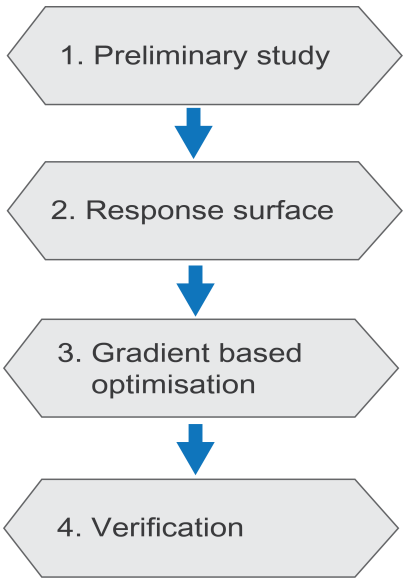

Figure 7.1: Illustration of the procedure including the 4 main steps.

7.1 Preliminary Study

In this section the results from the hydrodynamic analysis from the preliminary study is presented. Table 7.1 shows a overview over all the results. Hydrodynamic analysis showing the effect on piston mode by increasing or decreasing one variable individually and comparing it to a reference case is shown on Figure 7.2, 7.3, 7.4, 7.5, 7.6 and 7.7.

Table 7.1: Variables and results of the Preliminary tests.

Case	***Di1***	***Di2***	***T1***	***T2***	***T3***	***DT***	***Piston Mode***
0 (Reference)	40	35	30	30	30	10	22
1	40	35	**20**	30	30	10	21,5
2	40	35	**40**	30	30	10	23
3	40	35	30	**20**	30	10	21
4	40	35	30	**40**	30	10	23,5
5	40	35	30	30	**20**	10	21
6	40	35	30	30	**40**	10	23,5
7	40	**30**	30	30	30	10	20,5
8	40	**40**	30	30	30	10	25
9	**35**	35	30	30	30	10	20
10	**45**	35	30	30	30	10	24,5
11	40	35	30	30	30	**5**	22
12	40	35	30	30	30	**15**	22

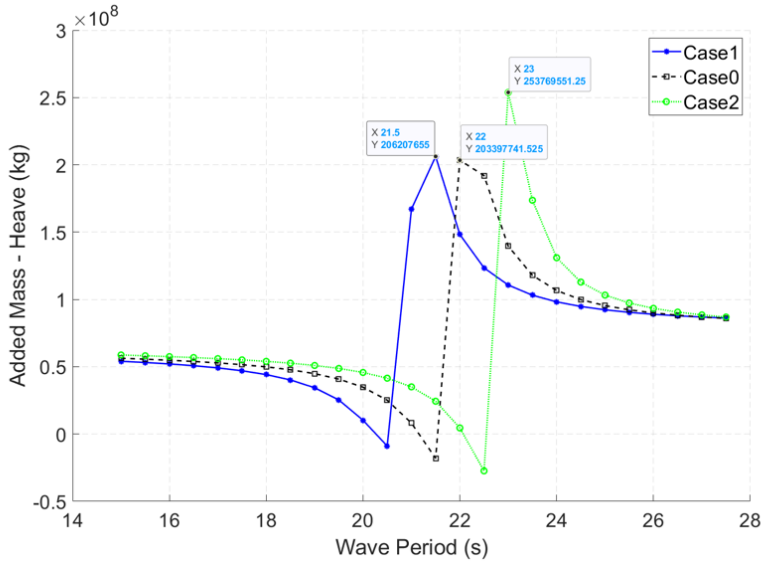

Figure 7.2: Preliminary test showing the effect on piston mode by change in T1.

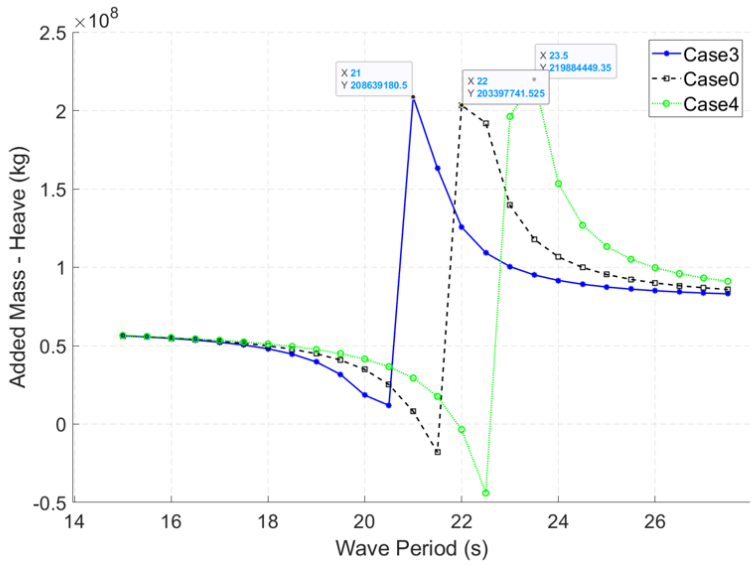

Figure 7.3: Preliminary test showing the effect on piston mode by change in T2.

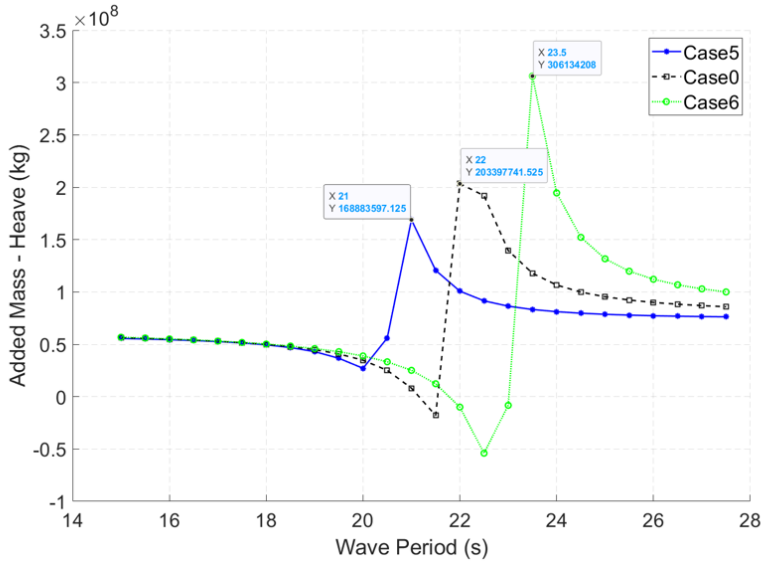

Figure 7.4: Preliminary test showing the effect on piston mode by change in T3

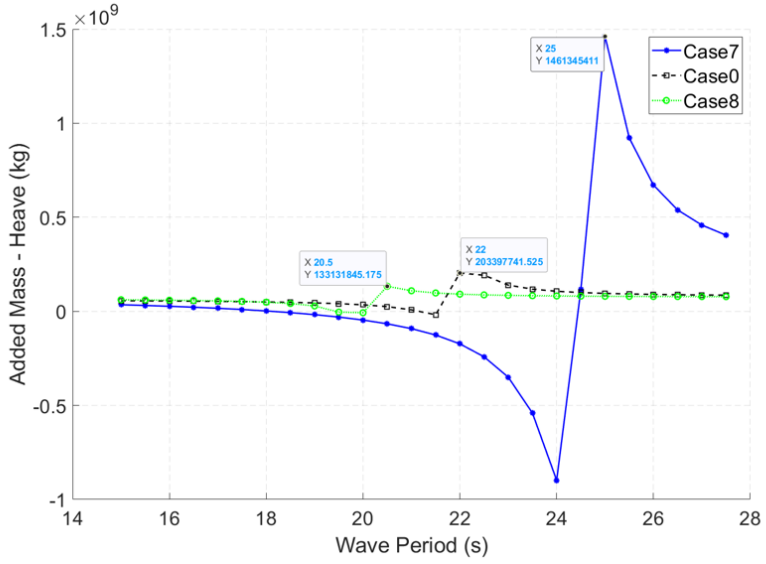

Figure 7.5: Preliminary test showing the effect on piston mode by change in Di2

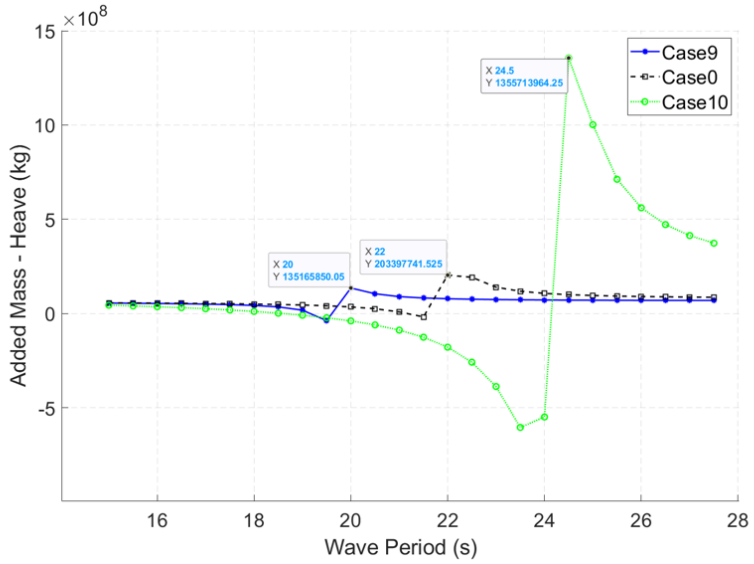

Figure 7.6: Preliminary test showing the effect on piston mode by change in Di1

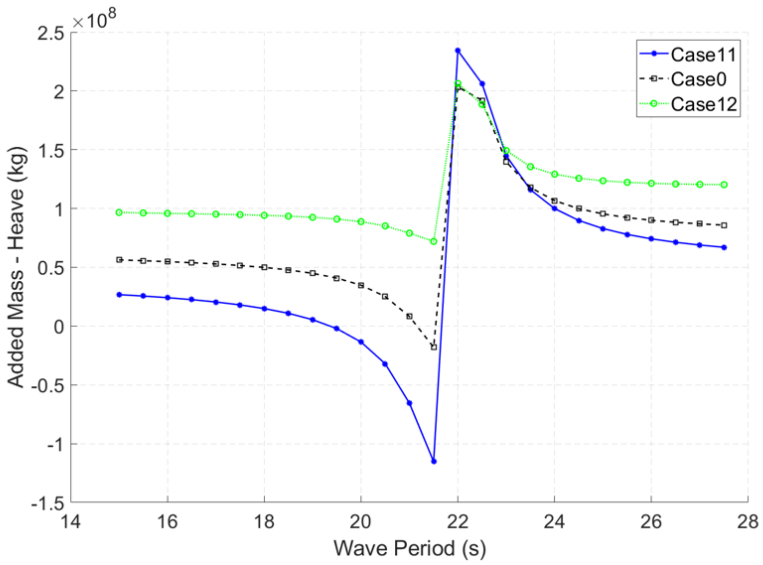

Figure 7.7: Preliminary test showing the effect on piston mode by change in DT

7.2 Response Surface

This chapter includes polynomial response surfaces, gaussian process regression based models and artificial neural network based models.

7.2.1 Polynomial Response Surface

This section presents different polynomial response surfaces which show how the different design variables affect the piston mode resonance period and which design variables has the biggest impact.

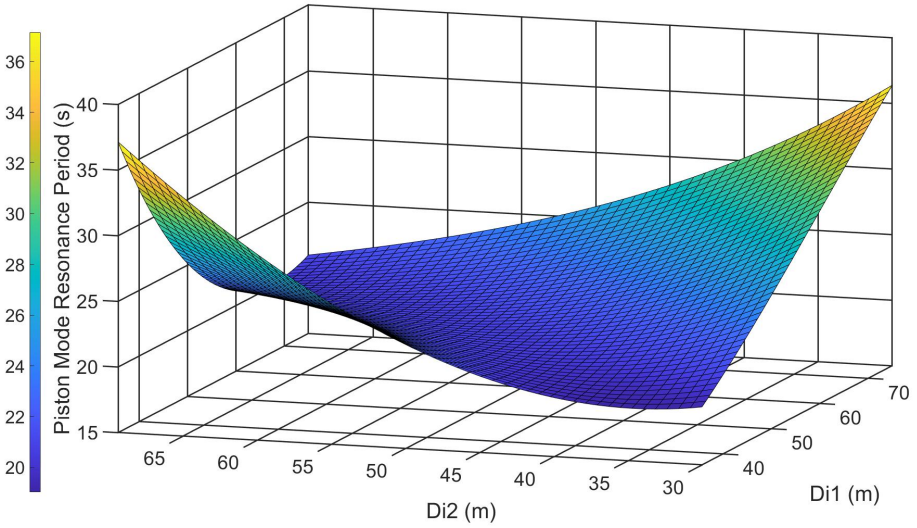

Figure 7.8: Polynomial response surface showing how the upper radius Di1 compared to the lower radius Di2 affects the piston-mode period.

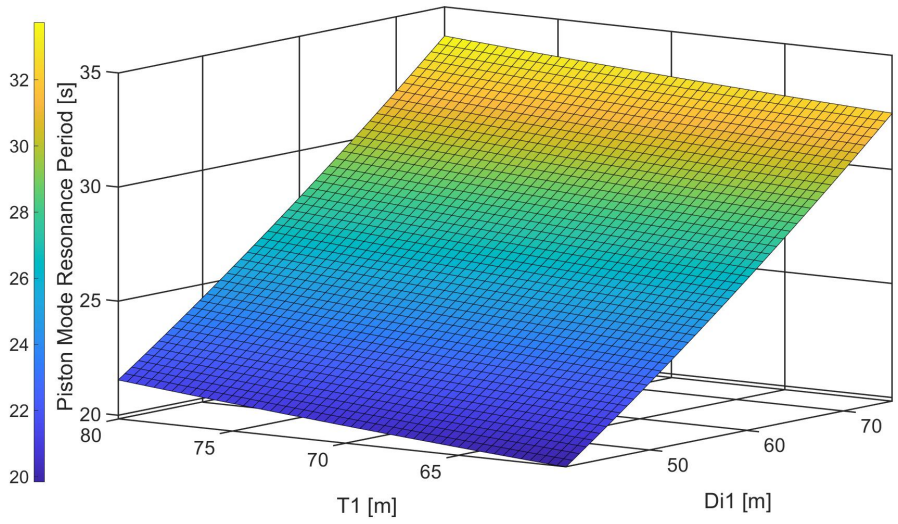

Figure 7.9: Polynomial response surface showing how the upper radius Di1 compared to the upper height T1 affects the piston-mode period.

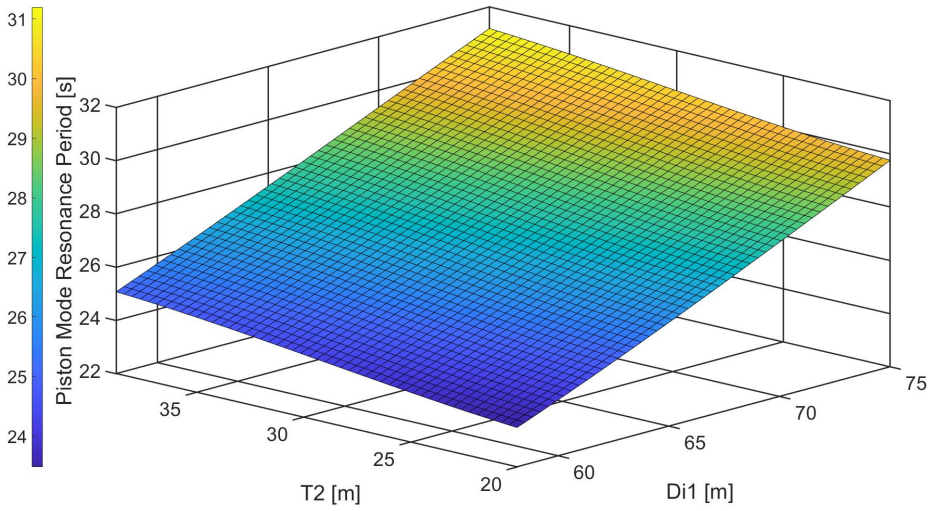

Figure 7.10: Polynomial response surface showing how the upper radius Di1 compared to the middle height T2 affects the piston-mode period.

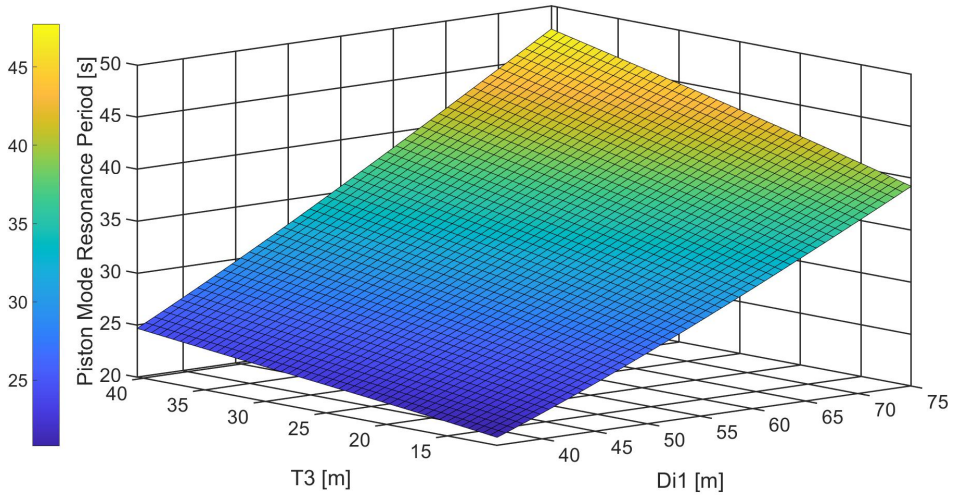

Figure 7.11: Polynomial response surface showing how the upper radius Di1 compared to the lower height T3 affects the piston-mode period.

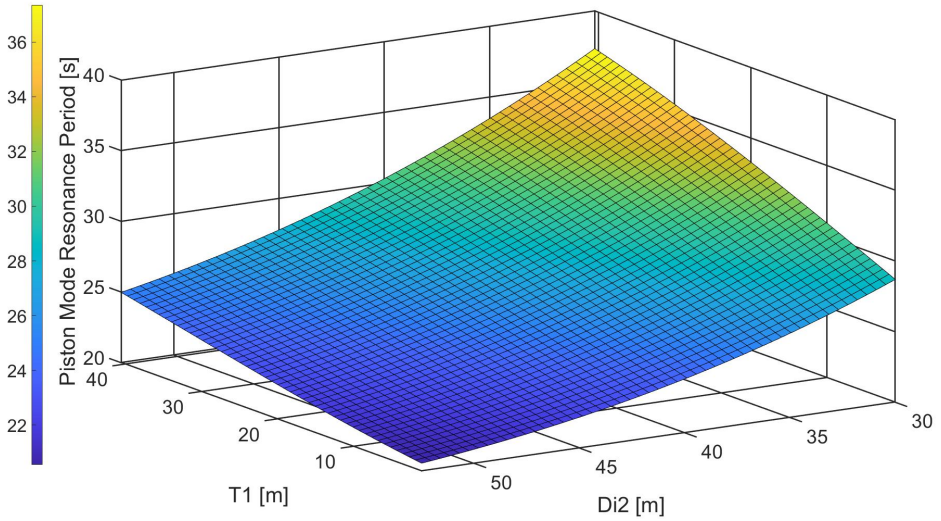

Figure 7.12: Polynomial response surface showing how the lower radius Di2 compared to the upper height T1 affects the piston-mode period.

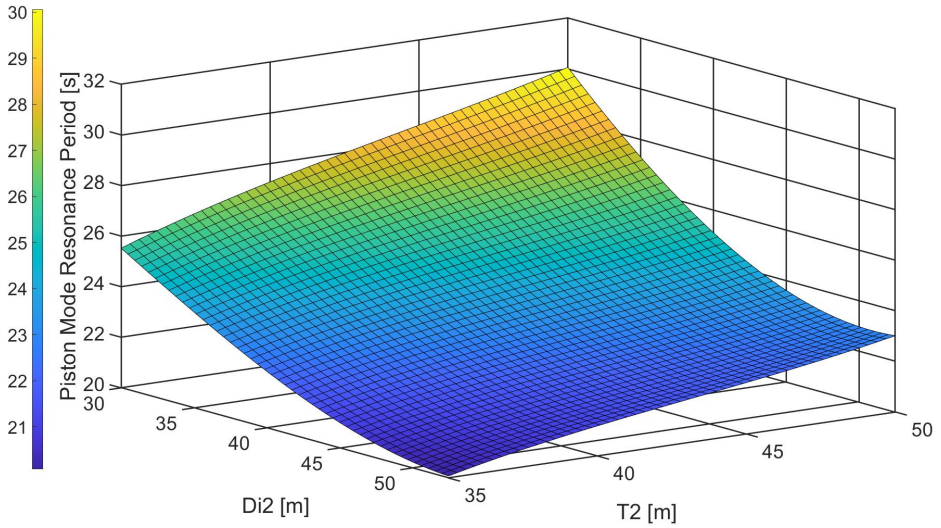

Figure 7.13: Polynomial response surface showing how the lower radius Di2 compared to the middle height T2 affects the piston-mode period.

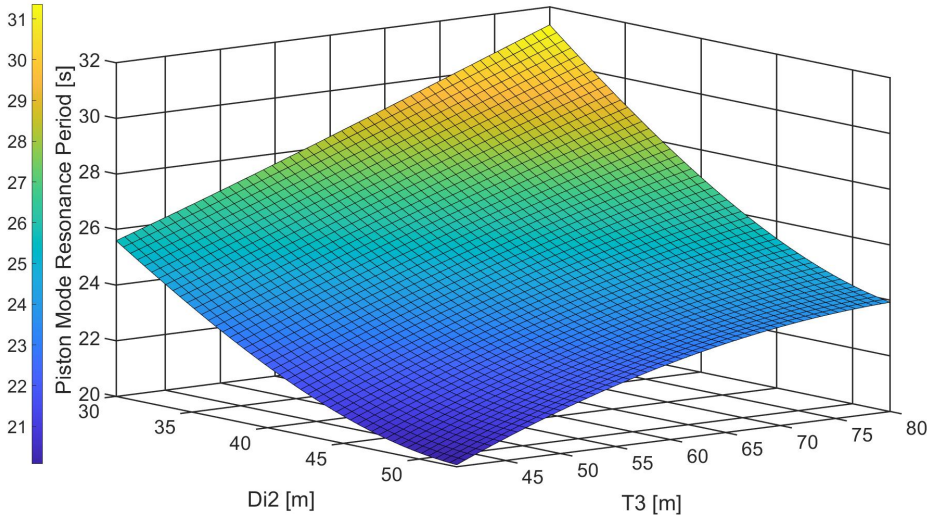

Figure 7.14: Polynomial response surface showing how the lower radius Di2 compared to the lower height T3 affects the piston-mode period.

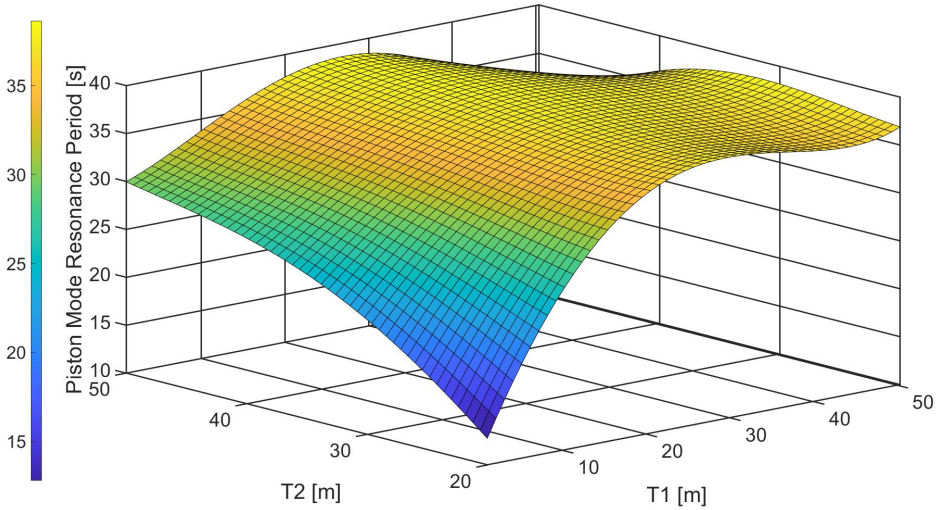

Figure 7.15: Polynomial response surface showing how the upper height T1 compared to the middle height T2 affects the piston-mode period.

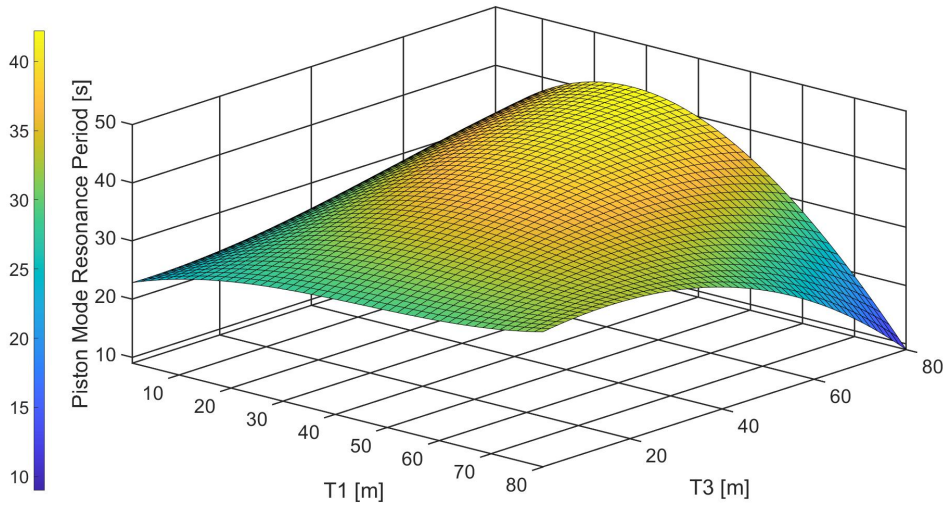

Figure 7.16: Polynomial response surface showing how the upper height T1 compared to the lower height T3 affects the piston-mode period.

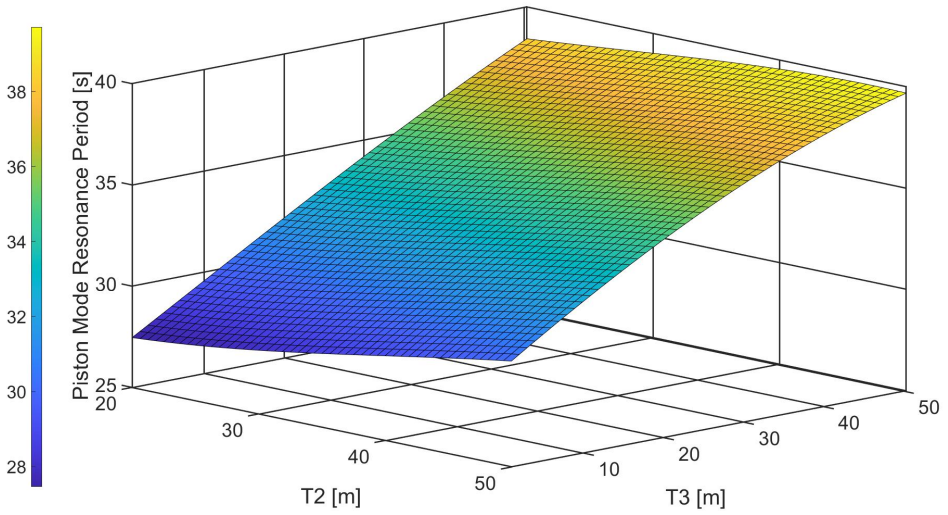

Figure 7.17: Polynomial response surface showing how the middle height T2 compared to the lower height T3 affects the piston-mode period.

7.2.2 Gaussian Process Regression

This sections presents comparisons between the results from the hydrodynamic analysis and predictions from gaussian process regression based models with three different covariance functions. It also includes a graph of probability density function for the relative error between the models and the results from the hydrodynamic analysis.

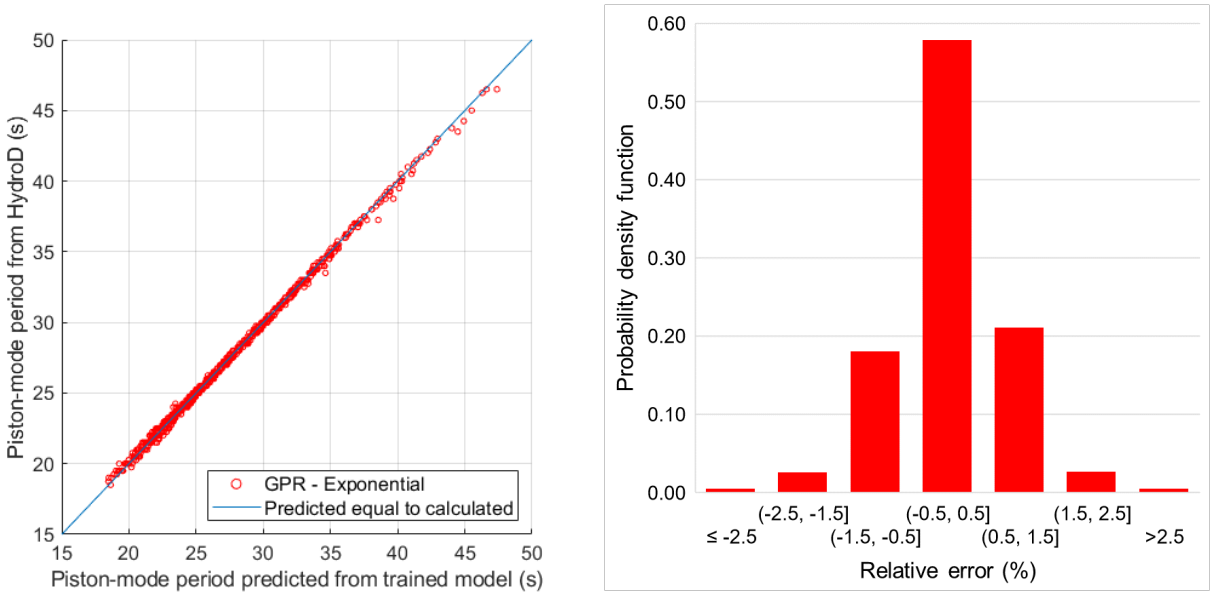

Figure 7.18: HydroD results compared to predictions by the trained model based on Gaussian process regression with exponential covariance function and a probability density functionr.

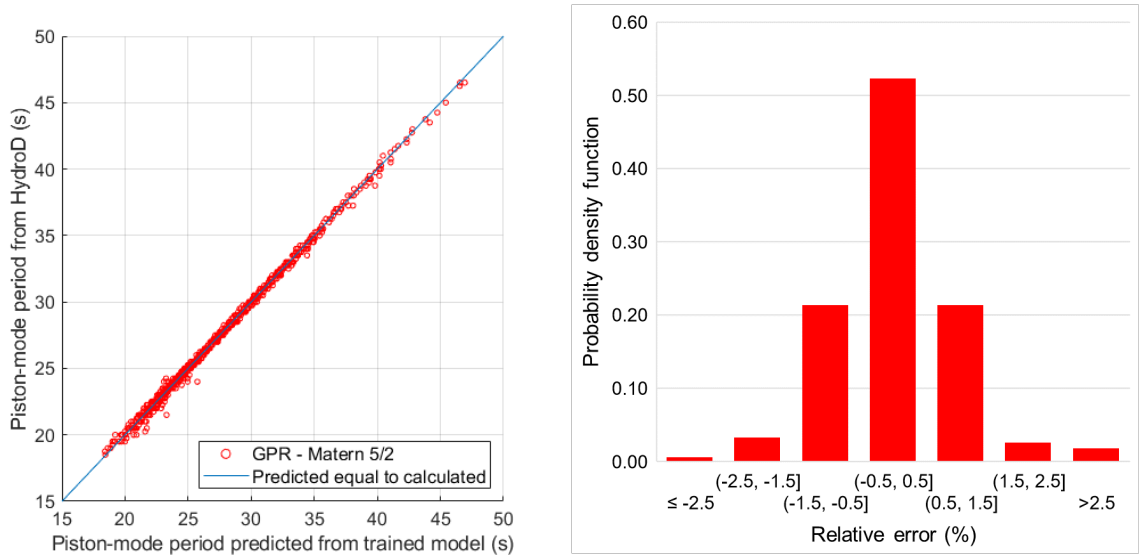

Figure 7.19: HydroD results compared to predictions by the trained model based on Gaussian process regression with matern 5/2 covariance function and a probability density function.

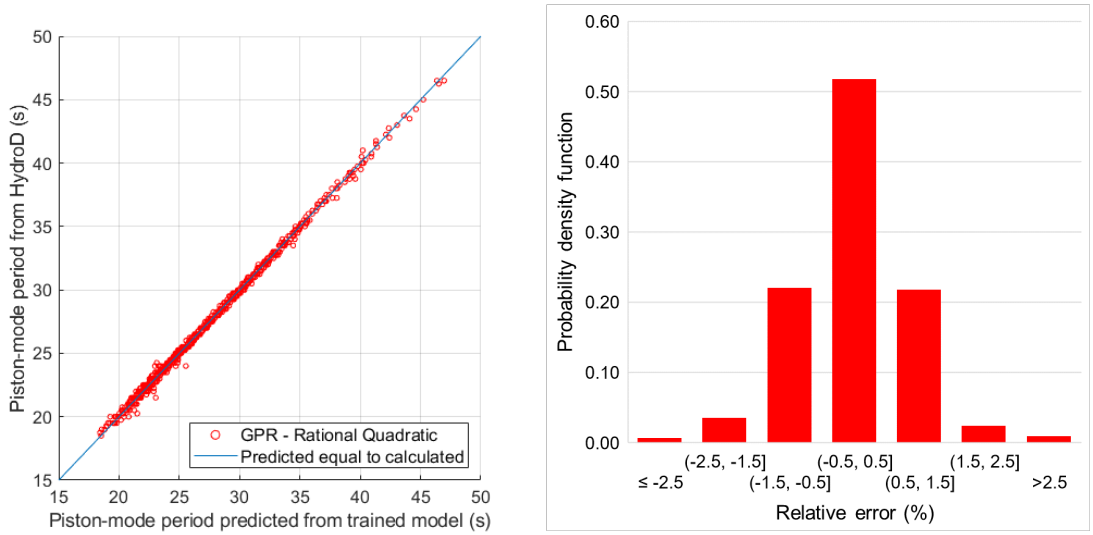

Figure 7.20: HydroD results compared to predictions by the trained model based on Gaussian process regression with rational quadratic covariance function and a probability density function.

7.2.3 Artificial Neural Network

This sections presents comparisons between the results from the hydrodynamic analysis and predictions from Artificial Neural Netwerk based models. Three different types of models is included. It also includes a graph of probability density function for the relative error between the models and the results from the hydrodynamic analysis.

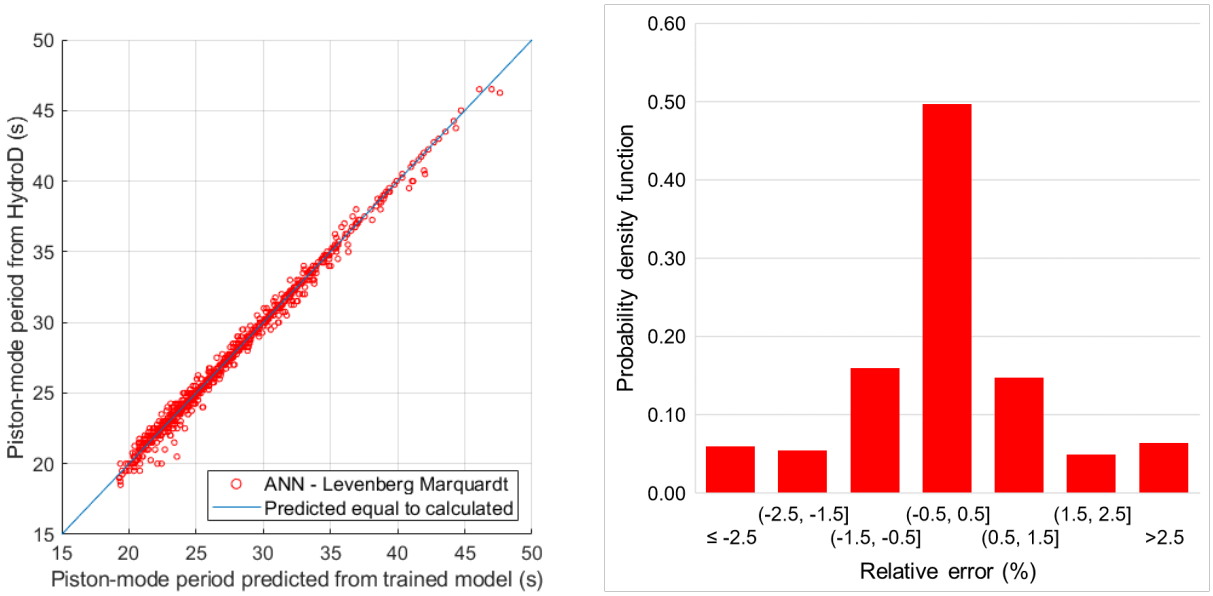

Figure 7.21: HydroD results compared to predictions by the trained model based on artificial neural network Levenberg Marquardt and a probability density function.

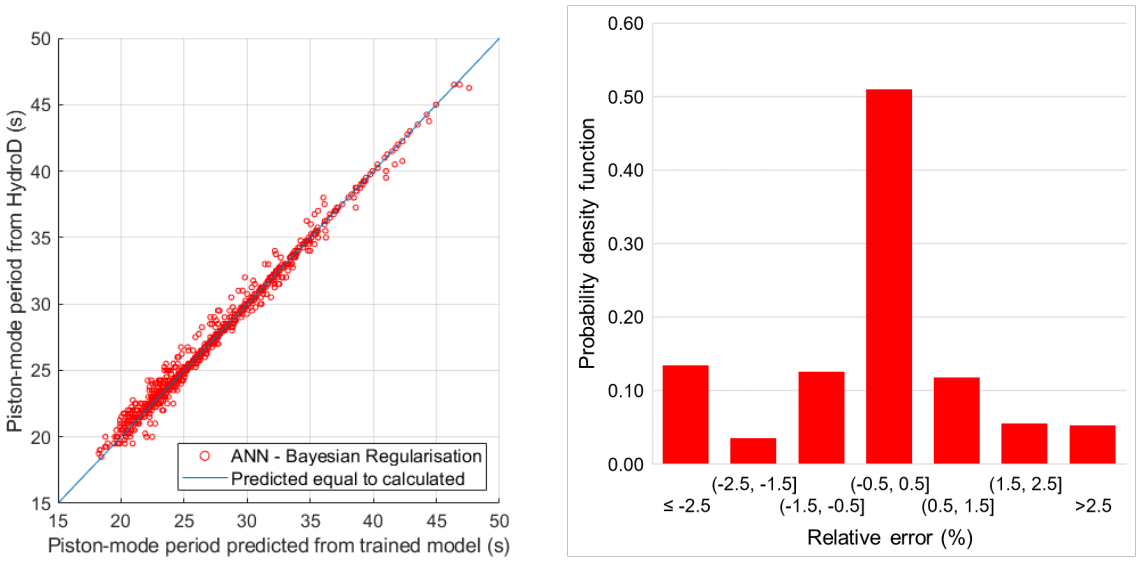

Figure 7.22: HydroD results compared to predictions by the trained model based on artificial neural network bayesian regulerisation and a probability density function.

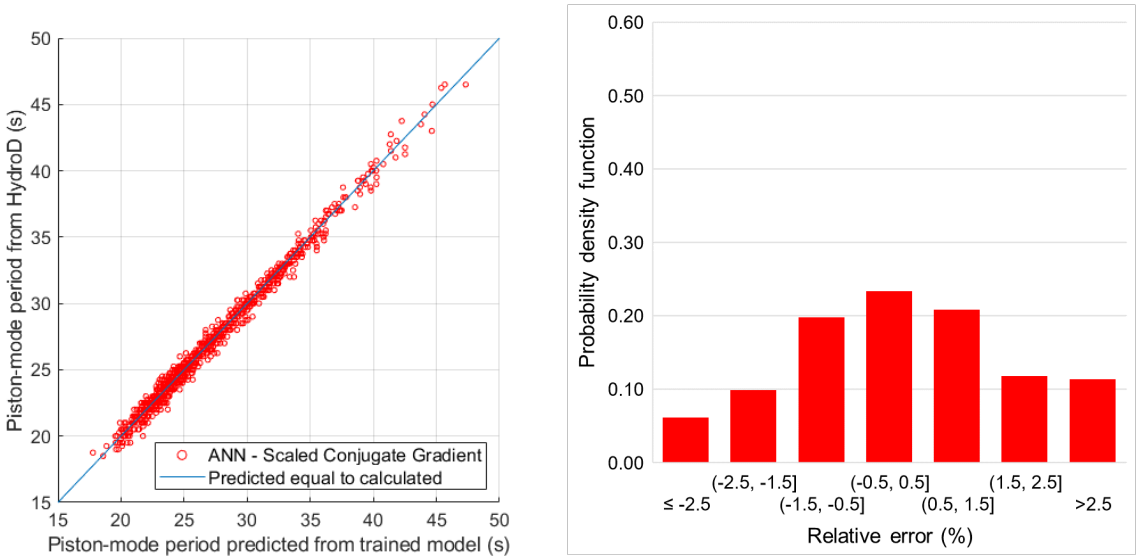

Figure 7.23: HydroD results compared to predictions by the trained model based on artificial neural network scaled conjugate gradient and a probability density function.

7.2.4 Comparison of the Trained Models

The figure shows a comparison of all the tested models. The maximum negative value is shown as "Min" on the figures. The average is calculated with absolute values.

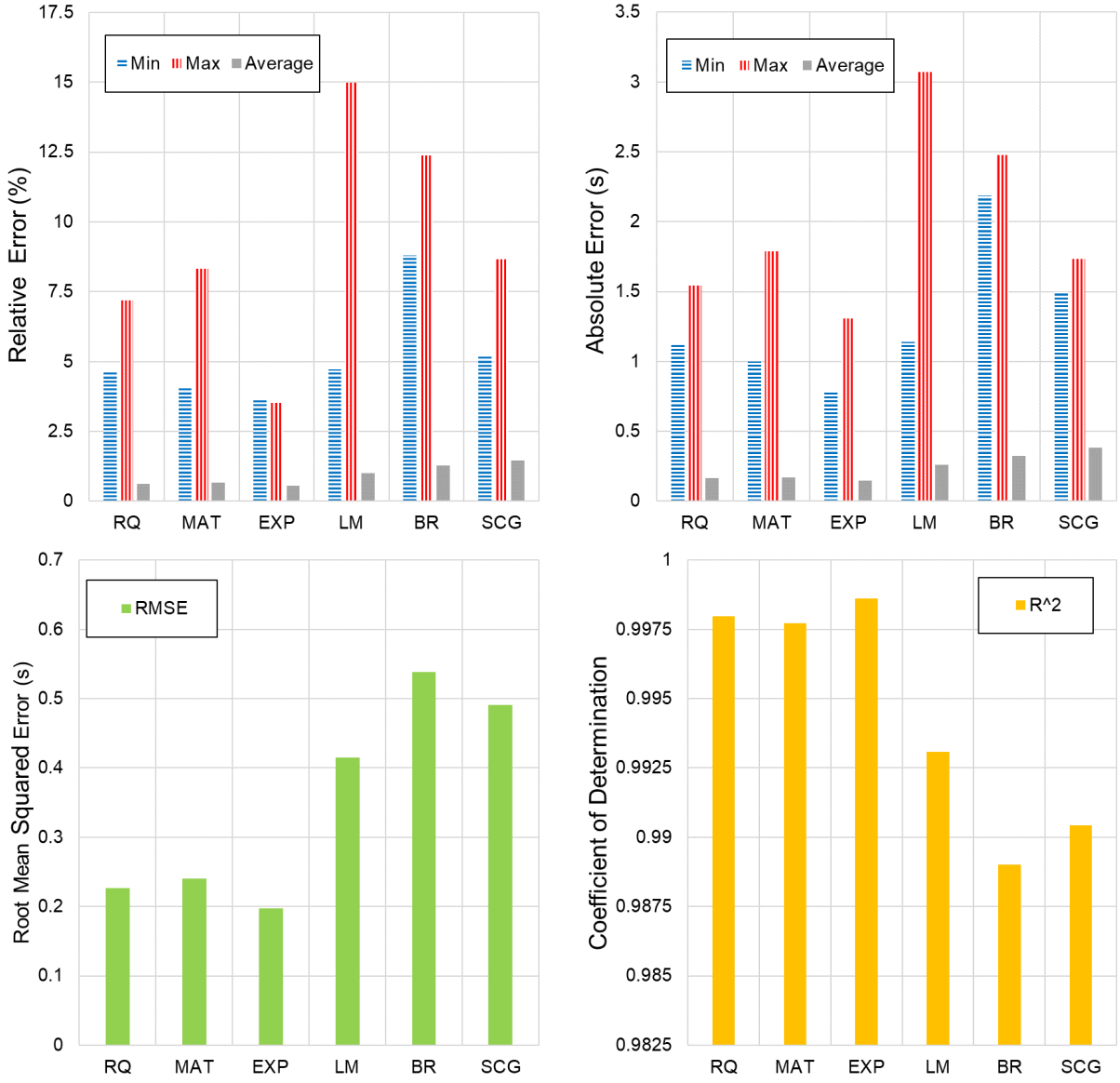

Figure 7.24: Comparison of statistics on the trained models based on gaussian process regression and artificial neural network.

7.3 Gradient-Based Optimisation

This section presents three optimum docks found. Figures showing optimum shape, iterations of variables, iterations of boundaries and the change in shape during early iterations is included.

Table 7.2: Overview of the sensitivity study

	Tt=20	**Tt=25**	**Tt=30**	**Without boundary**
Tn=17	Found	*Skipped*	*Skipped*	Found
Tn=19	Found	Found	*Skipped*	Found
Tn=21	Found	Found	Found	Found
Tn=23	Failed	Failed	Failed	Found

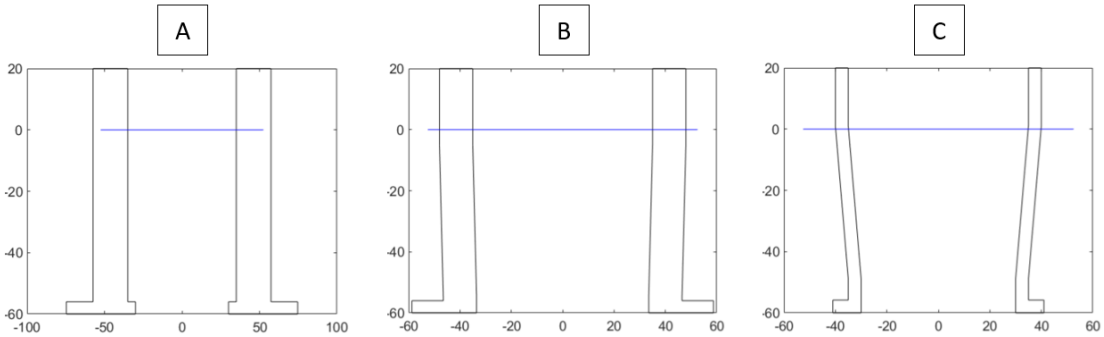

Figure 7.25: Illustration of the three optimum docks presented in this section in operational state.

Design variables	***Symbols***	***A***	***B***	***C***
Dock upper inner radius	Di1	35	35	35
Dock lower inner radius	Di2	35	33.5089	30
Dock thickness	Dt	22.4351	12.9717	5
Dock height upper	T1	25	25	18.8666
Dock height middle	T2	50	50	50
Dock height lower	T3	1	1	6.9524
Bilge tank height	Hsk	4	4	4.1810
Bilge tank outward extension	Hskout	17.1988	12.2525	6
Bilge tank inward extension	Hskin	5	0	0
Height of water ballast in operation	Hbwo	42.6559	32.6087	0
Height of water ballast in transit	Hbwt	0	0	7.7277
Dock freeboard in operation	Fo	20	20	20
Dock draft in operation	To	60	60	60
Dock freeboard in transit	Ft	59	50	16.7850
Dock draft in transit	Tt	21	30	63.2150

Table 7.3: Parameters of the three optimum docks presentated (m).

7.3.1 Main Study

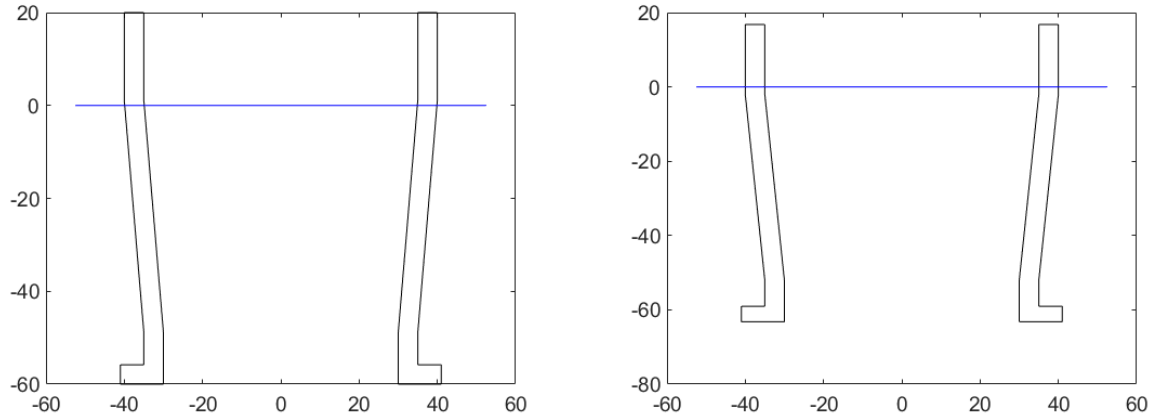

(a) Operation. (b) Transit.

Figure 7.26: Optimum shape of the floating dock in operation and in transit.

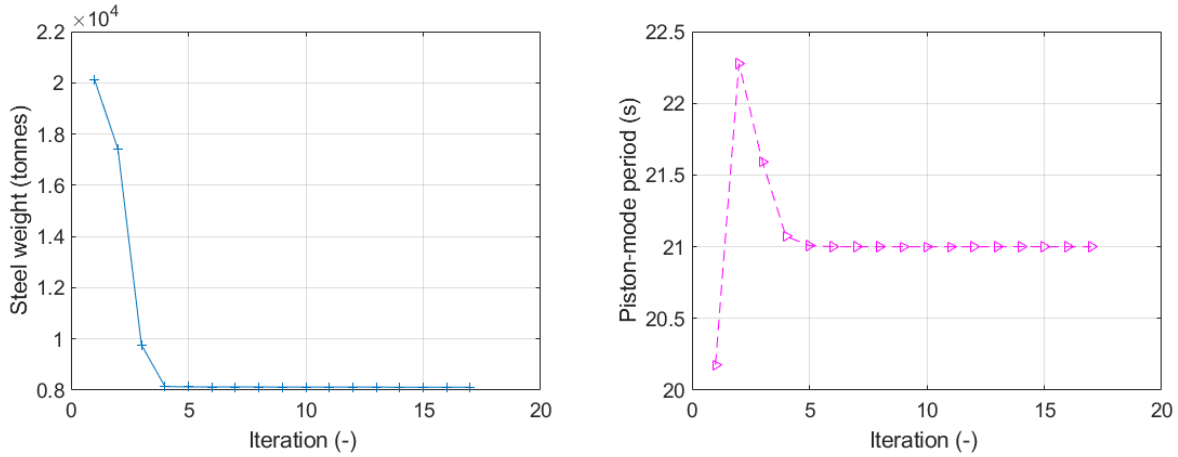

(a) Steel weight. (b) Piston period.

Figure 7.27: Iterations of optimisation objective steel weight and constrain piston-mode period.

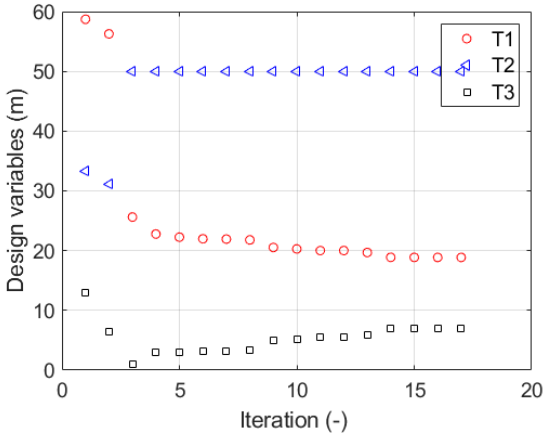

(a) T1, T2 and T3.

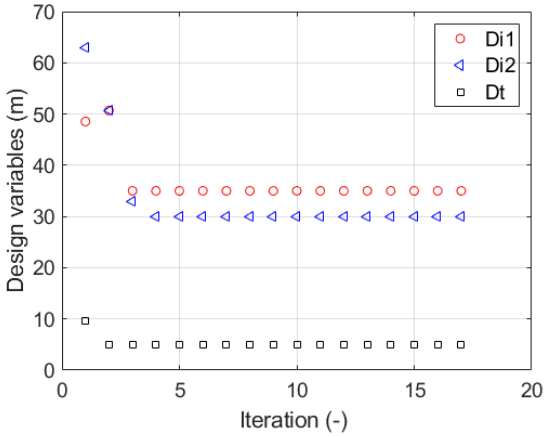

(b) Di1, Di2 and Dt.

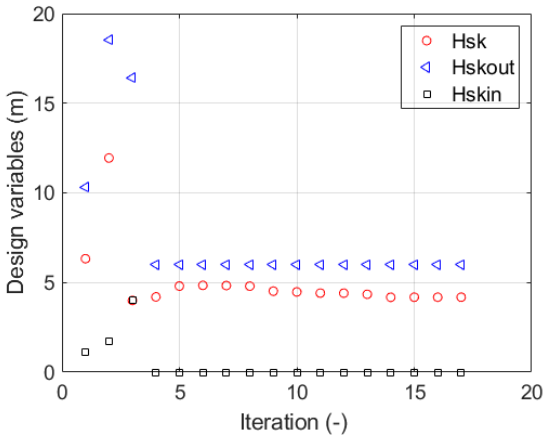

(c) Hsk, Hskout and Hskin.

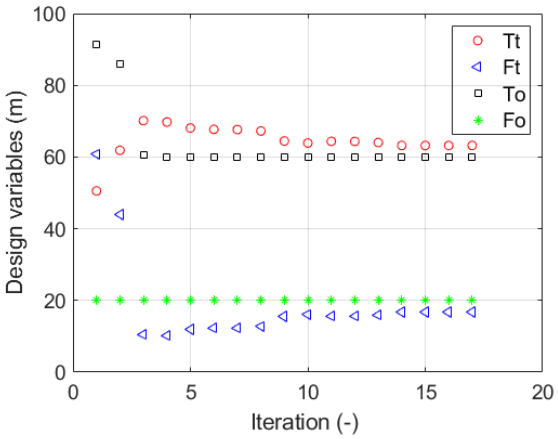

(d) Tt, Ft, To and Tt.

Figure 7.28: Iterations of design variables during the optimisation.

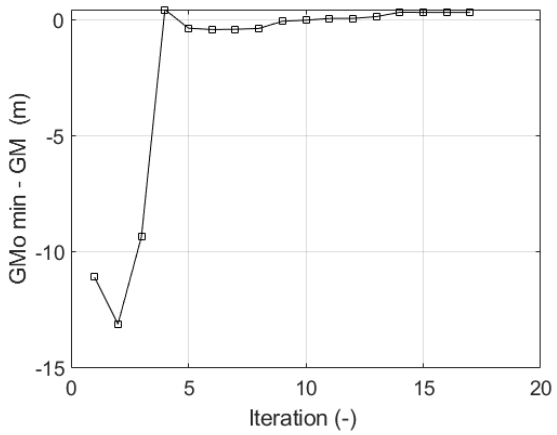

(a) Metacentric height in operation.

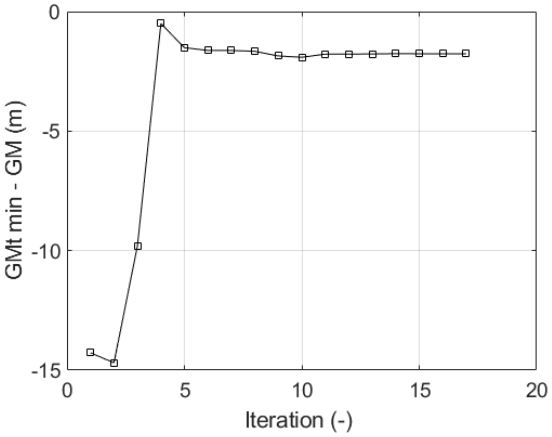

(b) Metacentric height in Transit.

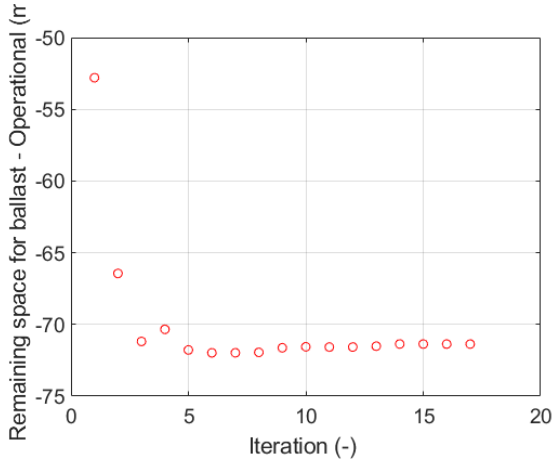

(c) Remaining space for ballast in operation.

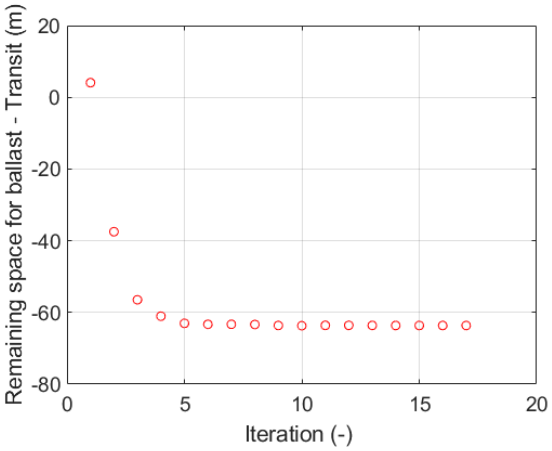

(d) Remaining space for ballast in Transit.

Figure 7.29: Iterations of boundaries during the optimisation.

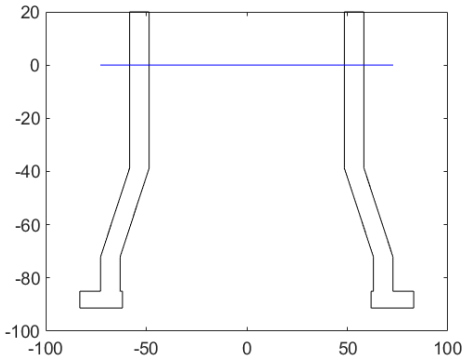

(a) Iteration 1.

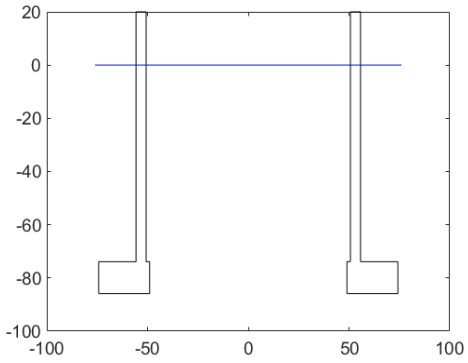

(b) Iteration 2.

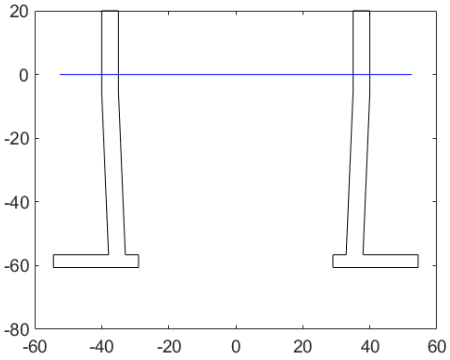

(c) Iteration 3.

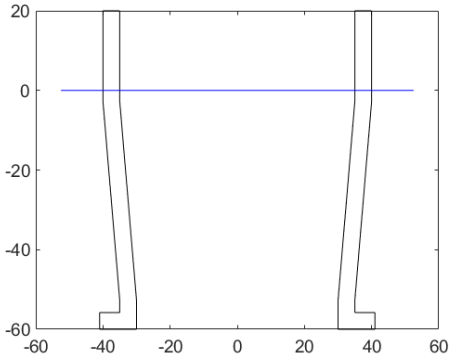

(d) Iteration 4.

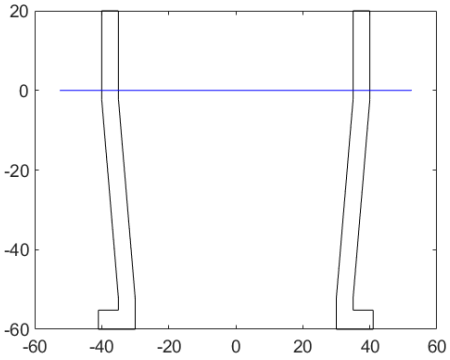

(e) Iteration 5.

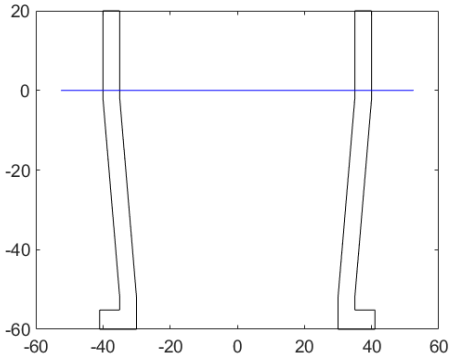

(f) Iteration 6.

Figure 7.30: The first iterations showing how the shape of the floating dock in operation changes.

7.3.2 Sensitivity Study

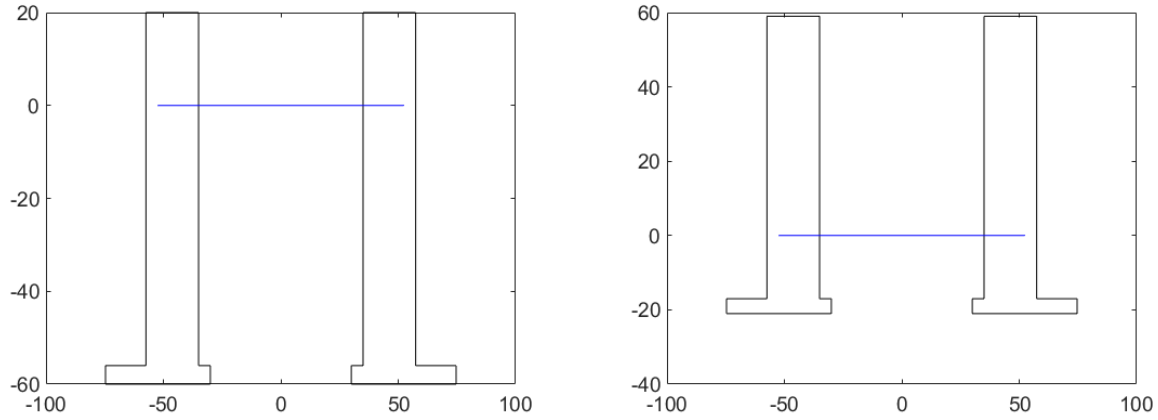

(a) Operation. (b) Transit.

Figure 7.31: Optimum shape of the floating dock in operation and in transit.

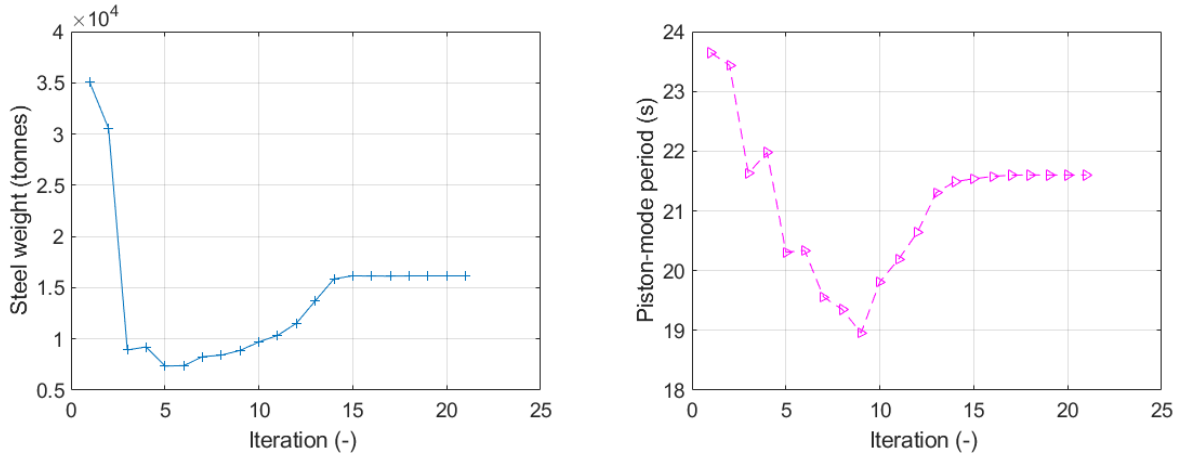

(a) Steel weight. (b) Piston period.

Figure 7.32: Iterations of optimisation objective steel weight and constrain piston-mode period.

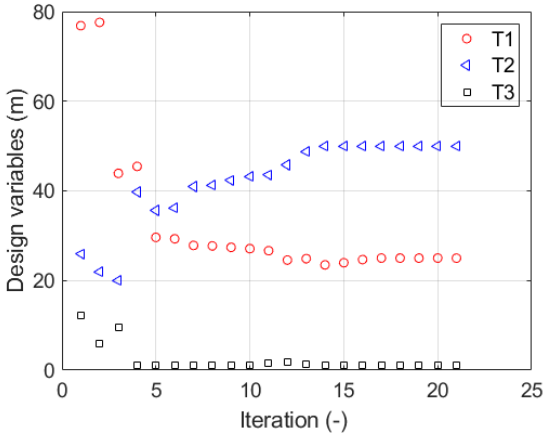

(a) T1, T2 and T3.

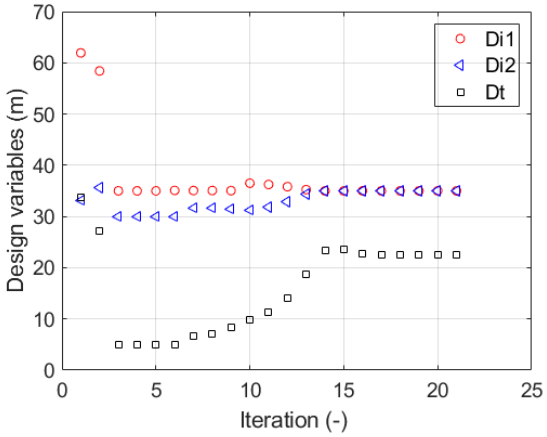

(b) Di1, Di2 and Dt.

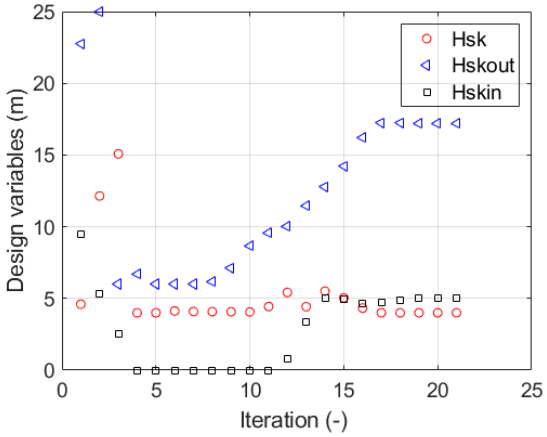

(c) Hsk, Hskout and Hskin.

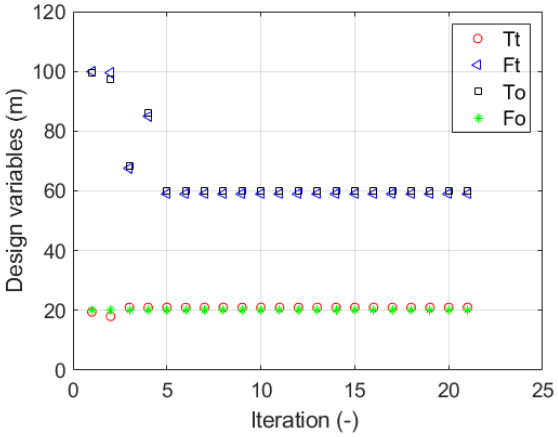

(d) Tt, Ft, To and Tt.

Figure 7.33: Iterations of design variables during the optimisation.

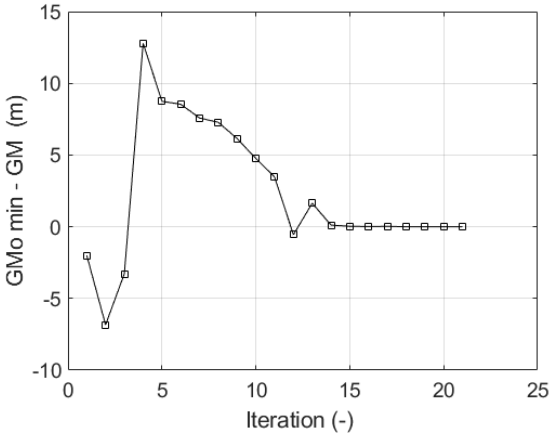

(a) Metacentric height in operation.

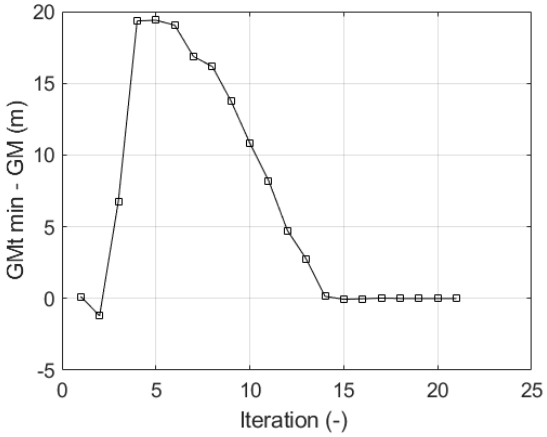

(b) Metacentric height in Transit.

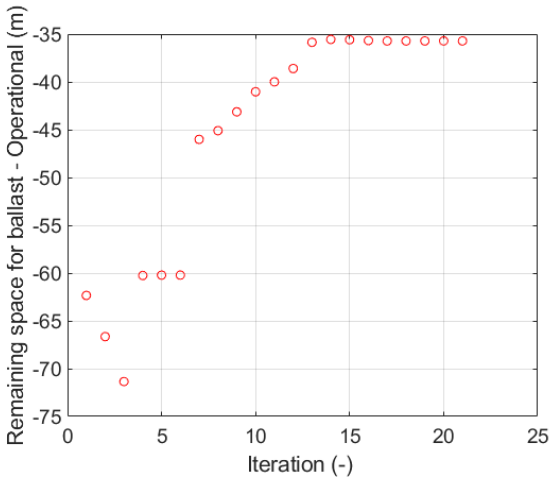

(c) Remaining space for ballast in operation.

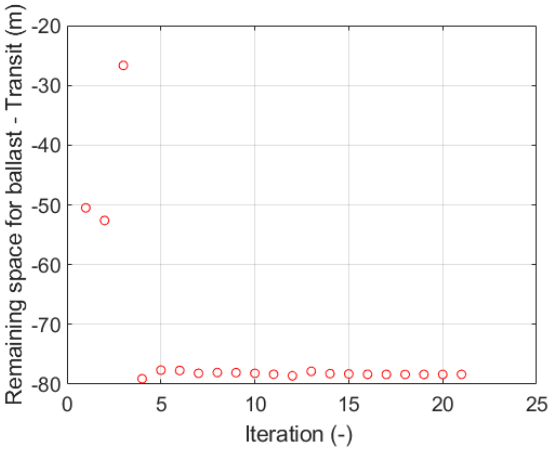

(d) Remaining space for ballast in Transit.

Figure 7.34: Iterations of boundaries during the optimisation.

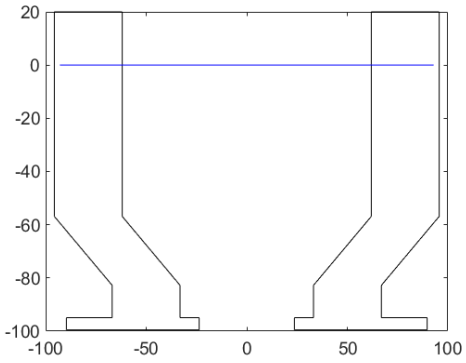

(a) Iteration 1.

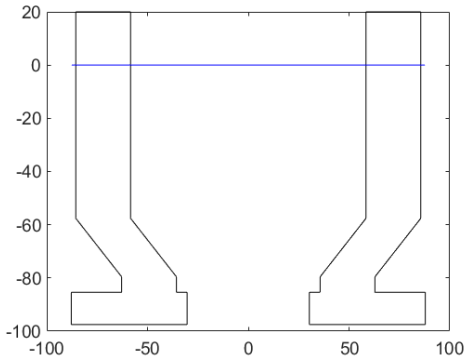

(b) Iteration 2.

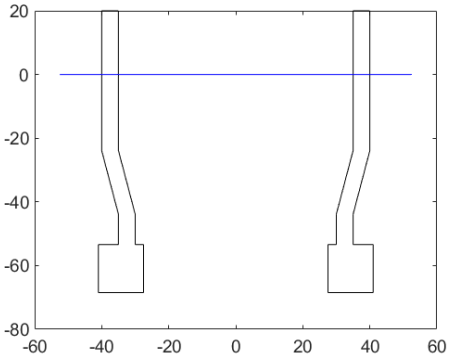

(c) Iteration 3.

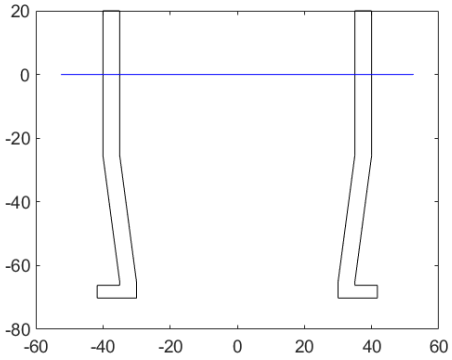

(d) Iteration 4.

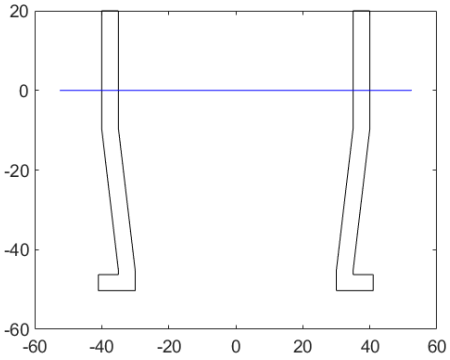

(e) Iteration 5.

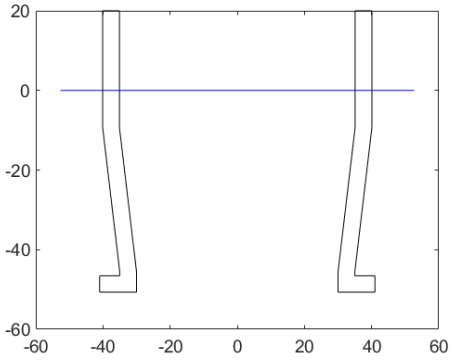

(f) Iteration 6.

Figure 7.35: The first iterations showing how the shape of the floating dock in operation changes.

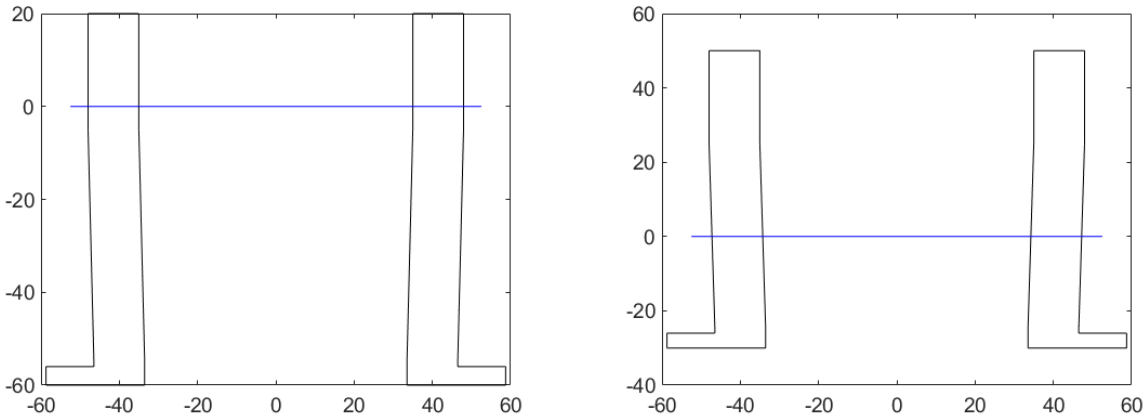

(a) Operation. (b) Transit.

Figure 7.36: Optimum shape of the floating dock in operation and in transit.

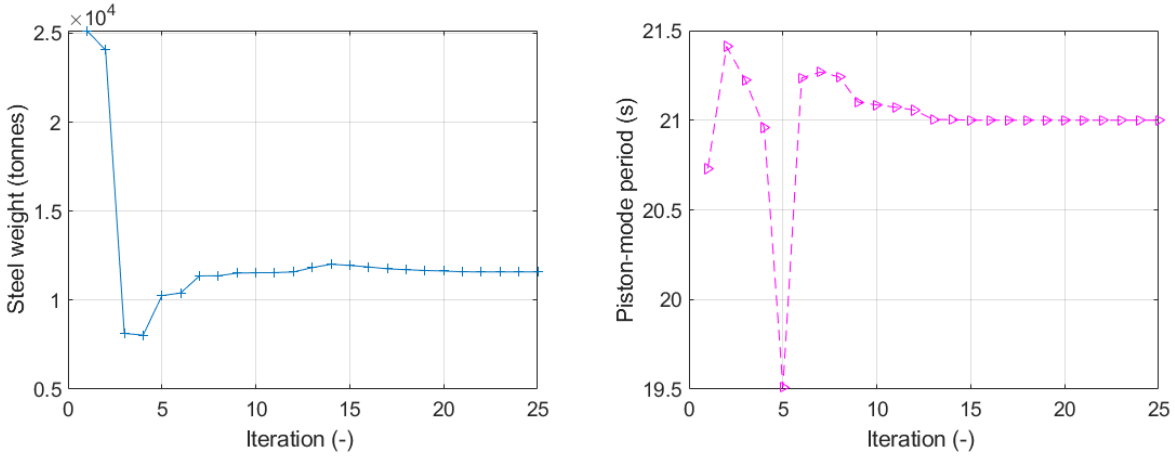

(a) Steel weight. (b) Piston period.

Figure 7.37: Iterations of optimisation objective steel weight and constrain piston-mode period.

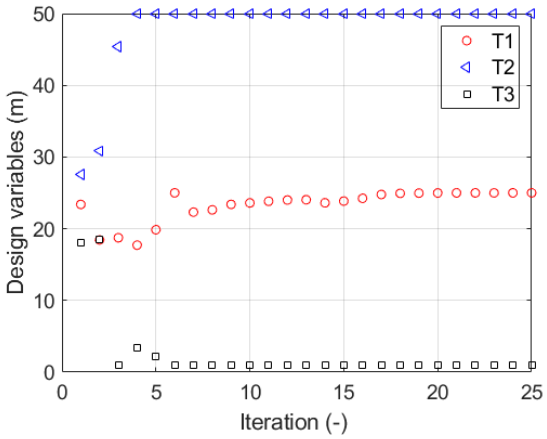

(a) T1, T2 and T3.

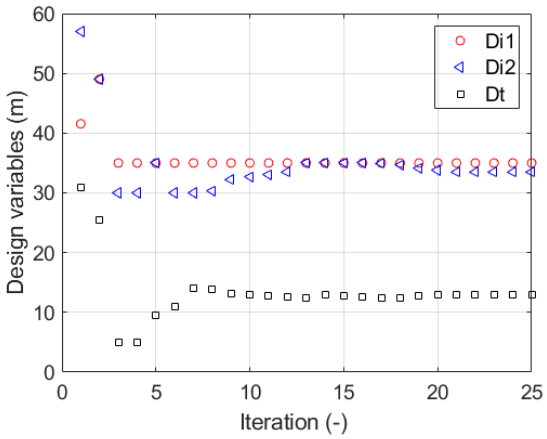

(b) Di1, Di2 and Dt.

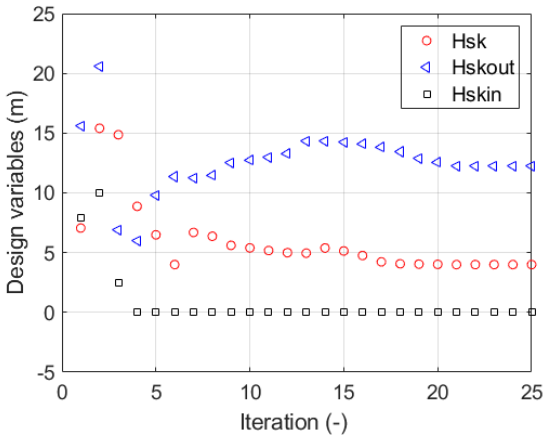

(c) Hsk, Hskout and Hskin.

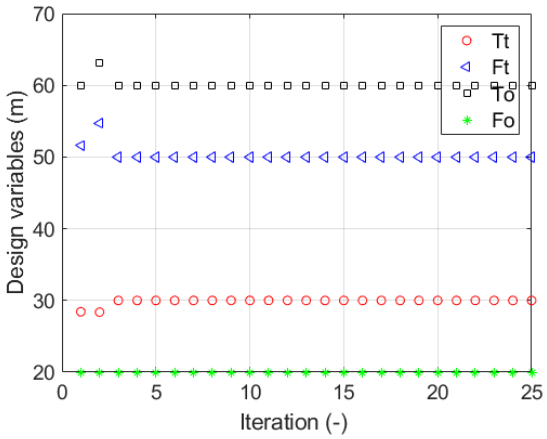

(d) Tt, Ft, To and Tt.

Figure 7.38: Iterations of design variables during the optimisation.

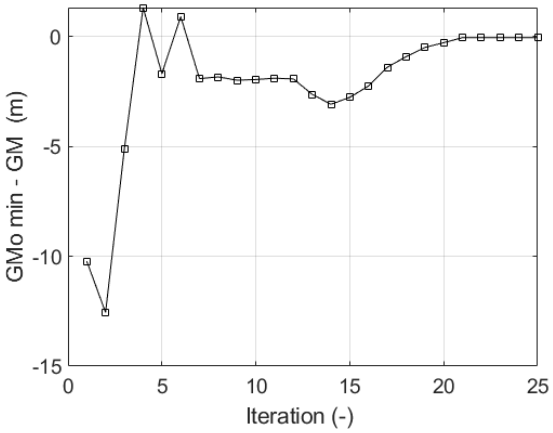

(a) Metacentric height in operation.

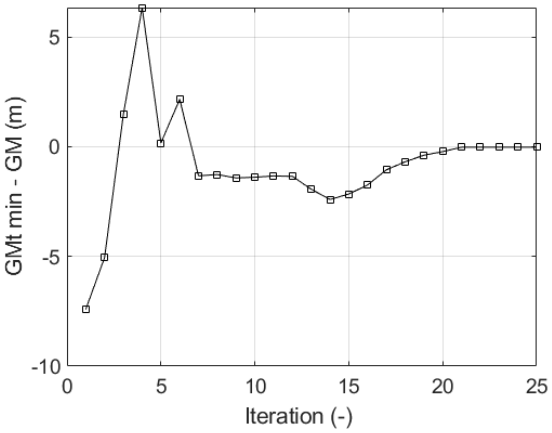

(b) Metacentric height in Transit.

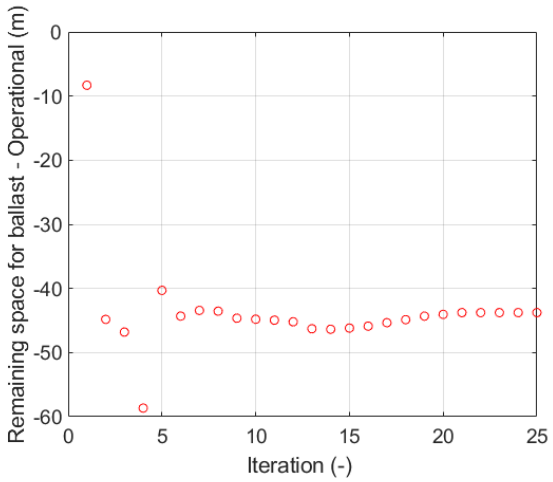

(c) Remaining space for ballast in operation.

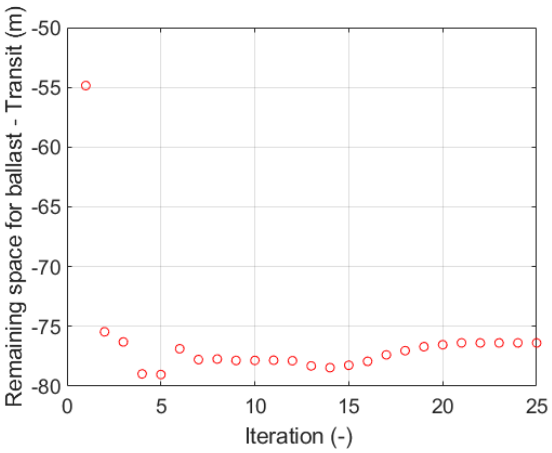

(d) Remaining space for ballast in Transit.

Figure 7.39: Iterations of boundaries during the optimisation.

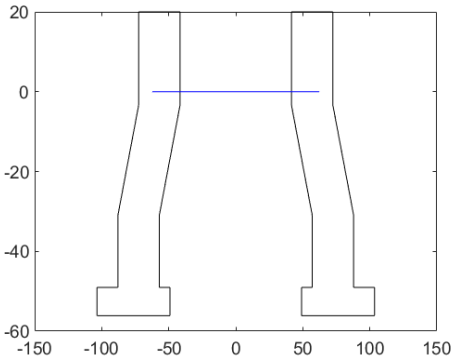

(a) Iteration 1.

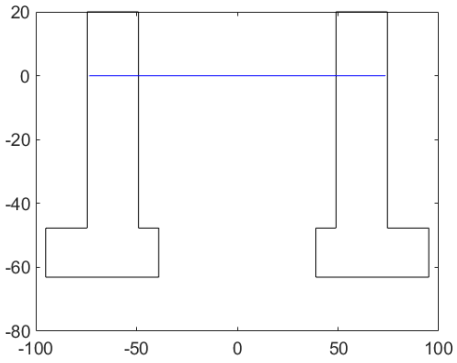

(b) Iteration 2.

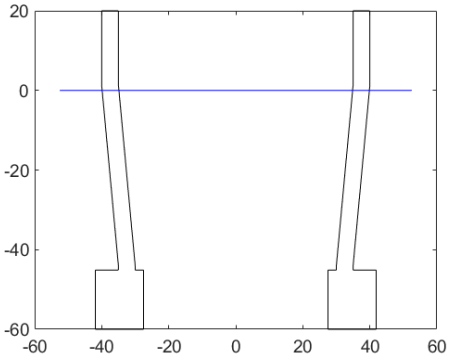

(c) Iteration 3.

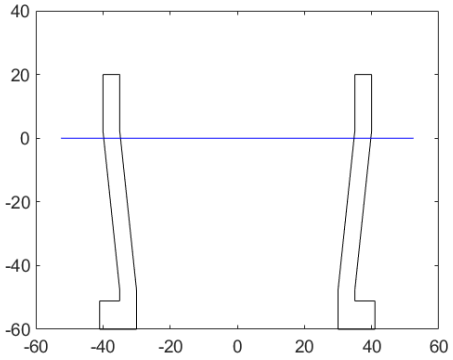

(d) Iteration 4.

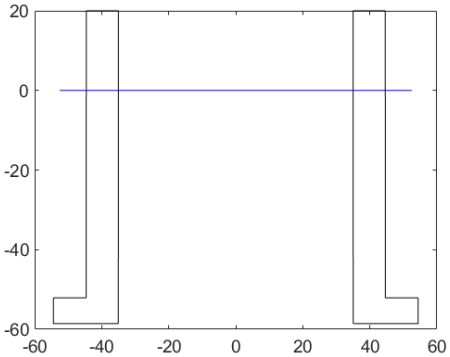

(e) Iteration 5.

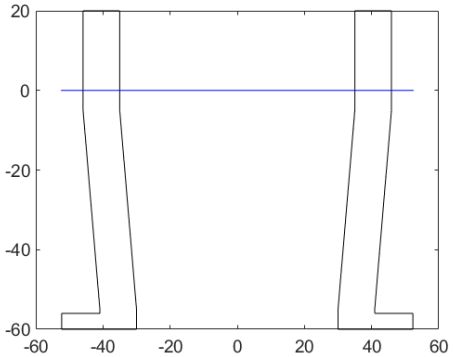

(f) Iteration 6.

Figure 7.40: The first iterations showing how the shape of the floating dock in operation changes.

7.4 Verification of the Optimisation Results

This section presents results of hydrodynamic analysis and from wave particle transfer function on the three optimum dock shapes found with gradient based optimisation. Piston-mode period is predicted from added mass in heave and from wave particle transfer function. Response amplitude operator of internal wave elevation is graphed for three points on the internal surface. Wave particle transfer function is used to make simulations where a grid for the entire internal surface is investigated. How piston-mode period is predicted from added mass in heave and from wave particle transfer function is explained in 3.5.5 and 3.5.7.

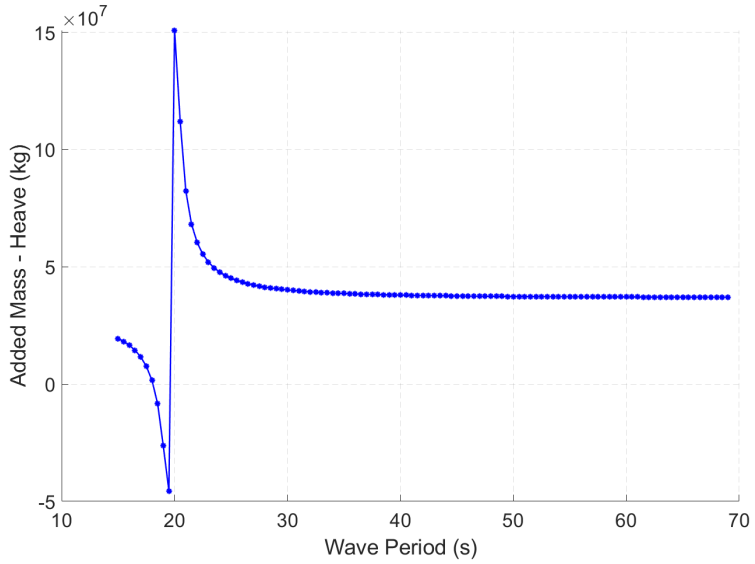

Figure 7.41: Added Mass in Heave from HydroD when Tt is without boundary. The peak is the piston-mode period which is 20s.

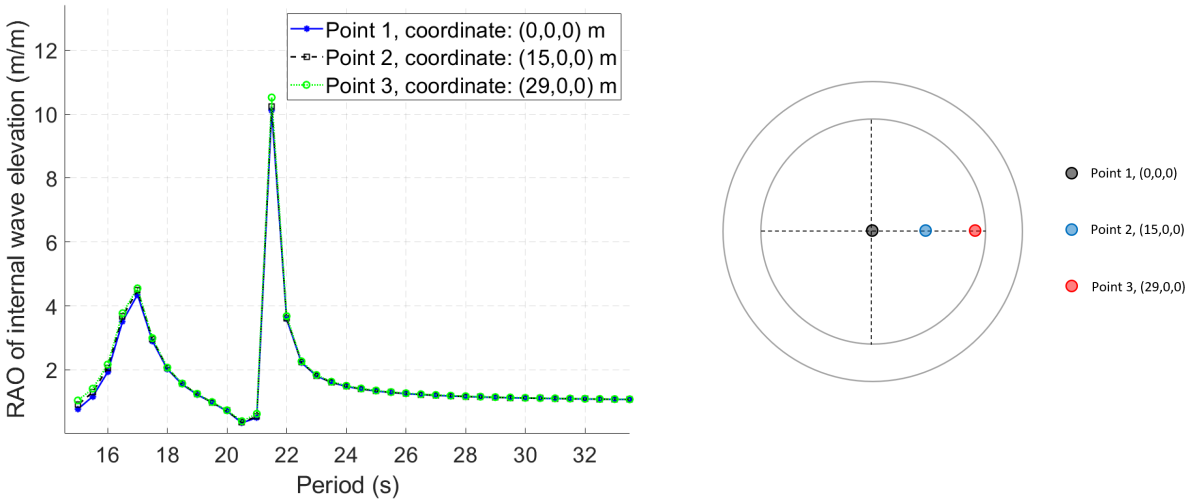

Figure 7.42: Response amplitude operator magnitude of internal surface points without damping where the first peak is the natural heave period and the second peak is the piston-mode period and a illustration of the placement of the offbody points seen from above.

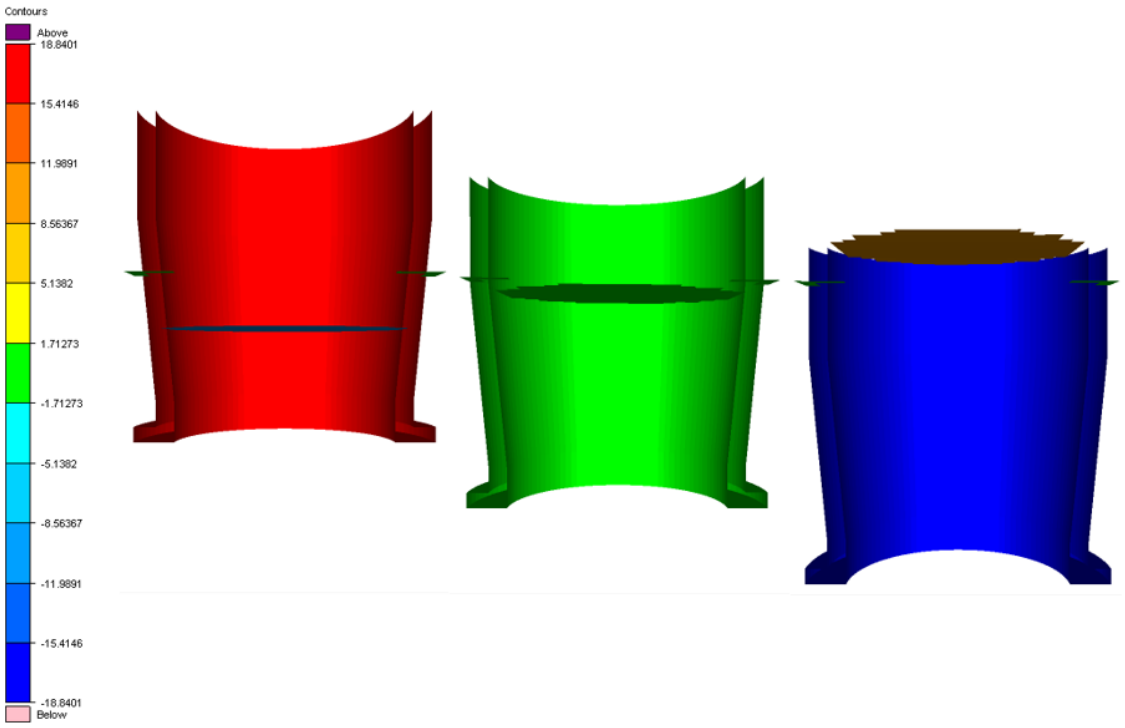

Figure 7.43: Visualisation of piston-mode period at 21.5s from simulations using wave particle transer funtion when Tt is without boundary

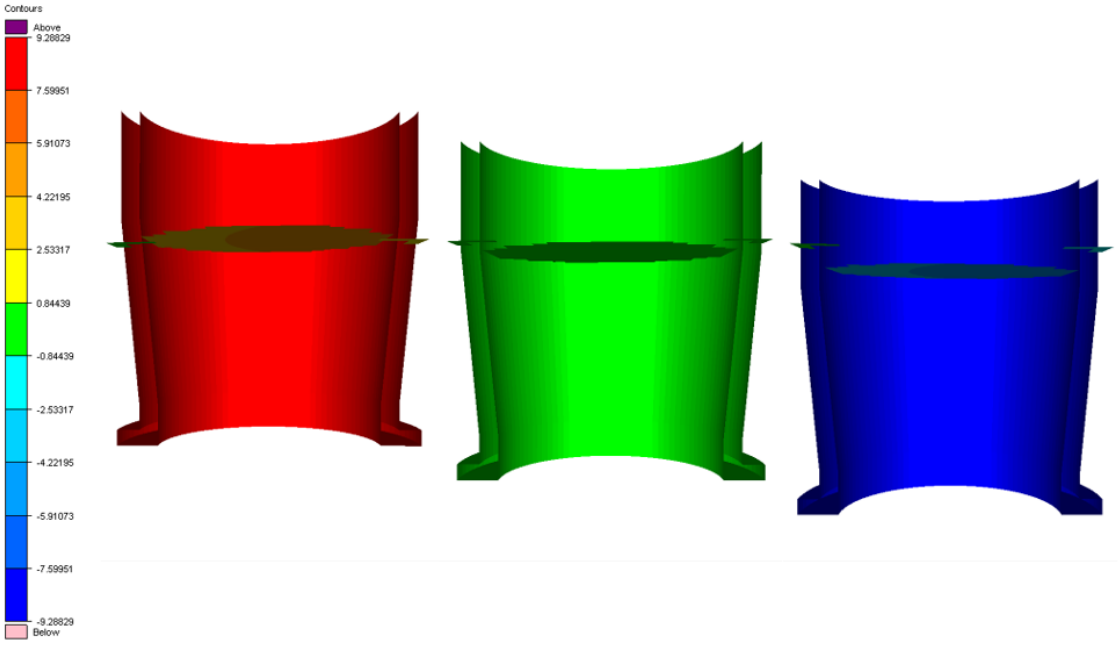

Figure 7.44: Visualisation of natural heave period at 17s from simulations using wave particle transer funtion when Tt is without boundary

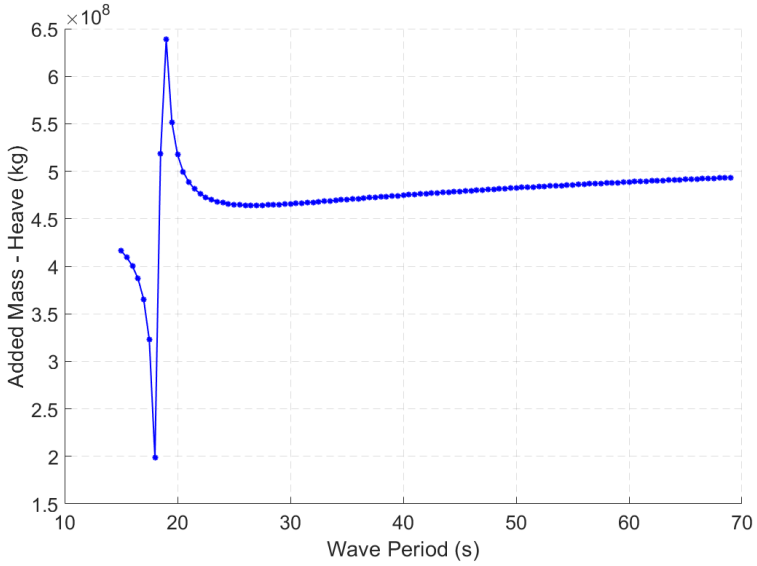

Figure 7.45: Added mass in Heave from HydroD when Tt is 20m. The peak is the piston-mode period which is 18.5s.

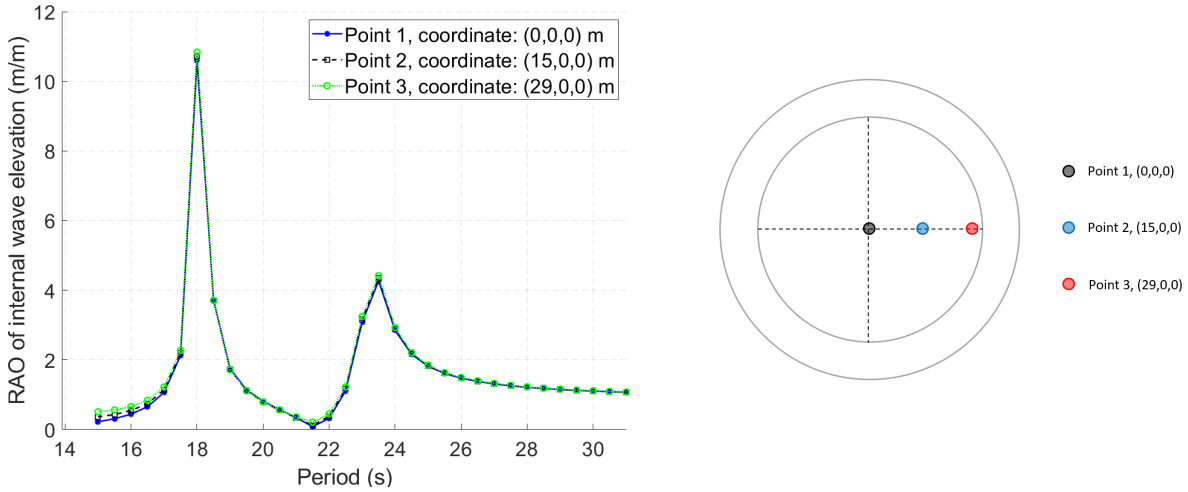

Figure 7.46: Response amplitude operator magnitude of internal surface points without damping where the first peak is the piston-mode period and the second peak is the natural heave period and a illustration of the placement of the offbody points seen from above.

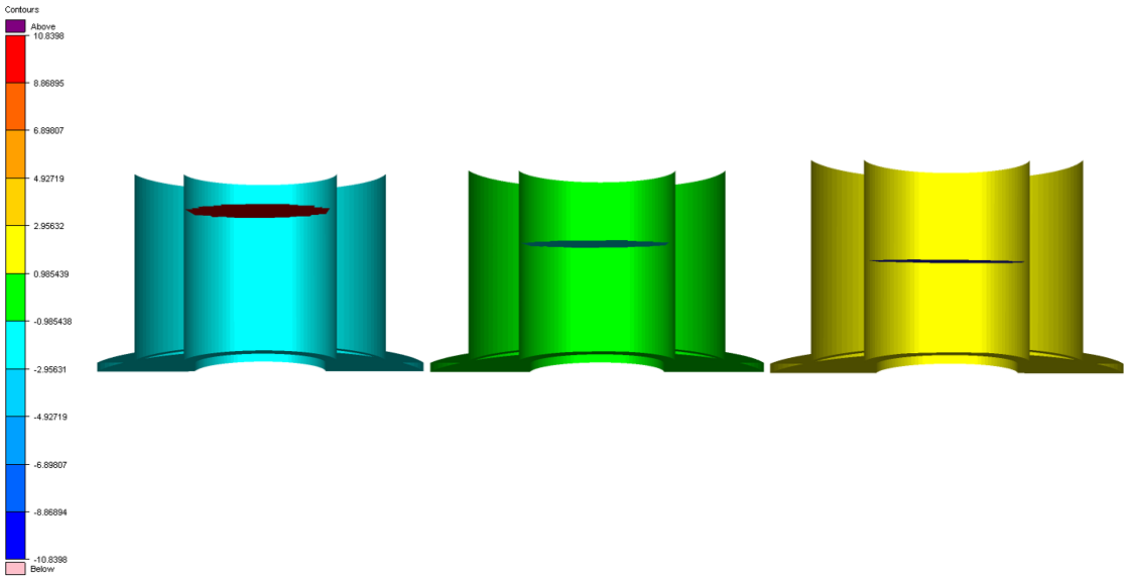

Figure 7.47: Visualisation of the piston-mode period at 18s from simulations using wave particle transer funtion when Tt is 20m

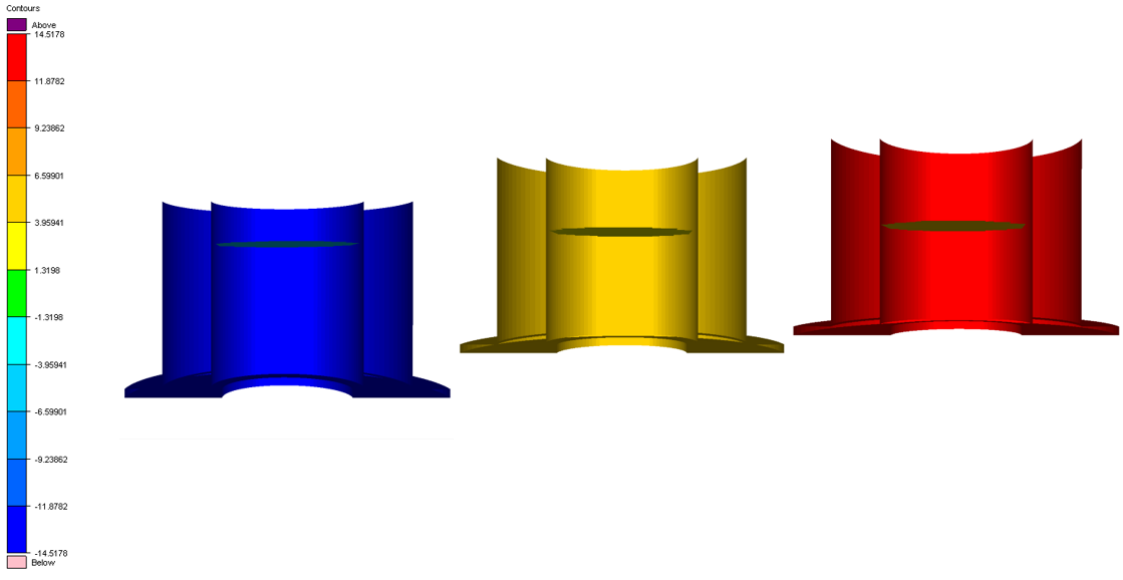

Figure 7.48: Visualisation of natural heave period at 23.5s from simulations using wave particle transer funtion when Tt is 20m

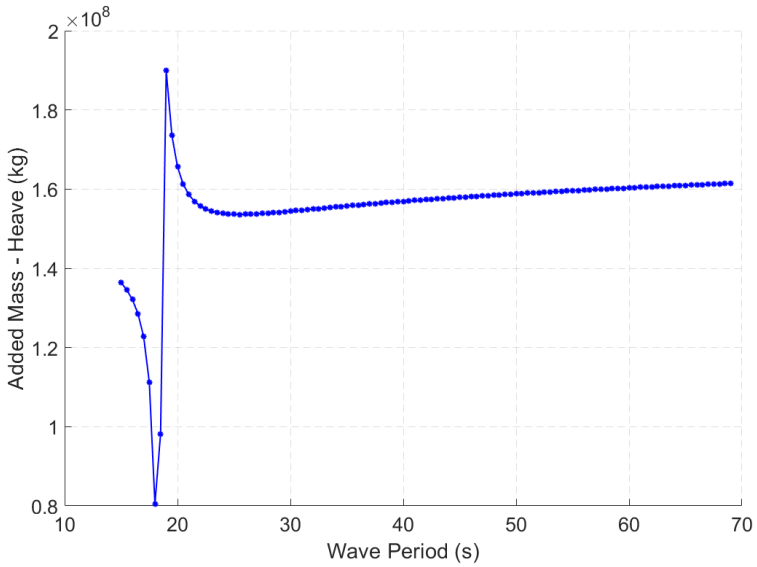

Figure 7.49: Added mass in Heave from HydroD when Tt is 30m. The peak is the piston-mode period which is 18.5s.

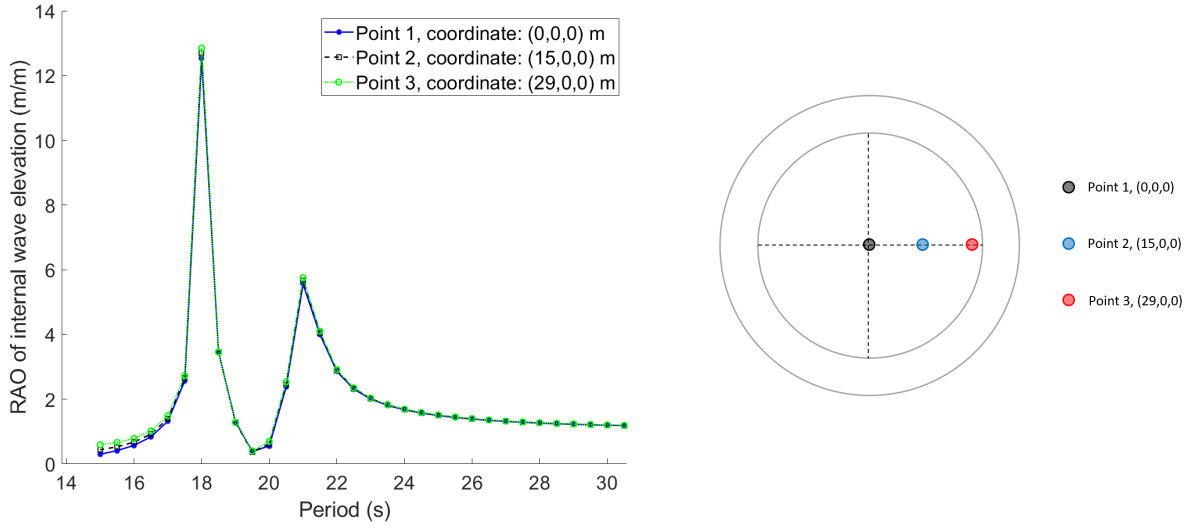

Figure 7.50: Response amplitude operator magnitude of internal surface points without damping where the first peak is the piston-mode period and the second peak is the natural heave period and a illustration of the placement of the offbody points seen from above.

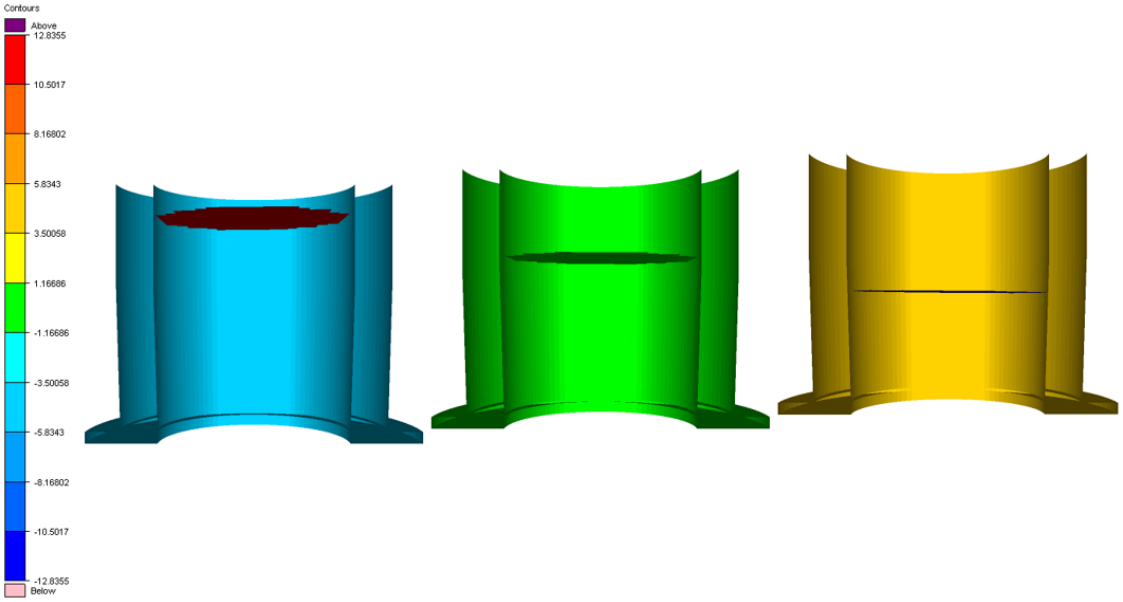

Figure 7.51: Visualisation of piston-mode period at 18s from simulations using wave particle transer funtion when Tt is 30m

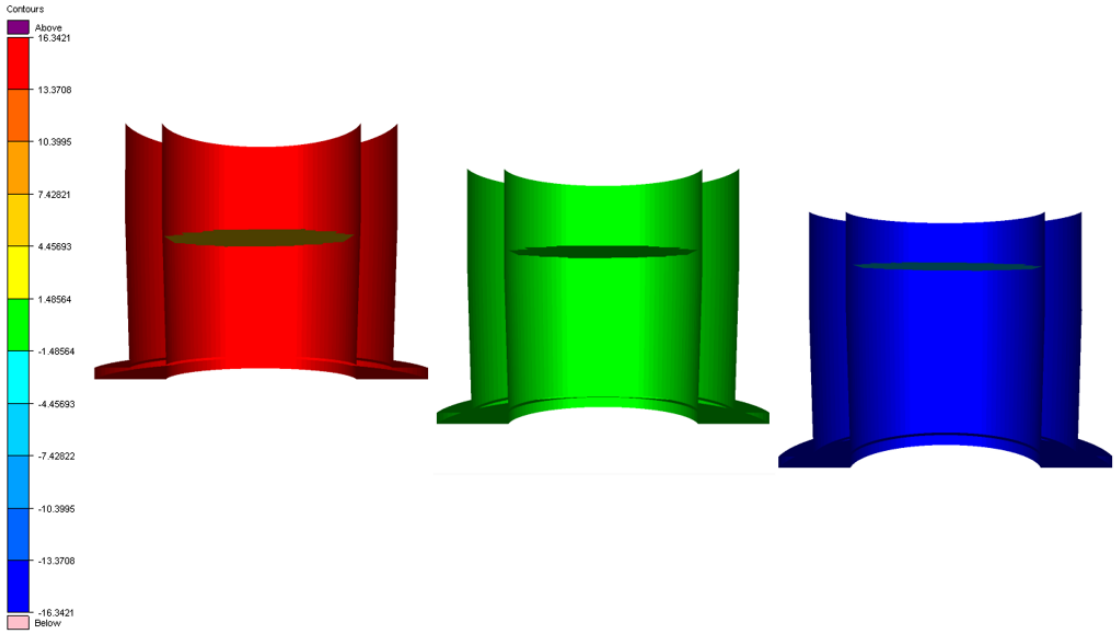

Figure 7.52: Visualisation of natural heave period at 21s from simulations using wave particle transer funtion when Tt is 30m

8 | Discussion

This chapter discuss the four main steps completed to investigate how a parametric design optimisation could be carried out for a funnel shaped dock intended for installation of floating wind turbine. This includes the preliminary study, response surfaces, gradient based optimisation and verification of the optima found.

8.1 Preliminary Study

The goal of the preliminary study was to investigate coherence between design parameters and the piston-mode period. A total of 13 tests was carried out; one reference and twelve indicator tests. The goal of the preliminary tests was to get an insight of how much influence the variables $Di1$, $Di2$, $T1$, $T2$, $T3$ and DT had on the result of piston-mode period. The table 7.1 shows that a change in $Di1$ and $Di2$ has the most significant influence on the piston-mode period, compared to the other variables. A change in DT don't influence the piston-mode period at all. This was expected as the thickness do not influence the inner geometric parameters in a direct manner. Change of the different heights $T1$, $T2$ and $T3$ did independently influenced the result similarly for each of the values. The results between the result that are listed in the table of the values below and above the reference values can be seen in the figures 7.2, 7.3, 7.4, 7.5, 7.6, and 7.7.

8.2 Response Surface

The response surface study investigates how the operational constraint of piston-mode period is affected by changes in design parameters. To visualize the individual impact of the design parameters on piston-mode periods, the parameters are separated and plotted in pairs as a 3D-surface representing piston-mode period in the polynomial response surface study. The artificial neural network and Gaussian process regression studies investigates the possibility of predicting a piston-mode period based on changes made in the design parameters. All data used for training and testing of the models should be considered noisy, as the frequency sets consist of data points every $0.5s$. The choice of $0.5s$ frequency intervals is made due to large amounts of computing time required for every frequency.

8.2.1 Polynomial Response Surface

To visualize the individual impact of the design parameters on piston-mode periods, the parameters are separated and plotted in pairs as a 3D-surface representing piston-mode period in the polynomial response surface study. As seen in figure 7.8, the design variables $Di1$ and $Di2$ are important for piston-mode period calculations. The surface looks exponential both along the x- and the y-axes. With lower $Di1$ and $Di2$ clearly leading to a low piston-mode period. When comparing $Di1$ to $T1$ in figure 7.9, it becomes clear that $Di1$ is still very important with respect to piston-mode periods of the structure, with the axis representing $Di1$ having a steeper curve compared to the axis representing $T1$. As both $Di1$ and $T1$ increase, piston-mode period increases. As seen in figure 7.10 and 7.11 $T1$, $T2$ and $T3$ are of very similar impact to piston-mode periods. This relation is reasonable as $T1$, $T2$ and $T3$ are all heights, and comparing them to a diameter without inputting data about the *other* heights gives a height-diameter chart for all three data sets. In total, a larger diameter and larger heights give higher piston-mode periods. This is explicable by looking at the volume of water which needs to move to create a resonating state. Larger upper diameters, with larger heights (in practice a larger dock) will give a heightened piston-mode period. The exception is $Di1$ compared to $T3$, figure 7.11, where it becomes obvious that the two variables essentially have nothing to do with each other. $T3$ is the height where $Di2$ is applicable and as such it changes the piston-mode period minimally in relation to $Di1$.

Comparing $Di2$ to $T1$, $T2$ and $T3$, as seen in figures 7.12, 7.13 and 7.14, the correlation between inner diameters and heights is comparable to the ones where $Di1$ is compared to $T1$, $T2$ and $T3$. Although it looks similar, one notable difference is how $Di2$ is closer to an exponential curve. With *lower* values leading to a larger piston-mode period. This is the opposite of $Di1$ and indicates that a smaller radius in the lower part of the dock will increase the piston-mode period. This phenomenon may be explained by looking at the principle behind piston-mode, where the wave energy outside of the dock needs to pass through the bottom of the dock as movement of volume to induce a resonating state. As the lower diameter is reduced, the cross-sectional area for water to pass through to get into the dock is reduced. This leads to a need of a larger amount of energy to create a resonating state.

As one starts to compare $T1$, $T2$ and $T3$ as in figures 7.15, 7.16 and 7.17, it becomes evident that $T1$ and $T3$, seem without correlation. As the heights are essentially dependent on $T2$ and the diameters in the top and bottom of this height, the diameters appear to have the largest impact on piston-mode periods.

Gaussian Process Regression

For the Gaussian process regression method of predicting data, three different covariance functions were tested for predicting piston-mode periods. All three are trained using the sequential HydroD results and tested using the randomized results. In the left graph of figures 7.18, 7.19 and 7.20 the blue line illustrates the cases from HydroD, where the calculated piston-mode period is set as the base for error-calculations from the prediction-model. Red circles illustrate the predicted values from the gaussian process regression models. The red circles close to the blue line show a small deviation from the prediction model to the HydroD simulation.

In the right graph of figures 7.18, 7.19 and 7.20 the probability density function as a relative error is shown. This figure illustrates what percentages of the cases deviate with what magnitude from the HydroD simulations.

Exponential Kernel

The model based on the exponential covariance function (figure 7.18) shows a smooth curve, without a large number of points far off the blue line. There are two predictions made in the region of $24s$ which are a bit high. In addition there are two predictions which seem a bit low int the areas of $34s$ and $37s$. The precision of the model is reduced as it passes approximately $35s$, and especially after $42 - 43s$, where the population density is very low. This does not necessarily have a large impact on the sensitivity study, as the piston-mode periods discussed fairly far below these values. As one looks to the probability density function, the largest number of predictions have an absolute relative error of less than 0.5%. Approximately 58% of the cases are in this part of the probability distribution. As one widens the absolute relative error to 1.5%, approximately 97% of all predictions land within this density function. A larger amount of the errors are with positive, meaning the predicted value is more often higher than the calculated value from HydroD. Overall this is a good approximation with the best predictions in the areas where the case-density is high.

Matern 5/2

Looking at the model based on the covariance function Matern 5/2 (figure 7.19) the first impression is a smooth curve. Although there are a few individual predictions which do not fit very well. The conspicuous cases are about 10 cases which are predicted a bit high in the area between $20s$ and $25s$. For this thesis this is the most important area to predict good values. Compared to the exponential kernel, the Matern-function predicts the piston-mode periods better in the areas above $35s$. This area of piston-mode periods is, however, not the most important in this case. Looking at the probability density model, it becomes evident that approximately 53% of the cases have an absolute relative error smaller than 0.5%. Widening absolute relative error to 1.5%, about 97% of the predictions are within this error margin. The errors are split evenly between negative and positive values, meaning the model does not always predic too low or too high values. Overall this is a good approximation, with better predictions in the higher piston-mode periods, where the case-density is lower.

Rational Quadratic

Looking at the statistics for the prediction model based on the rational quadratic kernel (figure 7.20) it looks like a nice and even fit at first glance. However there are a few conspicuous cases in the regions of $20s$ to $25s$. The errors seem to be divided between positive and negative values, meaning the model does not consistently predict high or low values. Even though there are both high and low predictions, these do not come at the same time. For instance, some values are predicted high at about $20s$ and $21.5s$, before they are predicted low at $23.9s$, high at $24s$ and low at $24.1s$. The model keeps predicting most values within a low relative error, but keeps predicting some values with errors in this *'s-shape'*. The probability density function is very similar to the one in 7.19, except it shows that the larger absolute relative errors build up in a low prediction, with the block between negative 1.5 and 2.5 about 50% larger than its positive counterpart. In total this is a good model, but the relative errors are larger than the two other gaussian process regression predictor models.

8.2.2 Artificial Neural Network

For the artificial neural network result, three different learning algorithms were considered and compared to the predicted piston-mode periods from HydroD. In the left graph of figures 7.21, 7.22 and 7.23 the blue line drawn from bottom left corner to top right, illustrates the cases from HydroD, where the calculated piston-mode period is set as the base for error-calculations from the prediction-model. Red circles illustrate the predicted values from the artificial neural network. In the right graph of figures 7.21, 7.22 and 7.23, the probability density function as a relative error is shown. This figure illustrates what percentages of the cases deviate with what magnitude from the HydroD simulations. The three different figures using the different types of algorithms are presented and discussed below:

Levenberg Marquardt

The predicted results using Levenberg Marquardt show a relatively smooth and uniform curve, without too much deviation from the blue line in the left part of figure 7.21. Compared to the results in GPR, the spread of the prediction made by the network appear to be a bit larger, thus the more thick spread in the left part of the figure. There are some cases in the area between 21 - 24 seconds and above 35 seconds that are a bit low and do not follow the "curve". But the relative error confirms that the majority, close to 50 % of the results are close to the blue line. On the other hand the right figure shows that there is a slight increase of cases with a relative error beyond ± 2,5%, compared to the cases in the area ± 1,5% - 2,5%

Bayesian Regularisation

The model based on the Bayesian regularisation algorithm is presented in figure 7.22. The visual first impression of this figure is that the predicted values using the algorithm is a bit fuzzy and not as smooth as i.e. the results in GPR. There is no particular area where the values are more smooth than not. Although the result did not turn out ideal, the relative error shows that the majority of the values, just above 50 %, still are within the blue line with a relative error of $\pm 0,5\%$.

Scaled Conjugate Gradient

Figure 7.23 shows HydroD results compared to predictions by the trained model based on the artificial neural network algorithm, scaled conjugate gradient. The predicted result in the left of the figure are relatively smooth similar to the distribution of the result in figure 7.21, using Levenberg Marquardt algorithm for the prediction. The relaitve error shows that the deviation between the result and the blue line are pretty evenly distributed between zero and$\pm 2,5\%$. This error is not share any similarity to the previous results using artificial neural networks as a prediction tool.

Using ANN as a prediction tool gives results with decent accuracy. The first two algorithms presented in this section gave around 50% of its relative error within the interval of zero to $\pm 0,5\%$. The last presented algorithm was not very accurate, but had more of an even spread of the deviation between the prediction and the result in terms of relative error.

8.2.3 Comparison of the Trained Models

While investigating how to best predict piston-mode periods, statistical values for the numerous approaches have been compared. The data used to train and verify all models, both artificial neural networks and Gaussian process regressions, are based on data which is not completely *smooth*. All simulations run in HydroD which constellate both the training data and the verification data are run with a resolution of $0.5s$. This gives data sets which are to a certain extent pixelated.

From theory it is known that the Gaussian process regression method uses a probability distribution function to predict outcomes. This approach is known to be good for noisy data. With this information it is reasonable to expect the Gaussian process regression to produce good results with small errors (figure 3.16).

Investigating the statistical values of RMSE and R^2 for all trained models, the Gaussian process regression, based on the exponential kernel, stands out. The model boasts both the lowest root mean square error and a R^2 closer to 1. In addition, the lowest relative and absolute errors are acquired by the use of this model.

This evaluation laid the grounds for using the Gaussian process regression model based on the exponential kernel for predicting piston-mode periods during the optimisation process.

8.3 Gradient-Based Optimisation

The gradient based optimisation presents the optimum docks found given individually specified constraints, and makes it possible to investigate how the design variables, the design objective and the boundaries vary along iterations, and also which constraint that has the greatest impact on a given optimum found.

8.3.1 Main Study

The optimum from the main study is a dock without boundary for draft in transit, and a minimum piston-mode period constraint of 21 s. Figure 7.26a and 7.26b shows the optimum shape of the floating dock in operation and in transit given the constraints. The result shows a funnel-shaped dock which is really close to the edge out the range of the gaussian process regression based model for piston-mode period calculations. Therefore the result is close to valid. It is the lightest and thus cheapest dock found so far, which can be seen by comparing Figure 7.32a, 7.37a and 7.27a, with the estimated weight of about $0.8x10^4$ tonnes.

8.3.2 Sensitivity Study

The first optimum presented is a dock which has a maximum of 20m draft in transit, and a minimum piston-mode period of 21 s. Figure 7.31a and 7.31b shows the optimum shape of the floating dock in operation and in transit given these constraints. The result shows a cylindrical dock and not a funnel-shaped dock. An explanation for this can be understood by looking at the first iterations showing how the shape of the floating dock in operation changes in Figure 7.35a to 7.35f and comparing it to the iteration of the design objective in Figure 7.32a and the iterations of the metacentric height in Figure 7.34a and 7.34b. The figures shows that the optimisation process first tries to find a funnel shaped optimum since it can give higher piston-mode resonance with lower weight, but due to the constraints for metacentric height it is forced into a cylindrical dock. This makes the piston-mode resonance calculated by the gaussian process regression based model for this dock invalid as the model is only tested for funnel shaped docks and it is therefore outside the accepted range.

The second optimum presented is a dock which has a maximum of 30m draft in transit, and a minimum piston-mode period of 21 s. Figure 7.36a and 7.36b shows the optimum shape of the floating dock in operation and in transit given these constraints. The result shows a vaguely funnel-shaped dock which is also outside the range of the Gaussian process regression based model for piston-mode period calculations. The reason is the same as for the optimum found when the transit is maximum 20m. The constraint for the metacentric height in transit is hard to accomplish with the funnel shape. By looking at the constraint for piston-mode period in Figure 7.37b and comparing it to the first iterations showing how the shape of the floating dock in operation changes in Figure 7.40a to 7.40f it is clear that the funnel shape can give higher piston-mode period in operation if the draft in transit of the dock is not an issue.

8.4 Verification of the Optimisation Results

The optimisation results are evaluated to verify if the optima found are valid, and which potential errors exist within the models. The optimisation results show that the piston-mode period found with wave particle transfer function and from added mass in heave for the three cases presented do not fit the predictions from the Gaussian process regression based model. The geometry provided by the optimisation process is outside of the range where the Gaussian process regression model is trained to predict. The geometry is closer to a cylindrical dock and hence, the piston-mode period constraint is inaccurate for these optima. The last case where the draft in transit had no boundary was close to the valid prediction area, and therefore the piston-mode period from the trained model was closer to the results from wave particle transfer function and from added mass in heave. The expected optimum shape was a funnel shape, and the trained models were therefore trained with only funnel shaped docks. This means that the piston-mode period predicted for any other shape will include an error with unknown magnitude . It is still expected that the funnel shaped docks will give higher piston-mode periods with lower weight. To further investigate optima for funnel shaped docks, additional constraints can be added so the optimisation only consider funnel shaped docks in the range of the trained model. However this would not give say anything about docks outside the range of the trained model, and is therefore not the best solution. A new model that in addition to funnel shaped docks also includes bottle shaped and cylindrical docks can be trained so the piston-mode period for all shapes can be considered. This demands a lot of computing time but could potentially have the ability to expand the range of the model so that the true optimum could be found.

8.5 Limitations

There are some weaknesses in this work, som of which are already discussed. An overview over some of the most important limitations are listed here:

- The simplifications made for the simulations used in the sequential and randomised tests may cause an unknown amount of errors.
- The Gaussian process regression model is trained to predict piston-mode periods for funnel-shaped docks where $Di1 > Di2 + 5.625\ m$. The optimisation-constraints of $Di1 > Di2$ creates an issue, where the predictor-model might be predicting values for geometries it has not been trained for.
- The operational constraint of piston-mode period is predicted based on test-results from added mass heave, although the wave particle transfer function regarded as the most direct representation of the piston-mode period (ref sub-chapter 3.5.7).
- The optimised objective function only takes into account the physical mass of steel. Construction, maintenance or other costs are not included.

9 | Conclusion

This study investigated how a parametric design optimisation could be carried out for a funnel-shaped dock intended for installation of floating wind turbines. This was done in four main steps.

- The preliminary study investigated coherence between different geometrical design parameters and the piston-mode period of the funnel-shaped floating dock. The study revealed the heights, $T1$, $T2$ and $T3$, in addition to the diameters, $Di1$ and $Di2$, to be design parameters which significantly affect the piston-mode period.
- With this foundation, response surfaces investigating which design parameters are most important were created, and how the operational constraint of piston-mode period most accurately can be predicted for funnel-shaped docks by comparing different algorithms was explored. The response surfaces show that a reduction in the lower diameter $Di2$ and an increase in the upper diameter, $Di1$, will increase the piston-mode period. $Di1$ and $Di2$ are the most important design parameters considering the piston-mode period. At the same time, increasing the height of the dock will slightly increase the piston-mode period. A Gaussian process regression based model with a exponential covariance function gave the most accurate predictions compared to results from hydrodynamic analyses. This model shows an average relative error $< 0.75\%$, a maximum absolute error of $1.3s$, a R^2-value over 0.9985 and an $RMSE$ smaller than 0.2.
- The gradient based optimisation presents the optimum docks found given individually specified constraints, and makes it possible to investigate how the design variables, the design objective and the boundaries vary along iterations, and also which constraint that has the greatest impact on a given optimum found. During the iterations the design objective is minimized while the function is kept within the constraints. The lightest and, in terms of material cost, cheapest optimum was found in the main study. This was a funnel-shaped dock with an approximate mass of $0.8x10^4$ tonnes. For funnel-shaped docks with low draft in transit the metacentric height appears to be the governing constraint. While the shallow draft in transit is not a requirement the piston-mode period appear to be the governing constraint. These constraints have the greatest impact on the optimum design.
- The gradient based optimisation results were evaluated to verify whether the optima found are valid, and what potential errors exist within the models. The optimisation results show that the piston-mode period found with wave particle transfer function and from added mass in heave for the three cases presented do not fit the predictions from the Gaussian process regression based model. This is because this optimisation is run with the piston-mode period constraint being predicted for a geometry outside of the trained area and therefore the optima found are invalid. To solve this problem, a parametric design optimisation for funnel-shaped, cylindrical and bottle-shaped docks may be carried out by training a Gaussian process regression model which predicts valid piston-mode periods for these shapes.

10 | Suggestions for Further Work

This work has investigated the optimum geometry for a floating dock, given a set of operational and geometrical constraints. The work has found different optima, depending on the constraints. Although the work has found possibilities for a floating dock, there are limitations in the predictor models created for piston-mode periods which cause some of the parameters for the optima to be inaccurate. To further build on this work, the authors present the following possibilities:

- A new predictor model for piston-mode periods could be created, where the constraints of $Di1 > Di2$ are not included. This would open the the optimization process for accurately predicting dock geometries which are not exclusively funnel-shaped. This process would demand a massive computing time but would potentially have the ability to expand the range of the model so that true optima with given constraints can be found.
- A life cycle assessment could be conducted to compare the effect of the increase in wind turbines installed versus the environmental footprint for the life cycle of the floating dock.
- An analysis that investigates the possible increased rate of installations of wind turbines due to this concept and a cost analysis could be conducted.

Bibliography

[1] IRENA, "Floating foundations: A game changer for offshore wind power," *The International Renewable Energy Agency, Abu Dhabi.*, 2016.

[2] Equinor, "Hywind scotland - the world's first floating wind farm," *[Online]*, Available: https://www.youtube.com/watch?v=vKHJfuuYiOk.

[3] Saipem, "Hywind," *[Online]*, Available: https://www.saipem.com/en/projects/hywind.

[4] US Department of Commerce, National Oceanic and Atmospheric Administration, "Wave height explanation," *[Online]*, Available: https://www.weather.gov/dlh/WaveHeightExplanation (accessed: 18.11.2019).

[5] DNV GL, "Modelling and Analysis of marine operations," *Det Norske Veritas AS*, 2014.

[6] O. M. Faltisen, "Sea loads on ships and offshore structures," *Cambridge University press*, 1990.

[7] M. Schabrich, "Coupled dynamic analysis of a floating dock system for installation of a spar wind turbin," *Master's thesis, Norwegian University of Science and Technology*, 2019.

[8] Sewaqu, "Random data points and their linear regression," *[Online]*, Available: https://en.wikipedia.org/wiki/Linear_regression (accessed: 12.03.2020).

[9] Wheeler Willie, *Nonlinear Regression in R.*

[10] Berland, "Linear interpolation on data set," *[Online]*, Available: https://en.wikipedia.org/wiki/Interpolation (accessed: 06.05.2020).

[11] Berland, "Illustration of polynomial interpolation of a data set," *[Online]*, Available: https://en.wikipedia.org /wiki/Linear_interpolation (accessed 06.05.2020).

[12] Mathworks Inc., *Gaussian Process Regression Models*, Available: https://se.mathworks.com/help/stats/gaussian-process-regression-models.html (accessed: 27.05.2020).

[13] J. B. Ahire, *The Artificial Neural Networks handbook: Part 1*, Available: https://medium.com/coinmonks/the-artificial-neural-networks-handbook-part-1-f9ceb0e376b4 (accessed: 03.06.2020).

[14] J. Gilis, "Gradient ascent," *[Online]*, Available: https://en.wikipedia.org/wiki/File:Gradient_ascent_(contour).png (accessed: 18.05.2020).

[15] Mathworks Inc., "Machine learning in matlab," *[Online]*, Available: https://se.mathworks.com/help/stats/machine-learning-in-matlab.html (accessed: 01.06.2020).

[16] IRENA, "Renewable energy statistics 2019," *The International Renewable Energy Agency, Abu Dhabi*, 2019.

[17] IRENA, "Innovation outlook: Offshore wind," *The International Renewable Energy Agency, Abu Dhabi*, 2016.

[18] WINDEUROPE, "Offshore wind in europe: Key trends and statistics 2018," *WINDEUROPE, Belgium.*, 2018.

[19] K. H. lIEN, "Hywind scotland – marine operations," *[Online]*, Available: http://www.norcowe.no/doc/konferanser/2016/SMI%20Stavanger%20presentasjoner/Lien%20Statoil%20Hywind%20Scotland%20Marine%20Operations.pdf.

[20] L. I. Hatledal, H. Zhang, K. H. Halse, and H. P. Hildre, "Numerical study for a catamaran gripper-monopile mechanism of a novel offshore wind turbine assembly installation procedure," *ASME 36th International Conference on Ocean OMAE2017–62342, Offshore and Arctic Engineering*, 2017.

[21] Z. Jiang, L. Li, Z. Gao, K. H. Halse, and P. C. Sandvik, "Dynamic response analysis of a catamaran installation vessel during the positioning of a wind turbine assembly onto a spar foundation," *Marine Structures 61 1–24*, 2018.

[22] Z. Jiang, Z. Ren, Z. Gao, P. C. Sandvik, K. H. Halse, and R. Skjetne, "Mating control of a wind turbine tower-nacelle-rotor assembly for a catamaran installation vessel," *International Society of Offshore and Polar Engineers, Sapporo, Japan*, 2018.

[23] Z. Jiang, R. Yttervik, Z. Gao, and P. C. Sandvik, "Design, modelling, and analysis of a large floating dock for spar floating wind turbine installation," *Marine Structures Vol. 72 - 102781*, 2020.

[24] Statistisk Sentralbyrå, "Omsetning i fiskenæringen," *[Online]*, Available: https://www.ssb.no/jord-skog-jakt-og-fiskeri/statistikker/fiskeri/ (accessed: 19.02.2020).

[25] The Norwegian Government, "Norsk oljehistorie på 5 minutter," *[Online]*, Available: https://www.regjeringen.no/no/tema/energi/olje-og-gass/norsk-oljehistorie-pa-5-minutter/id440538/ (accessed 19.02.2020).

[26] Norwegian Ministry of Finance, "Statsbudsjett 2020," *Finansdepartementet*, 2019.

[27] Einar-Are Drivenes, *NORSK POLARHISTORIE III.* Gyldendal, 2006.

[28] H.-O. Pörtner, D. Roberts, V. Masson-Delmotte, P. Zhai, M. Tignor, E. Poloczanska, K. Mintenbeck, A. Alegría, M. Nicolai, A. Okem, J. Petzold, B. Rama, and N. W. (eds.), "Ipcc special report on ocean and cryosphere in a changing climate (SROCC)," *Intergovernmental Panel on Climate Change*, 2019.

[29] Friedlingstein et al., "Global carbon budget 2019," *Earth System Science Data*, 2019.

[30] P. Støa, "130.000 nye arbeidsplasser i industrien før 2050," *SINTEF Energi AS*, 2020.

[31] International Energy Agency, "Offshore wind outlook 2019," *International Energy Agency [Online]*, Available: https://www.iea.org/reports/offshore-wind-outlook-2019.

[32] H. Veldkamp and J. var der Temple, "Influence of wave modelling on the prediction of fatigue for offshorewind turbines," *Wind Energy*, 2005.

[33] J. Journée and W. Massie, "Offshore hydromechanics," 2001.

[34] O. M. Faltinsen, "Sea loads on ships and offshore structures," *Cambridge University Press*, 1990.

[35] J. Journée and W. Massie, "Offshore hydromechanics," *Delft University of Technology*, 2001.

[36] O. Faltinsen and A. Timokha, "Sloshing," *Cambridge University Press*, 2009.

[37] D. GL, "Sesam user manual xtract," *DNV GL, Høvik, Norway*, 2013.

[38] D. C. Montgommery, *Design and Analysis of Experiments.* John Wiley & Sons, Inc., 2013.

[39] C. A. Petersy, "Statistics for analysis of experimental data," 2001.

[40] J. Fox and S. Weisberg, *An R Companion to Applied Regression, Third Edition.* Sage, Thousand Oaks, California, 2019.

[41] H. J. M. . L. A. Ransnas, "Fitting curves to data using nonlinear regression: a practical and nonmathematical review," *Department of Pharmacology, University of California*, 1987.

[42] C. E. Rasmussen and C. K. I. Williams, "Gaussian processes for machine learning," *MIT Press. Cambridge, Massachusetts*, 2006.

[43] Mathworks Inc., "trainlm," *[Online]*, Available: https://se.mathworks.com/help/deeplearning/ref/trainlm.html (accessed: 02.06.2020).

[44] Mathworks Inc., "trainbr," *[Online]*, Available: https://se.mathworks.com/help/deeplearning/ref/trainbr.html (accessed: 02.06.2020).

[45] Mathworks Inc., "trainscg," *[Online]*, Available: https://se.mathworks.com/help/deeplearning/ref/trainscg.html (accessed: 01.06.2020).

[46] J. Nocedal and S. J. Wrigh, *Numerical Optimisation.* Chapters 1-2. Springer Science & Business Media, LLC, 2006.

[47] M. Mitchell, *An Introduction to Genetic Algorithms.* Cambridge, MIT Press, 1996.

[48] Randy L. Haupt and Sue Ellen Haupt, *Practical Genetic Algorithms, Second Edition.* Wiley-Interscience, 2004.

[49] W. J. Cook, W. H. Cunningham, W. R. Pulleyblank, and A. Schrijver, *Combinatorial Optimization.* Wiley International, 1997.

[50] N. R. Draper and H. Smith, *Applied Regression Analysis, 3rd Edition.* Wiley, New York, 1998.

[51] S. Ruder, *An overview of gradient descent optimization algorithms*, Available: https://ruder.io/optimizing-gradient-descent/index.html#references (accessed 23.05.2020).

[52] N. Qian, "On the momentum term in gradient descent learning algorithms," *Elsevier*, 1999.

[53] V. Gran, Z. Jiang, and P. Zhiyuan, "Hydrodynamic analysis of floating docks with alternative geometries for floating wind turbine installation," *Submitted to ASME OMAE*, 2020.

[54] DNV GL, "Offshore standard dnvgl-os-c301, stability and watertight integrity," *DNV GL*, January, 2017.

[55] DNV GL, *Sesam User Manual - WADAM - Wave Analysis by Diffraction and Morison theory, Version 9.6-19, 2019*, 2019.

[56] Matworks Inc., "Getting started with matlab," *[Online]*, Available: https://www.mathworks.com/products/matlab.html.

[57] Mathworks Inc., "Matlab documentation," *[Online]*, Available: https://www.mathworks.com/help/matlab/.

[58] Microsoft Inc., "Microsoft excel training," *[Online]*, Available: https://www.microsoft.com/en-us/microsoft-365/excel (accessed: 11.05.2020).

Appendices

A Appendix 1

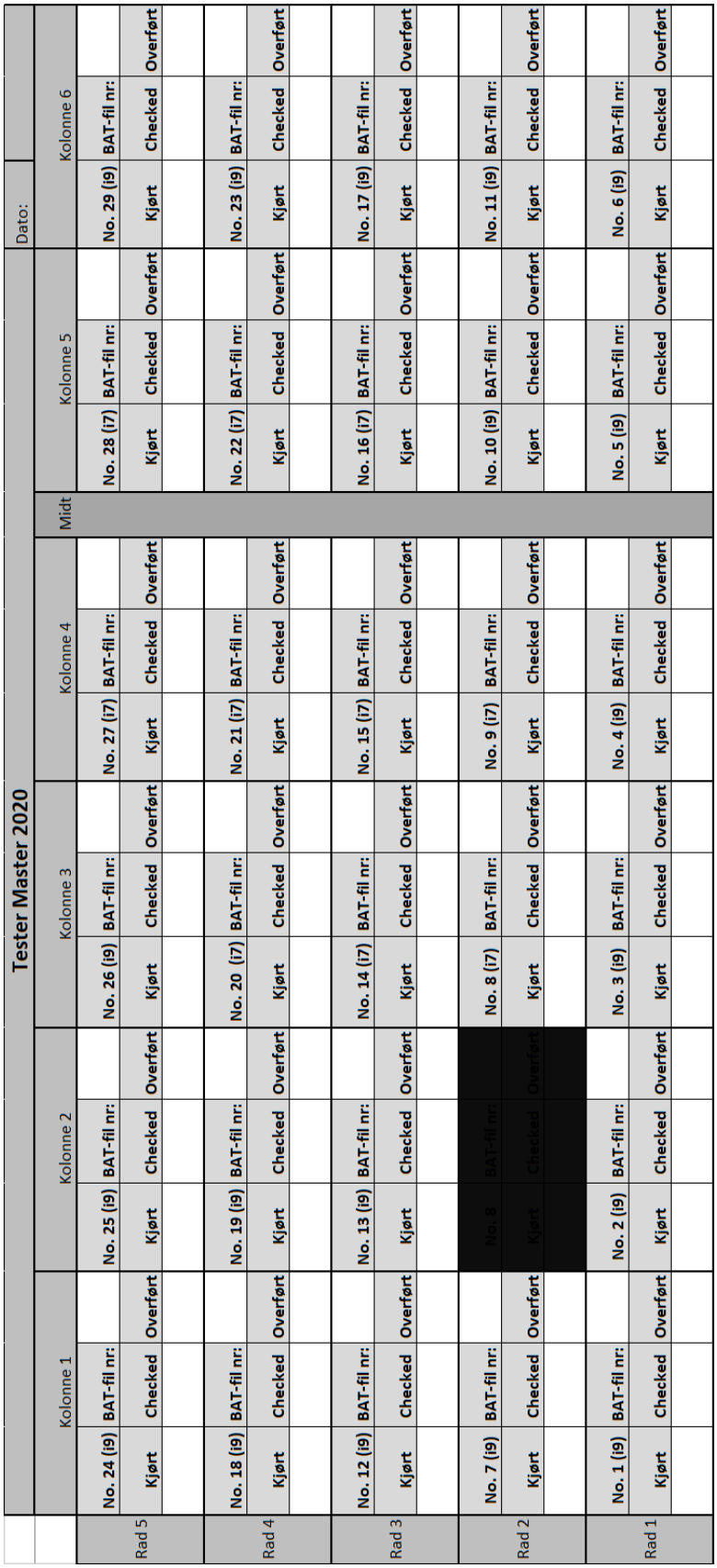

Figure 1: Document used to log the progress of the analyses.

B Appendix 2

- *VEDLEGG.zip.* MATLAB-code developed during this work.
- *Møteinnkalling, master.pdf.* Overview of mettings.

UiA Universitetet i Agder | BYG508-G 20V Masteroppgave

Title:

Design optimisation of a funnel- shaped floating dock for installation of offshore wind turbines.

Candidates:

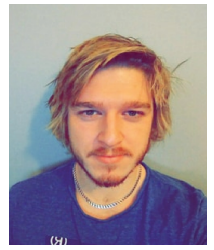

Viktor Gran

Simen N. Pedersen

Oscar Widestam

Supervisor:
Zhiyu Jiang, UiA

Summary

This master thesis investigated how a parametric design optimisation could be carried out for a funnel-shaped dock intended for installation of offshore floating wind turbines.The study revealed that the variables for different height and diameter affect the piston-mode period. A Gaussian process regression (GPR) based model with an exponential covariance function gave the most accurate predictions. The optimisation results showed that the piston-mode period constraint was invalid due to the range of the GPR based predictor model.

Introduction

Installation of offshore wind turbines is a challenging task. This technology is sensitive to wave excitation during the installation process. The floating dock concept has been proposed expand the weather window and avoid delays. The idea is to use a dock to shield the a spar platform from motions caused by waves.

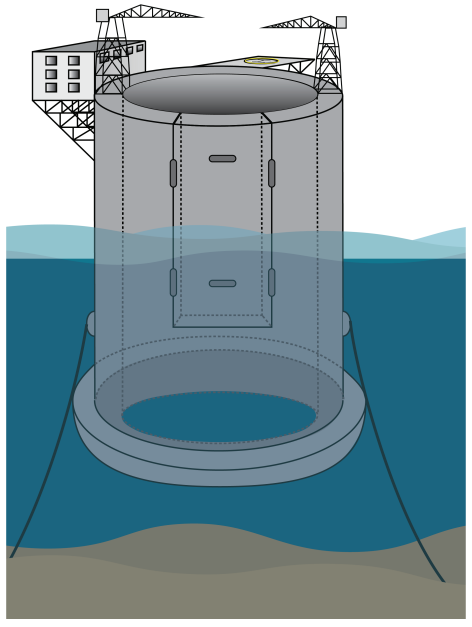

Figure 1 Schematic of floating dock consept

Case and materials

A previous study indicate that a funnel shaped dock has the potential to have improved performance in operating sea state.The variables used to define the geometry of the dock in this study are illustrated in the figure below.

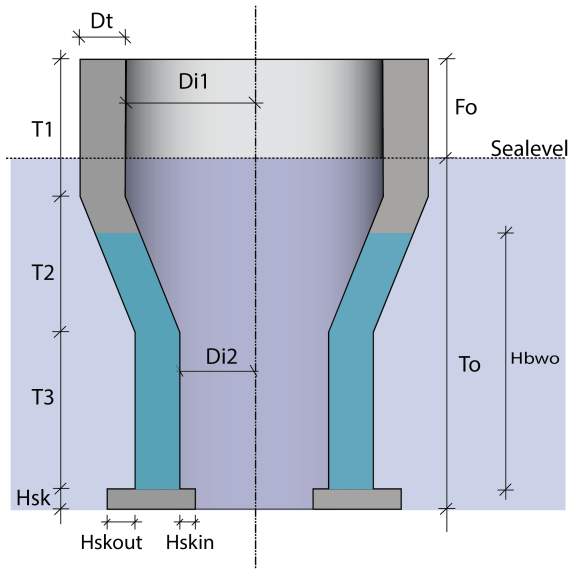

Figure 2 Funnel shaped dock

Research question

How can a parametric design optimisation be carried out for a funnel-shaped dockintended for installation of floating wind turbines?

- What are the most important design parameters?
- How can a response surface be created for certain operational constraints?
- Which constraints will have the greatest impact on the optimum design?
- How will the design objective vary along design iterations?

Theory

Piston mode causes resonance oscillations where the water surface moves as a rigid body in heave direction.

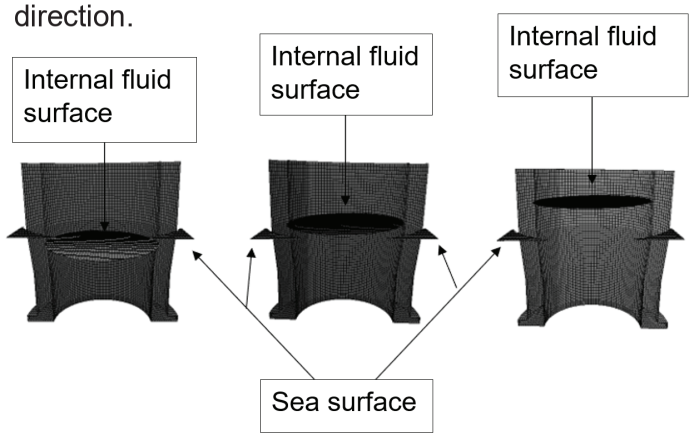

Figure 3 Piston-mode oscillation inside a floating dock.

Response surface methods are well-established statistical and mathematical ways of visualising and mapping correlations between a set of variables and an interesting output.

Gradient-based optimisation is a common denominator for optimisation algorithms which depend on differentiation of variables. Gradient descent is used for the optimisation in this thesis. The minimization is done by iterating gradients of the function. The gradients are foundby differentiating with respect to every variable.

Method

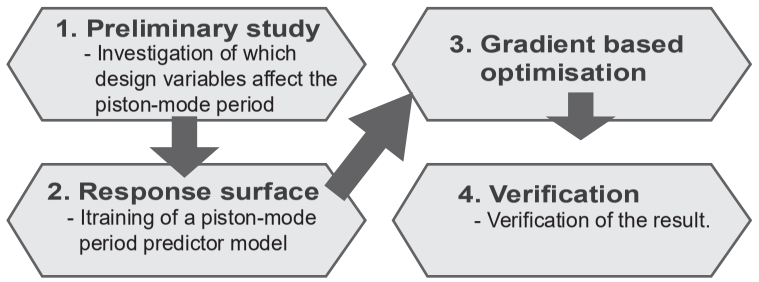

Figure 4 Flow chart of 4 main steps for the method

Results

The study revealed that the heights; T1, T2 and T3, in addition to the diameters, Di1 and Di2, are design parameters which significantly effect the piston-mode period. A gaussian process regression based model with an exponential covariance function gave the most accurate predictions compared to results from hydrodynamic analyses. The optimum found in the main study was a funnel shaped dock. This was the lightest and thus cheapest dock found and had an estimated mass of 8x10³ tonnes. The verification of the optimisation results show that the piston-mode from hydrodynamic analyses deviate from the predicted values from the GRP based model.

Conclusion

- The most important design parameters was Di1 and Di2.
- A gaussian process regression model with an exponential covariance gave the most accurate predictions for the operational constraint piston-mode period.
- For funnel-shaped docks with low draft in transit the metacentric height appear to bethe govering constraint. While the shallow draft in transit is not a requirement the piston-modeperiod appear to be the governing constraint.
- For a gradient-based optimisation, the design objective function will be reduced to a minimum within the defined boundaries and constraints.

The optima found in this study deviate from the predictions from the GPR based model as the geometry is outside the trained model-area. This can be solved with a new model which also includes bottle-shaped and cylindrical docks

Grimstad, Juni 2020